DYNAMIC HULL VANE

Motion and Resistance Reduction

MASTER THESIS - MARK PIETER DE JONGE

REVISION: 21 SEPTEMBER 2017

visit & mail us:
Costerweg 1B
6702 AA, Wageningen
The Netherlands

contact us:
T +31 (0)317 425818
info@hullvane.com
www.hullvane.com

company details:
IBAN: NL39ABNA0461251833
VAT: NL854243823B01
Chamber of Commerce: 61183199

follow us:

Thesis for the degree of MSc in Marine Technology in the specialization of hydrodynamics

Dynamic Hull Vane – Motion and Resistance Reduction

By

Mark Pieter de Jonge

Performed at

Hull Vane BV

This thesis is classified as confidential in accordance with the general conditions for projects performed by the TUDelft.

11-10-17

Company supervisors
Responsible supervisor: Kasper Uithof
E-mail: K.Uithof@hullvane.nl
Daily Supervisor(s): *separated by commas if necessary*
E-mail: *separated by commas if necessary*

Thesis exam committee
Chair/Responsible Professor: Riaan van 't Veer
Staff Member: Ido Akkerman
Staff Member:
Company Member: Kasper Uithof
Company Member: *Delete if inapplicable*

Author Details
Studynumber: 4172698
Author contact e-mail: markpieterdejonge@gmail.com

PREFACE

This document describes the research into the dynamic Hull Vane. I did this research over the course of seven months at Van Oossanen in Wageningen. During my study I got interested in CFD and the specialized knowledge of Van Oossanen quickly convinced me to do my research here. This led to the research about the dynamic Hull Vane, as it combines exploration into new possibilities for the Hull Vane and the use of advanced CFD methods. With this thesis, I complete my six year study of maritime technology with a master in ship hydrodynamics.

Writing this thesis would be impossible without the help of my colleagues at Van Oossanen. Firstly I would like to thank my daily supervisor Kasper, your revisions to this report were thorough and improved the overall quality greatly. Furthermore I would like to thank Nils, Vincent and Tijmen, you all contributed to my knowledge of fluid dynamics and CFD. I would like to thank the rest of my colleagues for contributing to the overall environment at the workplace. And of course Van Oossanen for giving me the opportunity to do this research.

Also thanks to the TU Delft for the education of the past six years. And thanks to Riaan van ‘t Veer and Ido Akkerman for steering the research in the right direction..

Lastly I would like to thank my family and friends for their support.

SUMMARY

Among other characteristics, two main performance parameters of a ship are fuel consumption and ship motions. Besides a well-designed hull, several appendages can be used to increase the performance. One of these is the Hull Vane (a fixed foil behind the transom of the ship). The Hull Vane has the potential to create large lift forces on the aft of the ship, thereby changing the resistance and dynamic position of the vessel.

In this thesis an algorithm is designed that controls the pitch angle and thus lift of the Hull. The goal is to investigate the potential of a dynamic Hull Vane for further reduction of resistance and ship motions. The resistance reduction is investigated by increasing the thrust on the Hull Vane trough an oscillating foil principle (vertically moving foil to create propulsion). The research is done with the use of the FINE/Marine CFD package. A model from the AMECRC OPV series in used for analysis, in combination with a previously optimized Hull Vane (Uithof, Hagemeister, Bouckaert, van Oossanen, & Moerke, 2016).

A literature review shows the relation between the oscillating foil theory and the dynamic Hull Vane. According to the oscillating foil theory, using a foil for propulsion can yield high propulsive efficiencies (≈60%) (Read, Hover, & Triantafyllou, 2002). In contrast to the oscillating foil, the ship does not need to supply the power for the vertical movement of the dynamic Hull Vane, thereby potentially increasing the efficiency. A preliminary study shows that the vertical motion of the Hull Vane is small, and the thrust will be generated by the oblique flow. This makes the working principles different from an oscillating foil where the thrust is mainly generated by the vertical motion. It can be concluded that a dynamic Hull Vane will not generate thrust in the same manner as an oscillating foil.

For proper control over the angle of attack, the relative flow direction on the Hull Vane is studied. It is caused by three systems; motion of the water caused by the waves, the vertical velocity of the Hull Vane (due to the ship's heave and pitch motions), and the variation of the pitch angle of the ship. A Computational Fluid Dynamics (CFD) analysis of the flow direction for the bare hull shows that the vertical velocity caused by the pitching velocity of the ship has the largest influence on change in angle of attack on the Hull Vane for this ship at the optimization condition (Fn = 0.4, H = 1.0m, $\omega_{enc} = 1.75\,{}^{rad}/_{s}$).

The working conditions of the foil profile are studied with both 2D and 3D wing theory, to calculate the optimal angle of attack for producing thrust. The induced drag limits the thrust production for larger angles of attack, i.e. a relatively small angle of attack will produce the most thrust (<≈5°).

The research is done using unsteady RANS (Reynolds Averaged Navier-Stokes) simulations. A test matrix was set up with three ship speeds and three wave encounter frequencies. The speeds are based on previous research in which the Hull Vane showed significant resistance reduction (Fn 0.30, Fn 0.40, Fn 0.50). The encounter frequencies of the waves were chosen based on the natural frequency of the ship (1.75 rad/s) and two frequencies next to it (1.25 rad/s and 2.25 rad/s). A grid study is done showing an uncertainty between 3% and 5%, depending on the method.

In total, four algorithms are tested based on different working principles. The first algorithm focuses on motion reduction by controlling the dynamic Hull Vane based on the pitch acceleration. At the moment the ship is accelerating bow up, the angle of attack is increased, to create more lift and thereby counteracting this motion. Different maximum angles are tested, which lead to a reduction of the pitching motion of up to 25.2% with little influence on the total resistance. The reduction in added wave resistance is comparable to the loss of thrust of the Hull Vane. Because maximum limits have to be defined for this algorithm, it is likely to give problems in irregular waves.

The second algorithm is designed to maintain a constant angle of attack during the waves based on the experience of the literature study. The result is a slightly more constant lift on the Hull Vane, although not stable enough to represent a constant angle of attack. The results show no significant effect on resistance or ship motions.

The third algorithm is based on measuring the vertical force on the Hull Vane, and use that to calculate the current angle of attack. This is then used to calculate the angle of the flow to the horizontal, which is compared to the optimal Hull Vane angle for maximum thrust according to the literature review. However, the resulting thrust is slightly smaller than the thrust of the static Hull Vane. This shows that when this algorithm would be optimized, no significant gain of thrust of the Hull Vane is possible.

For the final algorithm, the change in angle of attack is calculated with the pitch velocity. The dynamic Hull Vane then rotates in opposite direction, further increasing or decreasing the angle of attack. A few iterations with different control settings are tested, varying the neutral axis and the amplitude of the movement. The results show that good control over the lift on the dynamic Hull Vane is possible. The variation of the neutral axis can offset the mean lift, and the change in amplitude of the rotation changes the amplitude of the lift. This way of controlling the lift proved valuable for motion reduction, with little influence on the total resistance. The reduction in added wave resistance is again similar to the loss in thrust of the Hull Vane.

The final control algorithm proved easy to tune and was further tested in different conditions as setup based in the test matrix. Compared to the static Hull Vane, the dynamic Hull Vane reduced the ship motions between -13.4% to -28.4%, depending on the ship's speed and the wave encounter frequency. The total resistance in those conditions varies between a decrease of -1.3% and an increase of +2.3%. Changing the wave height at the optimization speed and wave encounter frequency, the dynamic Hull Vane shows a decrease in pitch motion between -24.8% to -21.3%. The resistance varies between -0.4% and +1.3%. At all wave conditions, the reduction in added wave resistance is similar to the decrease in Hull Vane thrust. For all conditions the dynamic Hull Vane reduces the pitch motions significantly, while its influence on total resistance was not uniform and varied.

CONTENTS

LIST OF FIGURES

LIST OF TABLES

LIST OF SYMBOLS

F_z^{HV}	Vertical force on Hull Vane
F_x^{HV}	Horizontal force on Hull Vane
h_0	Heave amplitude for oscillating foil
h_i	Typical cell size
R_{total}	Total ship resistance
C_D	Total drag coefficient
C_{FX}	Horizontal force coefficient
C_L	3D lift coefficient
C_T	Thrust force coefficient
C_d	2D drag coefficient
C_{di}	Incuded drag coefficient
C_l	2D lift coefficient
C_{l0}	2D lift coefficient for zero angle of attack
R_{hull}	Resistance on hull
R_{AW}	Added wave Resistance
U_{inf}	Undisturbed flow velocity
U_ϕ	Uncertainty of flow quantity
$V_{Z_{HV}}$	Vertical velocity of Hull Vane
V_Ω	Volume of entire domain
X_{HV}	Horizontal position of Hull Vane
r_i	Refinement factor
$\bar{u}$	Average flow component
$\acute{u}$	Fluctuating flow component
u_x	Horizontal flow velocity
u_z	Vertical flow velocity
z_{COG}	Vertical position of center of gravity
z_{HV}	Vertical position of Hull Vane
$\mathbb{P}_{ij}$	Stress tensor
$\hat{\theta}$	Pitch amplitude
$\bar{\theta}$	Pitch mean
θ_0	Pitch angle amplitude
τ_{ij}	Viscous stress tensor
ω_{enc}	Wave encounter frequency
ϵ_ϕ	Error of flow quantity
h	Heave motion
I_{xx}	Moment of inertia around x axis
K_{xx}	Inertia gyradius around x axis
K_{yy}	Inertia gyradius around y axis
K_{zz}	Inertia gyradius around z axis
Δ	Displacement
AR	Aspect ratio
Fn	Froude number
H	Wave height
LCG	Longitudinal center of gravity
LOA	Length over all
St	Strouhal number
V	Vector field
a	Amplitude
e	Planform efficiency factor
k	Wave number
α	Angle of attack
θ	Pitch
μ	Dynamic Viscosity
ρ	Density

ψ	Phase angle
ω	Angular frequency
ϕ	Flow quantity

Accents

$\widehat{}$	Amplitude
$\bar{}$	Mean
$\dot{}$	Time derivative

1. INTRODUCTION

This report describes the research done into a dynamic version of the Hull Vane[1] in waves, for which the pitch of the Hull Vane will be controlled. The goal of the dynamic Hull Vane is to further investigate the ship motion reducing capabilities of the Hull Vane and to develop thrust in combination with the vertical motion of the stern in waves, to reduce the total resistance of the ship. As an introduction to the dynamic Hull Vane, the background of the Hull Vane is explained in the introduction. Then the goal and general setup of the research is explained, followed by the structure of this thesis.

1.1 BACKGROUND

In the continuous search for the reduction of use of fossil fuel on ships, another fuel saving device was introduced in 1992. The Hull Vane was initially developed to reduce the dynamic trim of a catamaran, but its resistance reducing properties quickly led to additional research in the possibilities as a fuel saving device. According to Computational Fluid Dynamics (CFD) simulations done at Van Oossanen on multiple ships, the resistance can decrease by 25.5% but can also increase by 9.5% (Uithof, Moerke, Van Oossanen, Van Oossanen, & Zaaijer, 2014). This depends on ship speed, hull form, location of the foil and size of the foil. This shows that when designed correctly the Hull Vane can significantly decrease the total resistance, although each case needs to be researched individually before placement of the Hull Vane.

The four ways in which the static Hull Vane reduces the resistance are now briefly discussed. The background of the Hull Vane is largely discussed in (Uithof, Moerke, Van Oossanen, Van Oossanen, & Zaaijer, 2014).

1.1.1 THRUST FORCE

A schematic overview of the forces on the Hull Vane and a visualization of the flow can be seen in Figure 1. The flow direction has a vertical component right in front of the foil. As the generated lift on the foil is perpendicular on the flow direction, the lift has a positive horizontal component (Fx_{HV}). As long as this horizontal component is larger than the drag of the foil, there is a positive thrust force. Depending of the ship and foil the drag resistance of the extra wet surface might be dominant for low speeds. The direction of the flow is, for example, dependent on the buttock angle and the transom wave of the ship. For low speeds the transom wave is short and has a larger vertical component. For high speeds the transom wave becomes long and further behind the ship. The vertical component of the flow becomes smaller and the buttock angle relatively more important. A more vertical flow is favorable for thrust generation, but could also increase the pressure resistance of the hull. A wider and constant buttock angle creates a uniform flow over the entire width of the transom, this makes the hull more suitable for a Hull Vane.

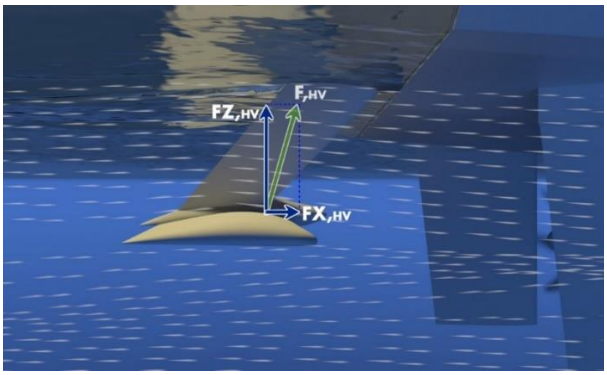

Figure 1: Lift and thrust force on Hull Vane (Bouckaert, Uithof, Moerke, & Van Oossanen, 2016)

1. Hull Vane® is a registered trademark of Van Oossanen & Associates bv

1.1.2 TRIM CORRECTION

The Hull Vane is primarily designed for fast (non-planing) displacement ships (Fn 0.2 – Fn 0.7). These ships generally have the urge to trim backwards (bow up), which tends to have a negative effect on the resistance. The lift force produced by the Hull Vane reduces excessive trim of the ship and thereby reduces the resistance. Because of the thrust component in the lift of the Hull Vane it is more efficient than trim wedges, stern flaps or interceptors. Although these can also lead to a total resistance decrease, they have resistance on their own.

1.1.3 WAVE REDUCTION

The flow over the Hull Vane creates a low pressure region on the top side of the foil. This low pressure region can interact with the high pressure region created by the transom wave. This effectively reduces the wave pattern of the ship. Proper placement ensures that the low pressure region of the Hull Vane will match the high pressure zone of the transom wave. Furthermore the Hull Vane creates a more straight flow which also reduces the wave. This effect can be so significant that it can be observed by the eye. In Figure 2 the wave profile of a 55 meter supply vessel is shown, with and without the Hull Vane at a speed of 13 knots. The wave profile is clearly reduced with the Hull Vane at the right.

Figure 2: Comparison of wave profile on the 55 meter supply vessel without Hull Vane (left) and with Hull Vane (right) at 13 knots, as seen from the aft deck during sea trials (Uithof, Moerke, Van Oossanen, Van Oossanen, & Zaaijer, 2014)

1.1.4 MOTION REDUCTION IN WAVES

The Hull Vane also reduces the ship motions in head waves, as seen in (Uithof, Bouckaert, Van Oossanen, & Moerke, 2016). CFD computations by Van Oossanen Fluid Dynamics for five ships consequently showed reduction in pitch motion, varying from 2.3% to 20.5%. When the vessel is trimmed bow down, the angle of attack of the flow on the Hull Vane is reduced and thereby the lift is reduced. This reduces the ships trim again. A similar thing happens for bow up trim, this increases the lift on the Hull Vane and trims the ship bow down again. The vertical motion of the Hull Vane also changes the relative angle of attack, dampening the pitch motion. The motion reduction has a positive effect on the added wave resistance. For the same five ships the added wave resistance showed a decrease between 4.6% and 39.2%.

1.1.5 LOCATION

A lot of research has been done into the optimal position of the Hull Vane (Uithof, Moerke, Van Oossanen, Van Oossanen, & Zaaijer, 2014). The Hull Vane can achieve resistance reduction in multiple ways (as discussed above), the relative contribution of these effects is affected by the location.

When the focus is on resistance reduction by generating a thrust force, a more vertical flow component is beneficial to the Hull Vane. This leads to a Hull Vane placed underneath the ship and close to the hull. For high speeds, here the flow has the biggest vertical component, which would lead to a larger horizontal component in the lift. However, close to the hull the flow is still dominated by boundary layer effects. This means that the flow speed is significantly lower close to the hull which reduces the generated lift. The high turbulence near the hull also reduces the generated lift of the Hull Vane. If the Hull Vane ® is too close to the hull the Venturi effect will create a low pressure zone on the hull, this increases the resistance of the ship.

If the Hull Vane is placed behind the transom, it will interfere with the transom wave, reducing the wave profile. The optimal placement would be behind the transom close to the free surface, as there is still a big vertical component in the flow. However, the free surface effect, the possibility of slamming and the wake of the boundary layer (reduced flow velocity) requires the Hull Vane to be at a certain depth.

The incoming flow at the Hull Vane is also dependent on the hull shape. Due to these effects the optimal and location of the Hull Vane is different for each ship. But in general the optimal placement is behind the ship with sufficient depth, usually around 1 to 1.5 meter from the free surface.

1.1.6 PREVIOUS RESEARCH

Van Oossanen did extensive research into a combination of the Hull Vane and the 50m patrol vessel AMECRC#13 (dimensions in Appendix A) (Uithof, Hagemeister, Bouckaert, van Oossanen, & Moerke, 2016). Optimal placement was researched, and resulted in a resistance reduction up to 32.4%. The synergy between the Hull Vane and the AMECRC#13 makes it a good candidate for a dynamic Hull Vane. The idea being, that the effect of a dynamic Hull Vane will be clearly visible on a ship that showed good collaboration in previous tests with a static Hull Vane. Furthermore, the design of the AMECRC#13 is publicly available, so any results can be published without constraints to the hull form. Therefore the AMECRC#13 is used in this research for the dynamic Hull Vane.

1.2 THRUST GENERATION WITH OSCILLATING FOIL PRINCIPLE

Since the invention of the diesel engines, people have been using propellers for ship propulsion. But as engineers often get their inspiration from nature, recent research was done in the propulsion by a moving foil like a whale (Mattheijssens J. , Marcel, Bosschaerts, & Lefeber, 2012). The vertical flow on the foil is created by moving the entire foil up and down, while varying the pitch to generate lift, as shown in Figure 3. Like a whale moves her tail in water. The oscillating foil as designed for propulsion purposes showed a high propulsive efficiency (up to 70%) (Schouveiler, Hover, & Triantafyllou, 2005). This lead to the development of the O-Foil concept, an oscillating foil underneath a ship which would provide the propulsion, instead of a conventional propeller. The high efficiency of the oscillating foil used in experiments could not be replicated with an actual ship (Bergsma & Moerke, 2013). The practical constraints of the oscillating foil greatly hinder the efficiency. The imposing of the vertical motion on the foil requires large appendages which create a lot of additional resistance. Any efficiency gained by this propulsion method has to overcome the extra resistance of the appendages.

When a ship is sailing in waves, the relative vertical motion needed for the propulsion generation is already present. With proper movement of the pitch of the Hull Vane the oscillating foil principle could be replicated without the need for extra appendages or power for the heave motion. The heave motion is then dictated by the waves and the pitch will have to be adjusted accordingly. The only appendages needed are those for connecting the Hull Vane to the ship, which are already present. The Hull Vane is already reducing resistance without waves, so the extra resistance of the appendages is already compensated by the Hull Vane. Since no extra power is needed for the vertical motion of the Hull Vane, the power consumption of the system is a lot lower. These effects present a fair chance for a decrease in total power for the dynamic Hull Vane.

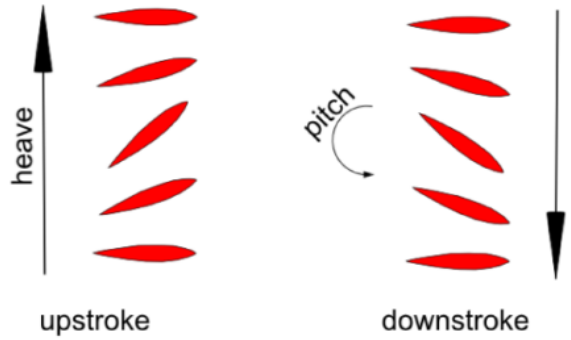

Figure 3: Heaving and pitching motion of a foil, (Mattheijssens J. , Marcel, Bosschaerts, & Lefeber, 2012)

1.3 SIGNIFICANCE

The necessary power of a ship is rarely dictated by its flat water resistance alone. In practice a ship will almost always encounter waves, which can significantly change the actual fuel consumption. A reduction of the fuel consumption is valuable for multiple parties involved with the ship. The most obvious one is the user, who will see a reduction in operational costs. But also when building the ship money could be saved, less required power means a smaller engine, a smaller propeller and smaller fuel tanks. The stricter regulations and the acceptance of climate change as an issue, call for ship owners to lower their fuel consumption and emissions. Therefore, ship owners are always looking for a way to reduce the necessary power of the ship.

Besides the fuel consumption, ship motions have large implications on the operating profile of the ship. The maximum speed of a ship is often limited by the behavior of the ship in waves. For workboats and ferries there are strict regulations for the maximum allowable accelerations and the owners of superyachts are always looking for ways to have a more comfortable trip. The relative motion of the ship to the waves is also of influence on the added wave resistance (Blok, 1993), so the reduction of ship motions could again lead to a reduction of total resistance.

The motion reducing and thrust generating capabilities of the Hull Vane lead to the question if this could be further improved by active control of the pitch of the Hull Vane. A proper control scheme could focus on the reduction of the ship motions, active thrust generation or a combination of both. This research will show if a dynamic Hull Vane has the capability to further reduce the ship motions and/or resistance.

For this initial research phase only the hydrodynamic and control issues of the dynamic Hull Vane are discussed. This includes different methods of controlling the Hull Vane. But does not include the structural implication of altering the pitch of the Hull Vane. This research will show the possibilities of a dynamic Hull Vane, while the practical limitations will not be investigated. For now a construction similar to the static Hull Vane is assumed.

1.4 PROBLEM DEFINITION

With the introduction of the project, the main research question and sub questions of the thesis can be introduced. The main research question will be:

Can a dynamic version of the Hull Vane on the AMECRC#13 reduce the ship motions in head waves, and/or reduce the total resistance by generating thrust using the vertical motion of the stern?

This question splits the research in two distinct directions. The first goal is the reduction of the ship motions in head waves. While the second part aims directly at reducing the total resistance by actively using the Hull Vane to generate thrust. For both cases the relevant parameters are the ship motion and the resistance, in comparison to a static Hull Vane and the bare hull.

For the first part the goal is to reduce the ship motions, while the second part focuses on the reduction of the total resistance. In practice a captain would probably want a combination of these two. But what combination is the optimum, is highly dependent of the ship, operating profile and crew. Therefore the research of this thesis is not focused on finding the best combination, this is more a design question and an optimum could be found based on the two limits. The goal of this research is to find the best possible motion reduction or resistance reduction with two different control algorithms. A possible practical combination of these two might be found.

A couple of topics will influence the answer to this question, which will need to be researched before the main question can be answered. The optimal movement an oscillating foil makes will be studied. Based on this the algorithm will be developed that is generating thrust by using the vertical motion of the stern. The pitching movement of the foil will need to match the vertical movement of the Hull Vane based on optimal Strouhal numbers found in the research. This is also dependent of the angle of attack of the flow on the Hull Vane in waves. The change of this needs to be studied to derive a control scheme that is making use of this effect. Lastly the characteristic of the NACA4412 profile are studied. The lift and drag coefficients are calculated and measured for a range in angle of attack. The thrust in combination with the AMERCR#13 is measured. This resulted in the following sub questions. These questions will be investigated in the literature review or during the research phase.

- What movement should an oscillating foil make to efficiently develop propulsion
- What is the angle of attack of the flow on the Hull Vane and how does it change in waves
- What are the operating characteristics of the Hull Vane in combination with the AMECRC#13

1.5 PROJECT SET-UP

The project will start with literature research to answer the sub questions. Previous research will show the working conditions of the oscillating foil, and how this relates to the dynamic Hull Vane. Then the flow around the dynamic Hull Vane will be investigated by using CFD. This will give insight in the effects that influence the change in flow on the Hull Vane. More literature review will show the working conditions of the Hull Vane, from possible lift to maximum thrust.

For the CFD Van Oossanen uses the commercial software FINE™/Marine, which is developed by NUMECA. A large part of setting up the computations has been automated by Van Oossanen, based on the best practices of NUMECA and the experience of Van Oossanen. Most of these settings will be used for this research, as they proved to be accurate enough for the research done at Van Oossanen. In this report the settings and reasoning will be explained, a grid refinement study will be done to show the accuracy of the settings.

FINE™/Marine contains the unstructured mesh generator HEXPRESS. This will be used to generate the mesh for the ship. Automation scripts are already developed by Van Oossanen to make the meshing consistent. The mesh will be shown in this report to discuss the quality. On the Hull Vane an overset grid will be used for the rotation.

Unsteady RANSE simulations are very computational intensive, this could limit the amount of runs to be used in the research. An Euler flow code would significantly reduce computation times and could still provide valuable insights during the initial phase of the research. However the Euler flow does not include viscosity and this will influence the result. Therefore a test is done, to see if the use of an Euler solver is viable. If the Euler solver provides valuable results, it can be used to test a variety of different algorithms and waves.

1.6 STRUCTURE

This report will describe the literature research to answer the sub questions. Then the method will be explained, including the grid refinement study. Finally several candidates for the algorithm will be described and tested in different conditions. The report ends with a conclusion and some recommendations for further research.

2. LITERATURE REVIEW

This section describes the relevant literature and research for this report, according to the sub questions. The working principles of the oscillating foil are discussed, the variation in flow direction behind the ship and the operating conditions of the foil. Each paragraph ends with the relevant conclusions for the dynamic Hull Vane and this chapter ends with an overview.

2.1 OSCILLATING FOIL PROPULSION

Nature has been a great source of inspiration for many engineers. In marine technology tails of fish as a form of propulsion have been of interest like bird wings for aviation. A lot of research has been done in the use of a foil to generate thrust (Xiao & Liao, 2010) (Schouveiler, Hover, & Triantafyllou, 2005) (Read, Hover, & Triantafyllou, 2002) (Bergsma & Moerke, 2013). The topic of this research varies from numerical simulations on finding the optimal angle of attack variation, experiments with a model scale oscillating foil, to CFD calculations for a full scale vessel propelled by an oscillating foil. An important variable for this research is how the angle of pitch of the Hull Vane needs to change to get the most thrust. The heave motion of the dynamic Hull Vane cannot be controlled, so the control of the pitch should match the heave motion of the aft. In this section the influence of the Strouhal number, phase angle, pitch bias, trajectory and finally the relevance to the dynamic Hull Vane is discussed. But first a small introduction of the mechanics of the oscillating foil.

2.1.1 BASIC SETUP

The oscillating foil uses a combined pitching and heaving motion to generate a thrust force, with a trajectory as shown in Figure 3. The heave (*h*) and pitch(θ) is described by the following two equations.

$$\boldsymbol{h(t) = h_0 sin(\omega t)} \quad \textbf{(1)}$$

$$\boldsymbol{\theta(t) = \theta_0 \sin(\omega t + \psi)} \quad \textbf{(2)}$$

The phase angle (ψ) is usually 90°, such that the highest pitch angle occurs at the highest vertical speed, and no pitch angle occurs at the top and bottom. The angle of attack of the foil is then given by the following equation.

$$\boldsymbol{\alpha(t) = -arctan\left(\frac{\dot{h}(t)}{U_{inf}}\right) + \theta(t)} \quad \textbf{(3)}$$

In which the free flow velocity is given by: U_{inf} and for constant heave and pitch amplitude the nominal angle of attack is given by: $\alpha_0 = -arctan\left(\frac{\omega h_0}{U_{inf}}\right) + \theta_0$

A dimensionless ratio for the speed of the stroke compared to the free stream velocity is given by the Strouhal number, as shown in equation (4). In which *f* is the frequency of the oscillation in Hz and *A* is the characteristic width of the wake, (approximated by $A = 2h_0$).

$$\boldsymbol{St = \frac{fA}{U_{inf}}} \quad \textbf{(4)}$$

An approximation for the maximum pitch angle of the foil can now be given based on the maximum angle of attack. This approximation is valid for low Strouhal numbers where the arctan(x) is nearly linear.

$$\boldsymbol{\theta_0 = \pi St + \alpha_{max}} \quad \textbf{(5)}$$

The force on the foil is measured and averaged over multiple periods as seen in equation (6), and the average power is calculated by equation (**7**).

$$\overline{F_x} = \frac{1}{T}\int_0^T F_x(t)dt \text{ for } T \gg {}^{2\pi}/_{\omega} \quad (6)$$

$$\overline{P} = \frac{1}{T}\left(\int_0^T F_y(t)\dot{h}(t)dt + \int_0^T Q(t)\dot{\theta}(t)dt\right) \quad (7)$$

The force and power data is reduced to coefficient form, resulting in the following equations. In which the area of the foil is calculated with the chord (c) and the span (s).

$$C_T = \frac{\overline{F_x}}{{}^1/_2\,\rho U^2 cs} \quad (8)$$

$$C_P = \frac{\overline{P}}{{}^1/_2\,\rho csU^3} \quad (9)$$

The propulsive efficiency of the oscillating foil can then be easily computed with: $\eta = \frac{C_T}{C_P}$

2.1.2 STROUHAL NUMBER INFLUENCE

Mostresearch to date measures or calculates the thrust coefficient for different Strouhal numbers. The goal of the research is to generate a positive thrust on the foil in an undisturbed flow. The Strouhal number thereby links the possibility of thrust generation (the oscillating frequency and wake) to the viscous resistance (free stream velocity). It also influences the direction of the lift, as this is defined as orthogonal to the undisturbed incoming flow. A relative high oscillating frequency with sufficient heave amplitude in relation to the free stream velocity, yields a relative long trajectory for the thrust generation and a positive thrust. This relation has been extensively researched by experiments and numerical simulations. An exhaustive research was done by D. A. Read, in “Oscillating Foils for Propulsion and Maneuvering of Ships and Underwater Vehicles” (Douglas Andrew Read & Triantafyllou, 2001) In these experiments a NACA 0012 foil was towed in the towing tank of the MIT Department of Ocean Engineering. Various combinations of oscillating frequency towing speed an angle of attack were tested, and the resulting forces on the foil were measured. This master thesis later led to a publication in the Journal of Fluids and Structures (D. A. Read, Hover, & Triantafyllou, 2002). Part of their results will be discussed here.

A harmonic motion for the heave and pitch was imposed as described in equation (1) and (2), where θ_0 is calculated with the maximum angle of attack as in equation (5). The thrust and efficiency coefficient are calculated as in equation (8) and (9). The thrust and efficiency contours are shown in Figure 4 and Figure 5. The largest thrust coefficients are obtained for the higher Strouhal numbers with large angle of attack variations, while the highest propulsive efficiency can be found at moderate angle of attack for a range of Strouhal numbers. In these figures the experiments were done with a heave/chord ratio of 1, similar results were obtained with a heave/chord ratio of 0.75.

For low Strouhal numbers a negative thrust coefficient was measured, this implies that the drag on the foil was bigger than the generated thrust. The highest thrust coefficient does not coincide with the highest efficiency coefficient. This in line with the highest lift coefficient of a foil profile not coinciding with the highest lift/drag ratio.

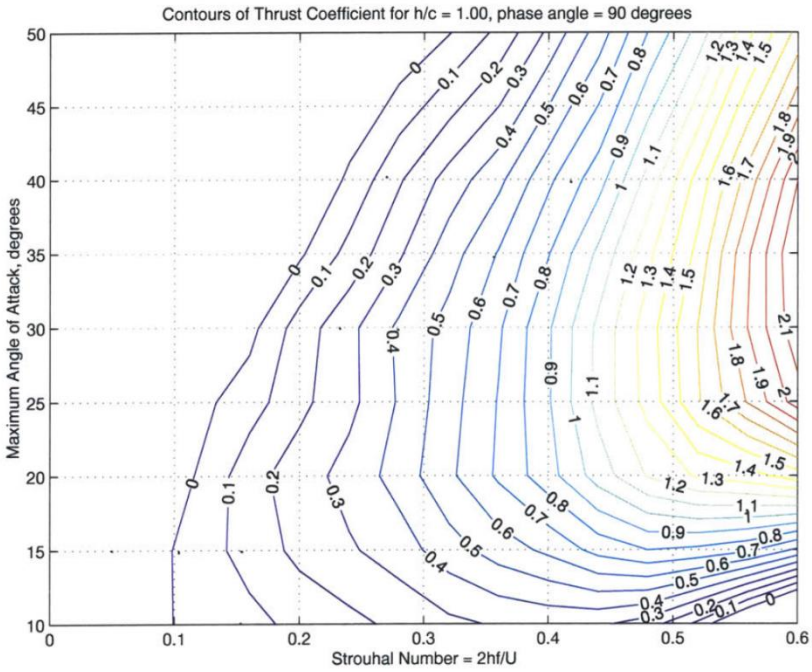

Figure 4: Thrust coefficient contours (Read & Trantafyllou, 2001)

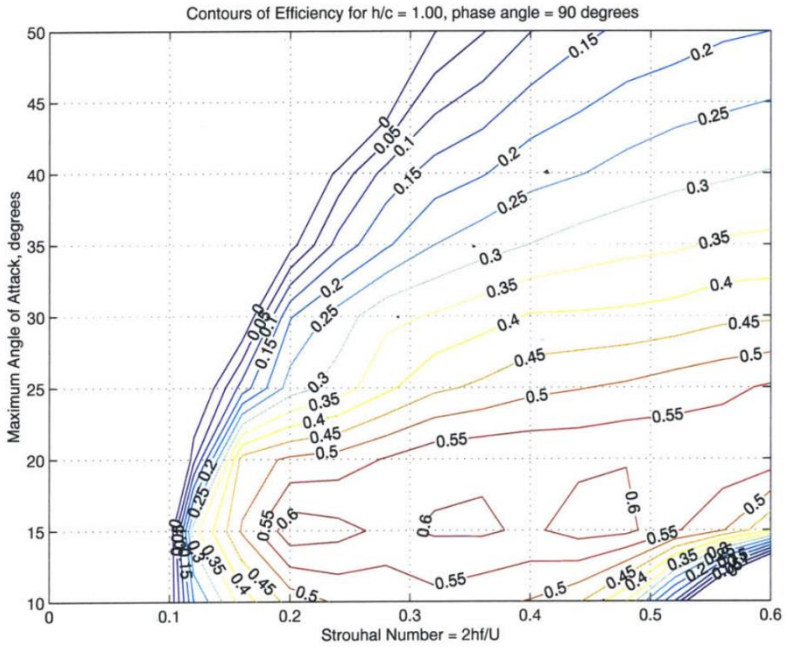

Figure 5: Efficiency Contours (Read & Trantafyllou, 2001)

2.1.3 PHASE ANGLE VARIATION

A logical starting point for the phase angle (ψ) is 90°, when the pitch of the foil is zero at the top and bottom of the heave motion (where the flow is horizontal) and maximum at the zero crossing of the heave motion (where the flow has the largest relative vertical component). Numerical simulations with a 10° lead or lag have been done by Q. Xiao and W. Liao (Xiao & Liao, 2010). The numerical simulations are done with a RANSE code on a 2D NACA0012 foil. In Figure 6 the effect of three different phase angles on the mean thrust coefficient is shown. It shows that for higher Strouhal numbers the thrust rapidly becomes negative, caused by the mismatch of the pitch angle to the heave. In Figure 7 the influence on the propulsive efficiency is shown. As the thrust coefficient becomes negative, this quickly changes the sign of the propulsive efficiency. Besides a small increases in efficiency at low Strouhal numbers, it has a negative effect overall.

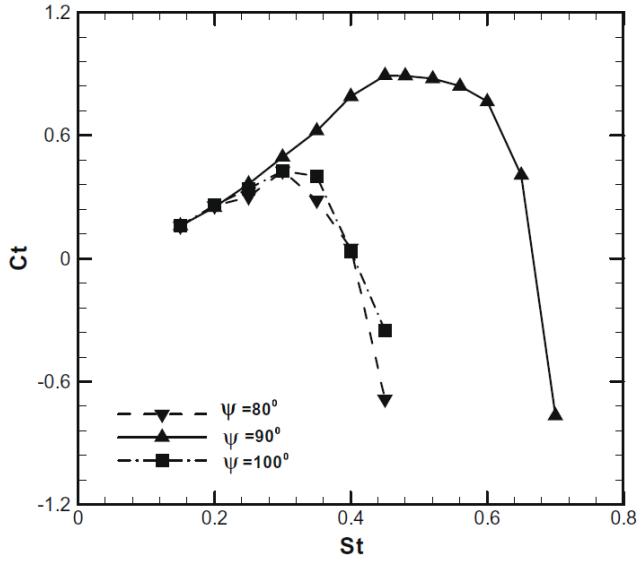

Figure 6: Effect of phase angle on mean thrust coefficient, for $\alpha_{max} = 15°$ and $h_0 = 1$ (Xiao & Liao, 2010)

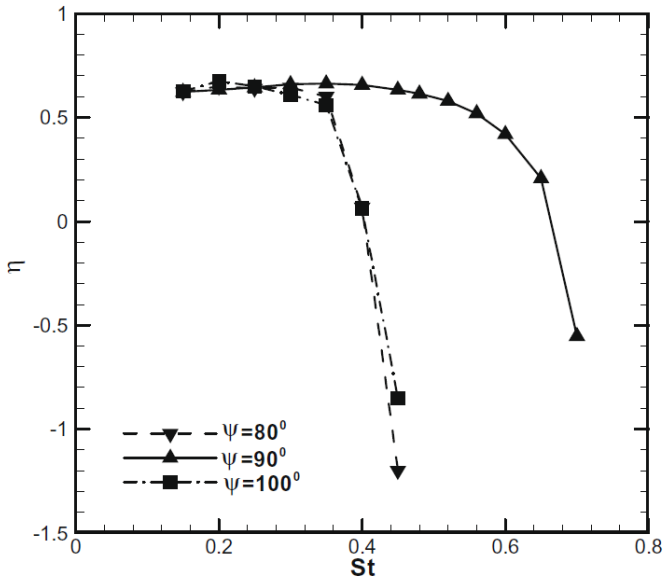

Figure 7: Effect of phase angle on propulsion efficiency, for $\alpha_{max} = 15°$ and $h_0 = 1$ (Xiao & Liao, 2010)

2.1.4 INFLUENCE OF PITCH BIAS

The lift generated on the foil consists mainly of a vertical component, as the flow is mostly horizontal. Only a part will produce thrust in the horizontal direction. But since it is an harmonic process, the mean force in vertical direction is zero. This can be made non-zero by offsetting the average pitch angle of the foil, thereby increasing the lift on one stroke and decreasing it in the other direction. The mean of the lift will now be non-zero. Again referring to the work done by A. D. Read, the large instantaneous lift forces could easily be turned in mean lift forces by simply adding a bias to the pitch (Read & Trantafyllou, 2001). It was observed that adding a bias to the pitch always decreases the thrust coefficient. In Figure 8 the mean thrust coefficient is shown for several pitch bias angles. The figure shows that the thrust coefficient decreases with bias angle. In Figure 9 the instantaneous and mean lift coefficients are shown, even without a pitch bias high lift coefficients are observed. The mean lift coefficient is increasing with pitch bias.

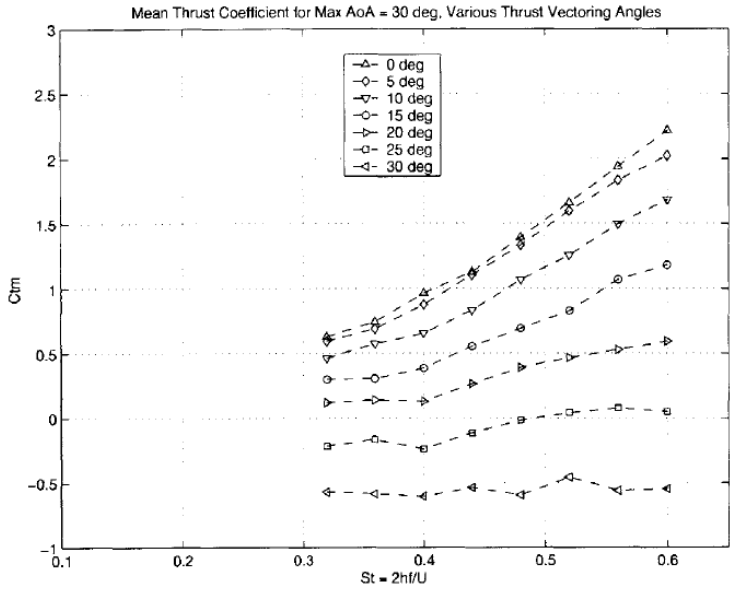

Figure 8: Mean thrust for various pitch bias angles (Read & Trantafyllou, 2001)

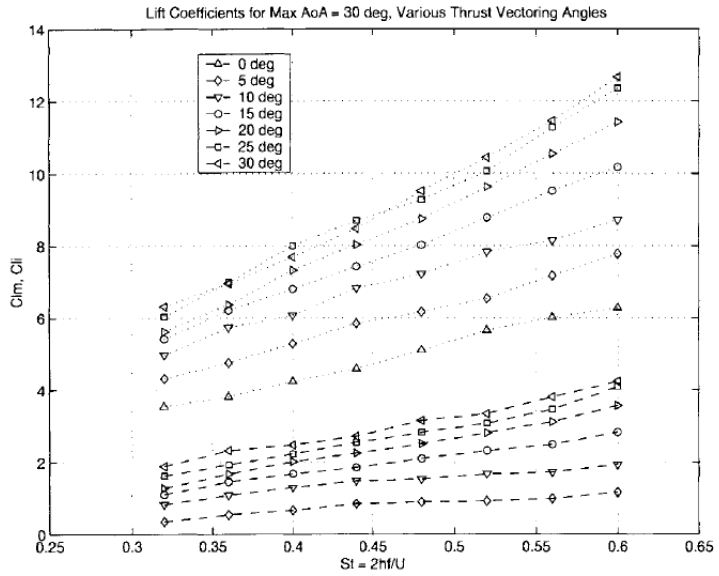

Figure 9: Mean and instantaneous lift coefficient (Read & Trantafyllou, 2001)

2.1.5 DIFFERENT TRAJECTORIES

For every foil profile there is an “optimal” angle of attack, depending on the use of the foil. An oscillating foil would be most efficient if it can keep this angle of attack during the entire stroke. Therefore a square heave motion is proposed and tested by J.A. Esfahani, E. Barati, H. R. Karbasian in (Esfahani, Barati, & Karbasian, 2013). In their research they simulated the foil with a hydrodynamic model based on an aerodynamic model for a flapping wing flight (Delaurier, 1993). A square heave profile would have a constant speed during the up and down stroke as much as possible. The angle of attack would then be almost constant along the strokes, thereby maximizing the amount of lift per stroke. However, a fully square profile would need infinite acceleration at the top and bottom, which is a problem for the control. Nonetheless the results of this new trajectory are interesting. A combination of a square and a cosine motion could be developed to further investigate the possibilities of the optimum angle of attack. In Figure 10 the results of the hydrodynamic model are shown. According to this research a fully square angle of attack profile could have almost doubled the thrust coefficient of the harmonic oscillation. A critical note has to be added to this research, as the mathematical model does not address the effects of the rapid change in direction of the foil. The model was validated for the harmonic motion, but the effects of the rapid change of direction are unclear. The generation of vortices during the quick redirection could considerably reduce the performance.

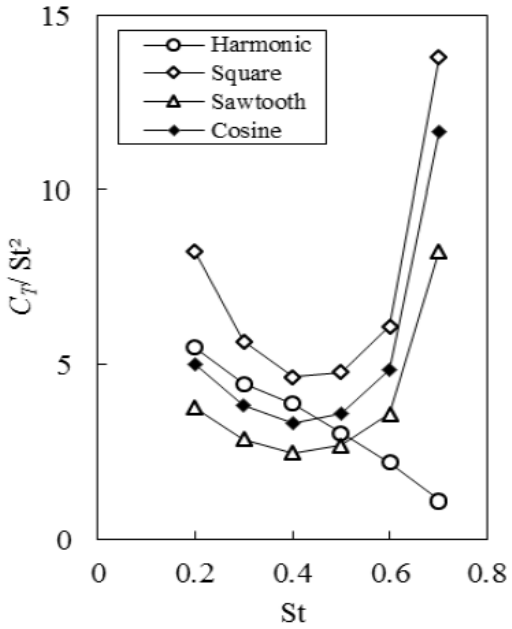

Figure 10: Comparison of different heave trajectories (Esfahani, Barati, & Karbasian, 2013)

A different approach to modifying the angle of attack during the strokes was presented by Q. Xiao and W. Liao (Xiao & Liao, 2010). For higher Strouhal numbers the angle of attack during the stroke becomes a higher order harmonic. In Figure 11 the effective angle of attack variation is shown during a stroke, for multiple Strouhal numbers. The large variation of angle of attack causes the very quick. degradation of thrust coefficient at high Strouhal numbers. Q. Xiao and W. Liao propose to change the heave and pitch motion to have better control over the angle of attack for high Strouhal numbers. In Figure 11 and Figure 12 the two modified motions and the result on the angle of attack are shown. In their research the better control over the angle attack greatly increases the thrust coefficient for high Strouhal numbers.

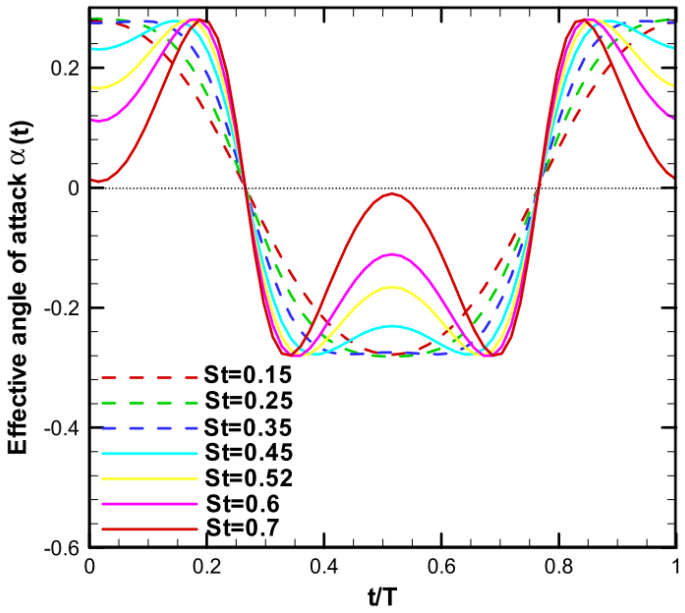

Figure 11: Angle of attack variation during stroke (Xiao & Liao, 2010)

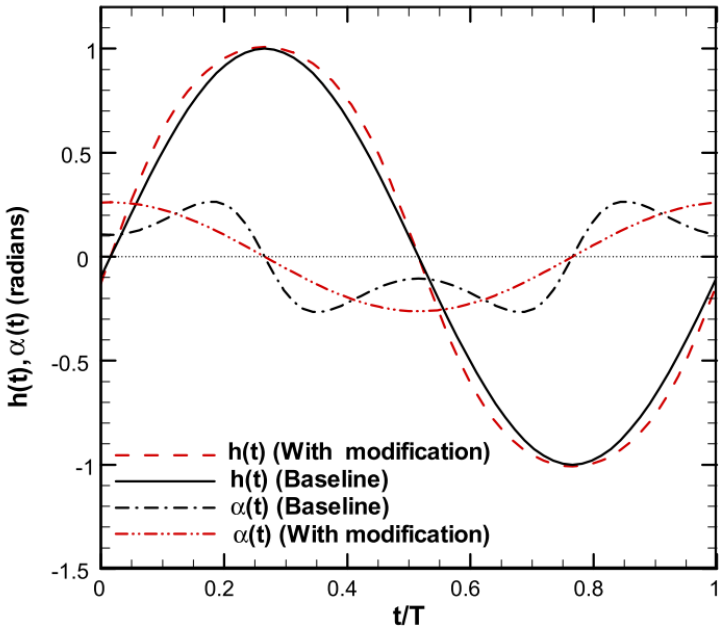

Figure 12: Angle of attack with modified heave motion, $h_0 = 1.0, \psi = 90, \alpha_{max} = 15°, St = 0.65$, (Xiao & Liao, 2010)

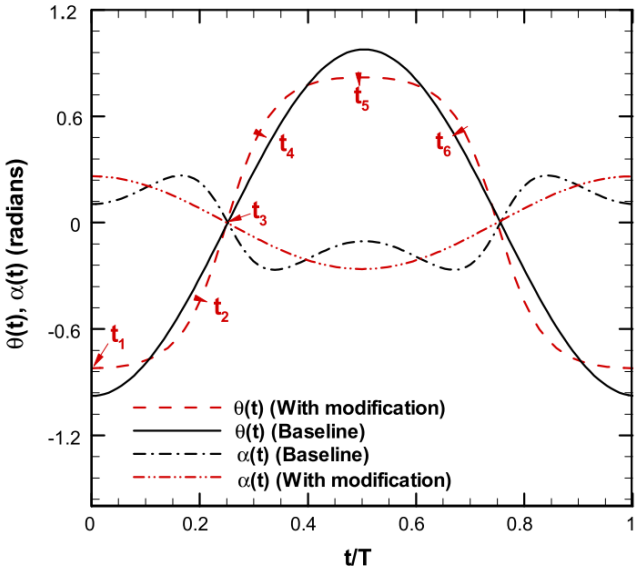

Figure 13: angle of attack with modified pitch motion, $h_0 = 1.0, \psi = 90, \alpha_{max} = 15°, St = 0.65$, (Xiao & Liao, 2010)

2.1.6 RELEVANCE TO THE DYNAMIC HULL VANE

The goal of this literature review is to understand the working principle of the oscillating foil, as this will help develop the dynamic Hull Vane. Therefore the effect of each component will now be discussed for the dynamic Hull Vane.

The basic setup of the dynamic Hull Vane is different form the oscillating foil. The principles of the oscillating foil cannot be directly used for the dynamic Hull Vane, this has positive and negative effects. The dynamic Hull Vane will simulate an oscillating foil, although the heave motion will not be controlled. Furthermore the flow field on the dynamic Hull Vane will be an oblique non-uniform flow field. This makes it more difficult to find a proper control algorithm for the dynamic Hull Vane. However the overall consumed power by the system will decrease significantly, because no power is needed for the heave motion of the foil. According to the discussed experiments the power for the heave motion was around 80% of the total required power (Read & Trantafyllou, 2001). The angle of attack variation will also be different for the Hull Vane as the oblique inflow will create a bias.

The Strouhal number at which the oscillating foil will operate, is dictated by the speed of the ship and the wave encounter frequency. For a fixed heave motion with 1 meter amplitude the Strouhal numbers are shown in Table 1. The vertical motion of the Hull Vane is dependent on the encounter frequency of the wave, but later results (Figure 36) showed this is gives a good indication. The Strouhal number is dependent on the encounter frequency, free-stream velocity and vertical motion. The heave amplitude will also change with wave encounter frequency, as the response of the ship is dependent on the frequency, but for the Strouhal numbers in Table 1 the heave amplitude is fixed to 1. Fixing the heave amplitude simplifies the calculation of the Strouhal number. In general the Strouhal number will be relatively low. In short waves it might be around 0.2, and in long waves it might be around 0.05. These are not absolute values (since the ship motion is fixed), but give an indication of the range.

Table 1: Overview of Strouhal numbers against wave encounter frequency and ship speed, for vertical motion of Hull Vane of 1 meter amplitude on a 50 meter ship

Strouhal	1.25 [rad/s]	1.5 [rad/s]	1.75 [rad/s]	2 [rad/s]	2.25 [rad/s]
Fn 0.2	0.090	0.108	0.126	0.144	0.162
Fn 0.4	0.045	0.054	0.063	0.072	0.081
Fn 0.6	0.030	0.036	0.042	0.048	0.054

At this low Strouhal number the viscous resistance will be relatively large, and according to Figure 4 the thrust coefficient will hardly be positive. This might be a problem for the dynamic Hull Vane and could ask for a different control algorithm.

The phase angle variation showed a small increase of the efficiency at low Strouhal numbers, but the influence on the thrust coefficient was negligible. The increase of the efficiency was primarily caused by the reduction of the power coefficient. The dynamic Hull Vane will operate primarily at low Strouhal numbers, but the power coefficient will already be a lot lower. Therefore the positive effect of the phase angle variation is not significant. However it is promising that a different phase angle will not diminish the thrust coefficient. As for the dynamic Hull Vane the heave motion is not controlled, it will be hard to match the pitch motion perfectly. A delay of 10° degrees phase angle or more could be a realistic situation in practice. The research showed this will not be catastrophic for the thrust.

The oblique inflow onto the dynamic Hull Vane can also be seen as a pitch bias on the oscillating foil, the only difference is the direction and definition of the thrust. In all abovementioned research the thrust is defined as the horizontal force, and the pitch bias as an offset of the pitch of the foil to the horizontal axis, while the inflow is still horizontal. For the dynamic Hull Vane with an oblique inflow, the thrust force is in horizontal direction, while the inflow has an angle to the horizontal axis. For the oblique flow, the thrust force will be larger on the down stroke, when the flow is more vertical and therefore the lift force more horizontal. On the up stroke, when the flow is more horizontal and the lift more vertical, resulting in a lower thrust force compared to the experiments with pitch bias. The average thrust over the entire stroke will be the same for the dynamic Hull Vane and the oscillating foil, but in a different direction. The research showed that adding a pitch bias will always reduce the thrust coefficient for the oscillating foil, but it also showed the development of a mean lift. For the static Hull Vane this has shown to reduce the trim of the vessel at high speed and thereby also reducing the resistance. The mean lift force is therefore an important characteristic for reducing the total resistance. Due to the offset of the flow to the horizontal axis, the mean lift on the oscillating foil results in a mean thrust force on the Hull Vane. The angle of attack of the oblique flow will show the pitch bias and could show what effect is dominant: the generation of thrust trough the vertical movement or the part of the lift in the horizontal direction. The low Strouhal number suggests that the thrust generated by the vertical movement is low compared to the viscous resistance.

The different trajectories showed potential for generating higher thrust and efficiency coefficients, by using two methods. Unfortunately the modifying of the heave motion is impossible and the altering of the pitch motion is only useful at higher Strouhal numbers (St>0.35). Altering the trajectory will therefore not benefit the dynamic Hull Vane. The normal cosine trajectory of the pitch will be most suitable for the dynamic Hull Vane.

In summary a few things can be noted.

- The dynamic Hull Vane will operate at a very low Strouhal number (0.05 - 0.20).
- The normal oscillating foil could have some problems with generating a positive thrust, so a different control scheme may be useful.

- Phase angle variation will not lead to any significant gains, but will also not really hinder the efficiency.

- The oblique flow on the dynamic Hull Vane can be compared to a pitch angle bias, this will produce lift but will also limit the amount of thrust. The oblique flow means that lift will also have a thrust component. This is dependent on the angle of attack of the flow, how large the angle of attack is will show the relative importance of this effect.

- Modifications to the pitch trajectory will not be of any benefit for the dynamic Hull Vane.

2.2 ANGLE OF ATTACK ON HULL VANE

As the ship moves, the angle of attack of the flow onto the Hull Vane changes. This is caused by multiple aspects, whereas the angle of attack of the oscillating foil is only changed by vertical movement. The goal of the dynamic Hull Vane is to have better control over the lift, which can only be done by controlling the pitch of the Hull Vane. In this paragraph the mechanism behind the changing of the angle of attack of the flow is studied. The influence of the water movement, pitch and heave velocity are compared. When the change of the angle of attack of the flow is understood, the control of the dynamic Hull Vane can be based on this. The study is done using CFD and probing the flow and the ship motions in 1 meter waves for the AMECRC#13 without a Hull Vane. The measurements are done at y=1 meter. The flow varies over the span of the Hull Vane, this was chosen as a representative average.

2.2.1 WAVE THEORY

Even without the movement of the ship, the waves already introduce a horizontal and vertical velocity. For deep water a good approximation of the velocity is given by linear wave theory. The horizontal velocity is given by equation (10) and the vertical velocity is given by equation (11). The maximum amplitude of both velocities is at the free surface and is equal to the wave amplitude. As the Hull Vane is at relatively low depth (~1m), the maximum velocity is used as representative for the velocity on the Hull Vane. In practice this might be between 10% to 20% less.

$$\boldsymbol{u_x(x,z,t) = a * e^{k*z} * cos(k * x - \omega * t)} \quad \textbf{(10)}$$

$$\boldsymbol{u_z(x,z,t) = a * e^{k*z} * sin(k * x - \omega * t)} \quad \textbf{(11)}$$

The maximum vertical velocity is now only dependent on the wave amplitude. For a 1 meter wave and a free stream velocity comparable to the ship sailing at Froude 0.4, the change of flow direction is shown in Figure 14. This is the effect of the undisturbed wave velocity at the flow direction at the aft of the ship. In reality the wave is disturbed here by the presence of the hull, but the figure shows the magnitude of this effect. It can be observed that in these conditions the relative flow can change about ±3 degrees.

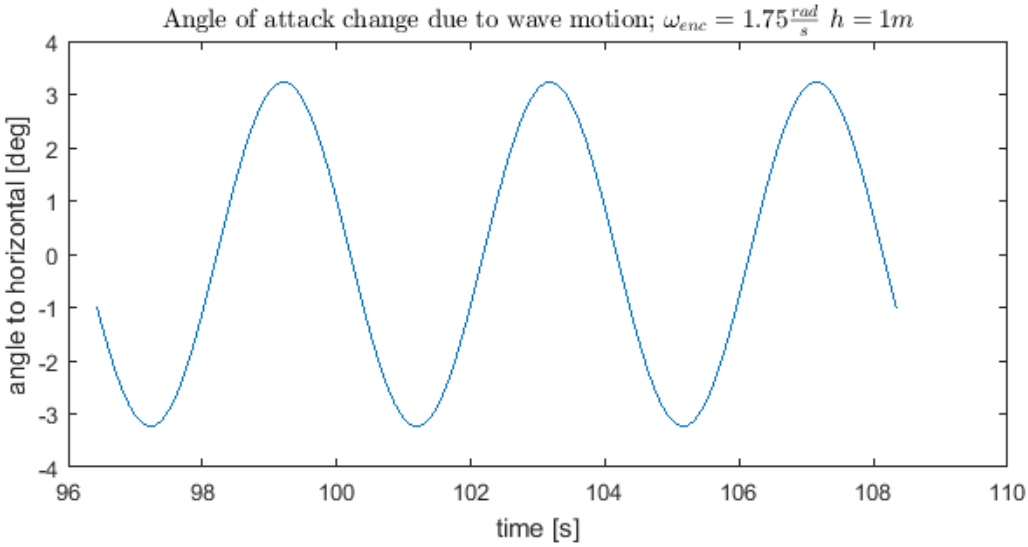

Figure 14: Chance of flow direction due to undisturbed wave, $U_{inf} = 8.59\ \frac{m}{s}$

2.2.2 PITCH

When the Hull Vane is fixed to the ship, its angle of attack changes with the pitch of the ship. This is also an effect that could be compensated by the dynamic Hull Vane. This can be a significant effect, as typical pitch angles for a ship in 1 meter waves on its natural pitch frequency can be an amplitude of multiple degrees. For the AMECRC#13 the pitch was found to oscillate between +2 and -3.5 degrees, for one meter waves with an encounter frequency close to the natural pitch frequency. An example of this is shown in Figure 15. A direct change of 5 degrees of angle of attack can be found, which can have a significant effect on the lift and drag coefficient.

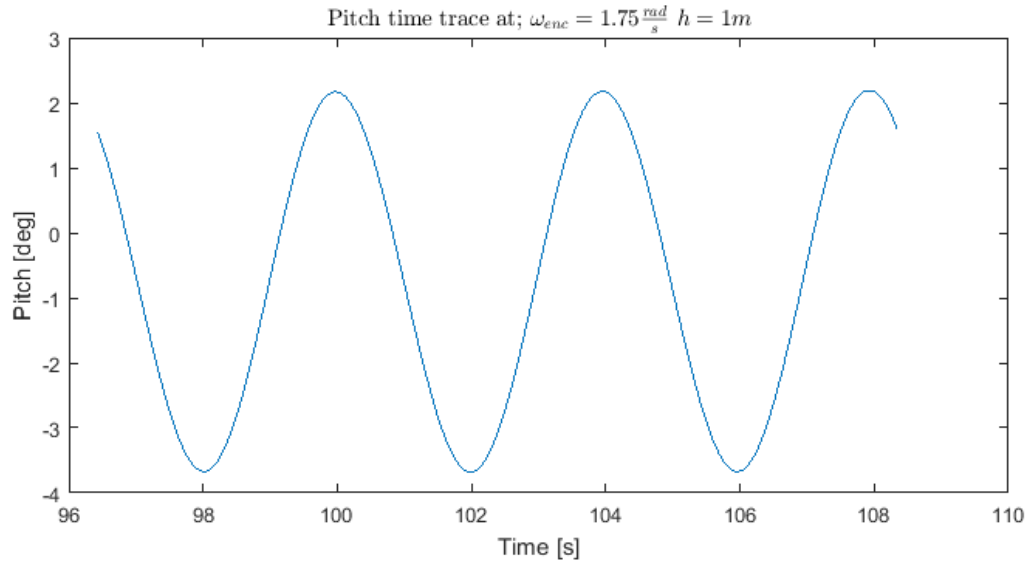

Figure 15: Typical pitch time trace, for Fn = 0.40

2.2.3 HEAVE VELOCITY

The vertical movement of the aft ship will cause a change in angle of attack, which is the driving mechanism for the oscillating foil principle. With the use of CFD the heave velocity and the pitch velocity is measured around the natural pitch frequency of the ship in 1 meter waves. The combined heave velocity of the aft ship is shown in Figure 16, the combined heave velocity is calculated by: $\dot{z_{HV}} = \dot{z_{cog}} - L_{cog_{HV}} * \sin(\dot{\theta})$. In which L_{cog_HV} is the distance from the center of gravity to the Hull Vane (which is negative).

Figure 16 also shows the heave velocity caused by the two combined motions. As observed, the phase difference causes a significant part of the combined motion to be cancelled out. The largest part of the heave motion at the aft is caused by the pitching motion at this frequency. It needs to be noted that the phase shift between the two motions will change with different wave encounter frequencies. Therefore this experiment is repeated for a wave encounter frequency of 1.25 rad/s and 2.25 rad/s. At these frequencies a small shift of the systems was observed, but the heaving of the Hull Vane still had the largest influence on the velocity.

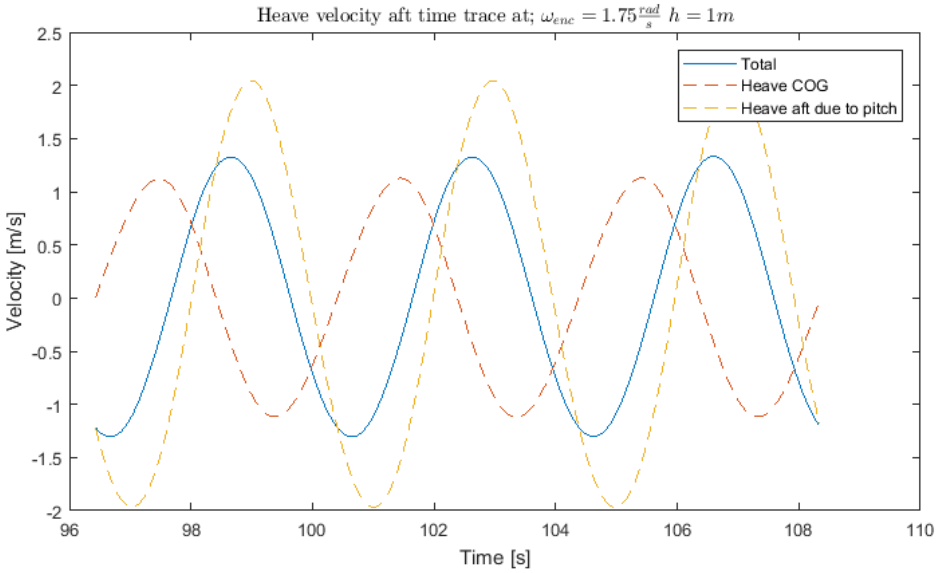

Figure 16: Comparison of heave velocity at aft, for Fn = 0.40

Due to the vertical velocity of the aft, the relative direction of the flow to the aft changes. The amount of change of the flow direction of a Hull Vane moving in a free flow is shown in Figure 17. As seen, the heave velocity of the Hull Vane would have the biggest influence on the angle of attack so far.

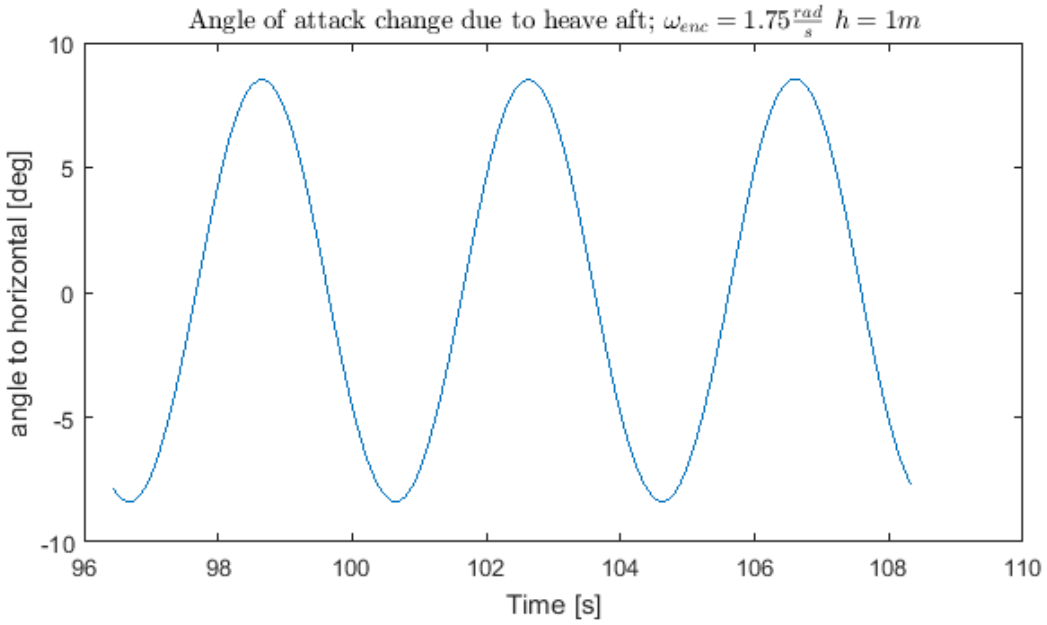

Figure 17: Change of angle of attack due to heave of aft ship, for Fn = 0.40

2.2.4 TOTAL CHANGE IN ANGLE OF ATTACK

The combined change in angle of attack on the Hull Vane consists of the previous three systems: vertical water movement due to waves, changing of the pitch of the ship and vertical velocity of the aft. In this section the relative importance of those systems is discussed. In Figure 18 the total change in flow direction relative to the ship coordinate system and relative to the earth fixed coordinate system is displayed. This is measured for a ship without Hull Vane at the position where the leading edge of the Hull Vane would be. In practice a ship with a Hull Vane would have less pitch and heave motions, resulting in a lower change in angle of attack, but this does give a good indication of the undisturbed flow. Interestingly the motion of the ship actually dampens the change in angle of the flow, so due to the movement of the ship the Hull Vane will experience a smaller change in angle of attack.

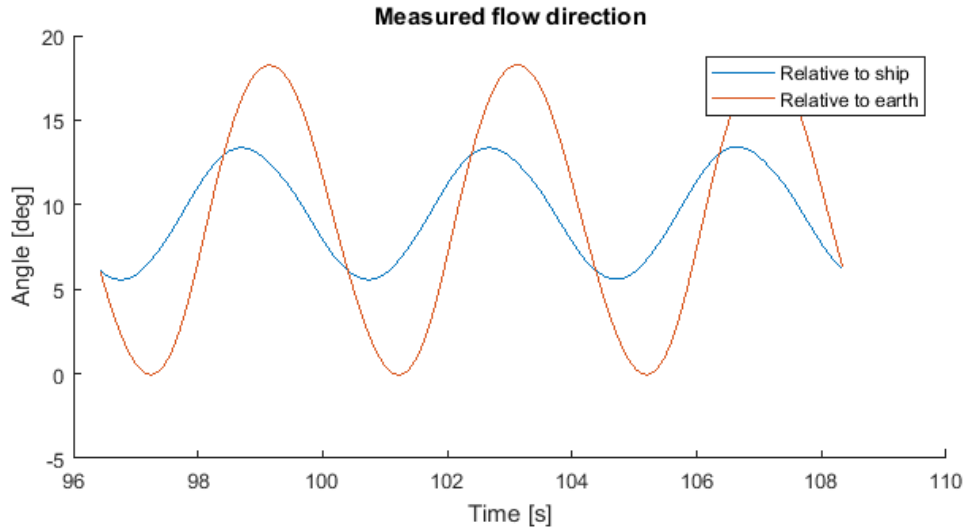

Figure 18: Flow direction relative to ship coordinate system and earth fixed coordinate system

The previous sections showed the contribution of each system to the changing of the angle of attack. We can now look at the total flow direction, but also at the contribution of each system. In Figure 19 the total measured flow direction and the separate components as discussed above are shown. Again

in the angle of attack is to the ship bound coordinate system, so it is the actual angle of attack on the static Hull Vane. Figure 19 shows that the vertical velocity of the aft has the largest amplitude and the largest influence on the flow direction. As seen in section 2.2.3 the vertical velocity is mainly caused by the pitching velocity. But the angle of attack change caused by the vertical velocity and caused by the direct pitch change are out of phase. The angle of attack change caused by the aft vertical velocity has changed phase because of the heave motion of the center of gravity. The two ways in which the pitching motion causes a change in angle of attack damp each other out. It is unsure in what way these effects will behave at different frequencies and wave lengths. The phase difference between the effects may change at different wave lengths, also the magnitude of the systems may change at different encounter frequencies. Therefore the same investigation was done for an encounter frequency of $\omega_{enc} = 1.25\,{}^{rad}/_{s}$ and for $\omega_{enc} = 2.25\,{}^{rad}/_{s}$, similar effects as for $\omega_{enc} = 1.75\,{}^{rad}/_{s}$ were found. Although the amplitude of the effects changed considerably, the main angle of attack change was still caused by the wave motion and heave motion of the aft caused by pitching velocity. This study must not be used as a definitive investigation into the relative contributions to the change of flow direction, but can be seen as an investigation of the effects that play a role and how they might work together.

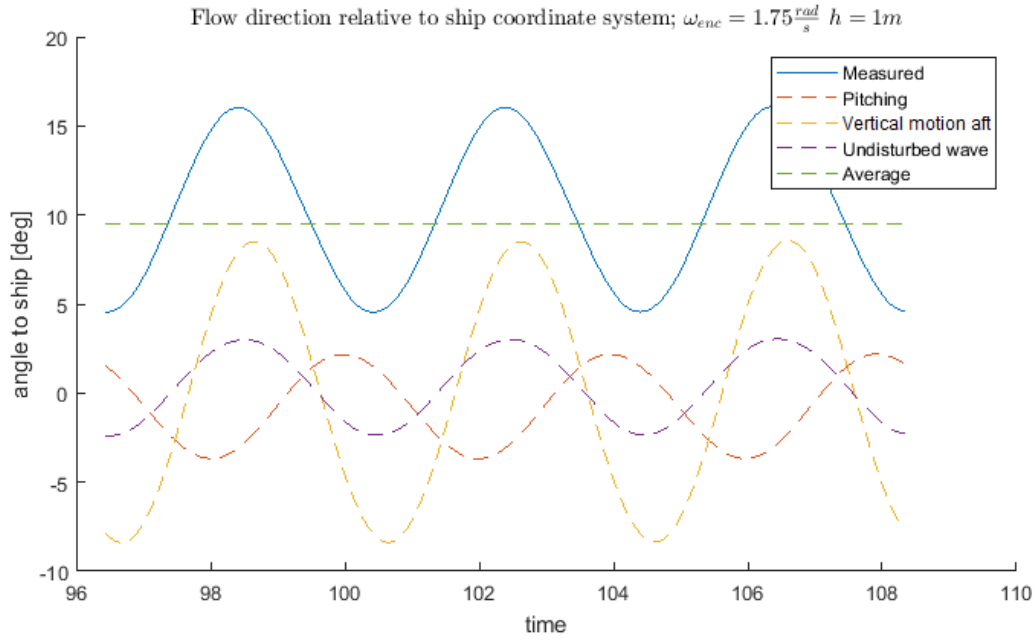

Figure 19: contribution of each system to the changing angle of attack

2.3 FOIL PROFILE CHARACTERISTIC

The foil profile will determine at what angle optimum lift coefficients or lift/drag ratios are obtained. Therefore it is important to match the profile with the operating conditions. This research does not provide a full investigation of all the different profiles, instead a proven combination of ship and foil profile has been chosen, for which the characteristics and advantages or disadvantages are discussed in this chapter.

2.3.1 2D PROFILE CHARACTERISTICS

In the previous research on this ship an asymmetric NACA4412 profile has been used. Extensive research has been done on the NACA profiles starting before the second world war. The NACA profiles were developed by the National Advisory Committee for Aeronautics, this was founded in 1915 and in 1958 transformed into NASA and started to focus on space technology. In 1938 the NACA4412 profile was tested which lead to a series of lift and drag coefficients for different Reynolds numbers and angles of attack (Pinkerton, 1938).

Figure 20 shows part of the result of these experiments. It can be noted that for small angles of attack the lift coefficient can be linearly estimated. The maximum lift coefficient and angle of attack seem to increase with a higher Reynolds number. The dynamic Hull Vane will operate at these high Reynolds number (between $5*10^6$ to $10*10^6$), so it is important to note this theoretical maximum lift coefficient and at what angle of attack it begins to stall. For the high Reynolds numbers it begins to stall around 16° and the maximum lift coefficient is obtained right before the foils starts to stall.

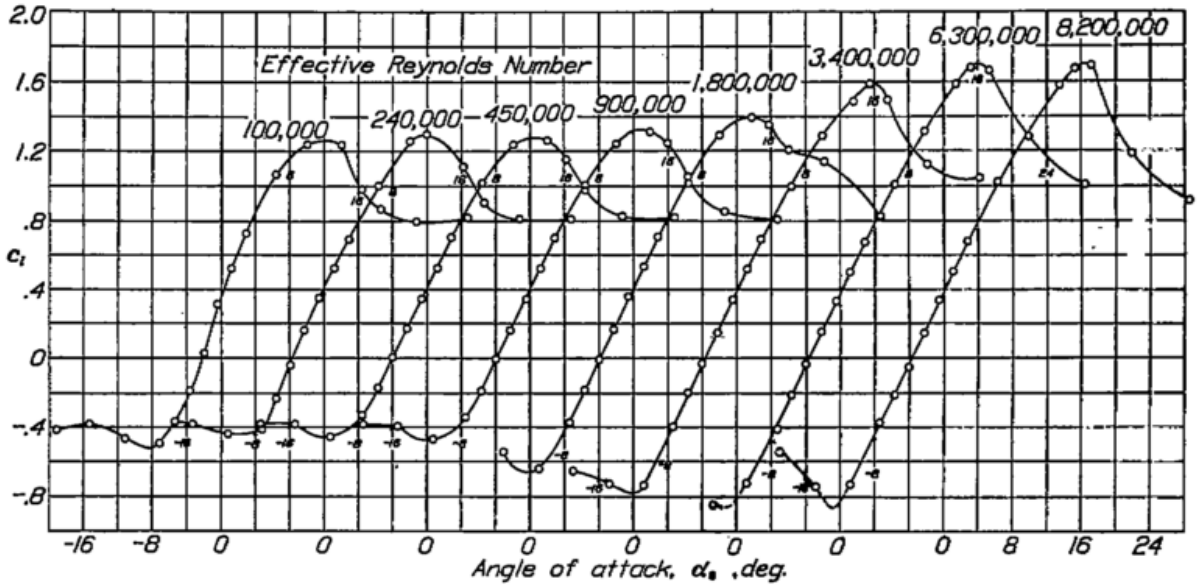

Figure 20: Lift coefficient for NACA4412 airfoil (Pinkerton, 1938)

More recent results can be found on the website www.airfoiltools.com. For a large collection of air foils the characteristics have been calculated using the software XFOIL, which can do viscous and inviscid pressure calculations over a 2D air foil. In Figure 21 the lift/drag ratio is given for various Reynolds numbers for the NACA4412 profile. It shows a higher peak at high Reynolds numbers, indicating a more efficient profile for higher Reynolds numbers.

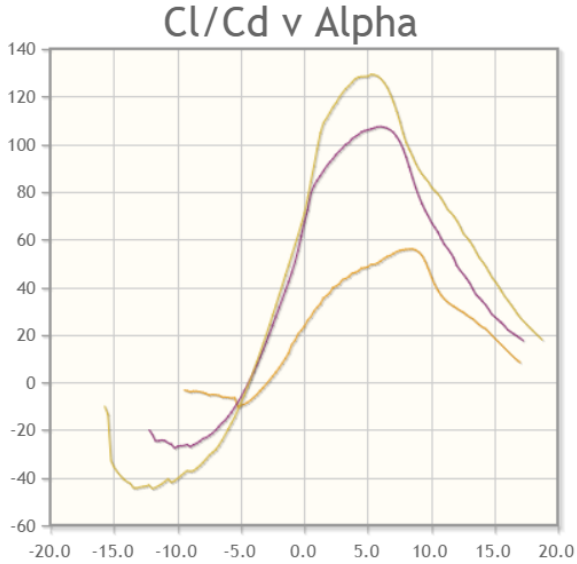

Figure 21: Lift/drag ratio for $Re = [1 * 10^5, 5 * 10^5, 10 * 10^5]$, (www.airfoiltools.com)

2.3.2 3D EFFECTS

So far the effects described in this literature review are for 2D foils, thereby ignoring the induced resistance and lift distribution of a 3D foil. The induced drag is a significant part of the resistance for a 3D foil. For an accurate prediction of the lift and drag coefficient the 3D effects need to be included. The Prandtl lifting-line theory is used to estimate the induced drag coefficient and 3D lift coefficient. The lift distribution over the wing is simplified to represent an elliptical circulation distribution. The 3D lift and drag coefficient can now be calculated with equation (12) and (13) (Abbott & Von Doenhoff, 1959).

$$\boldsymbol{C_L = (\alpha C_{l\alpha} + C_{l0})\left(\frac{AR}{AR+2}\right)} \quad \textbf{(12)}$$

$$C_{di} = \frac{{C_L}^2}{\pi ARe} \quad \textbf{(13)}$$

The 2D lift coefficient slope ($\boldsymbol{C_{l\alpha}}$) and zero-angle lift coefficient ($\boldsymbol{C_{l0}}$) are determined from the 2D lift characteristics. The aspect ratio of the foil is 7 and the planform efficiency factor (e) is estimated as 0.7. Literature on the planform efficiency factor for hydrofoils is very limited, a conservative planform efficiency factor for a hydrofoil is 0.7, for an ideal elliptical lift distribution it would be 1.

The total drag on the Hull Vane can now be calculated as the sum of the 2D viscous drag and the 3D induced drag.

$$\boldsymbol{C_D = C_{di} + C_d} \quad \textbf{(14)}$$

The 2D lift coefficient ($\boldsymbol{C_d}$) is dependent on the angle of attack and shown in Figure 22. The 3D drag coefficient can now be calculated and is shown in Figure 23. It can be noted that the induced drag is a significant part of the total drag. This implies that a higher angle of attack will produce a significant amount of extra drag and optimal lift-drag ratios will not be around the 5° as predicted by the 2D theory.

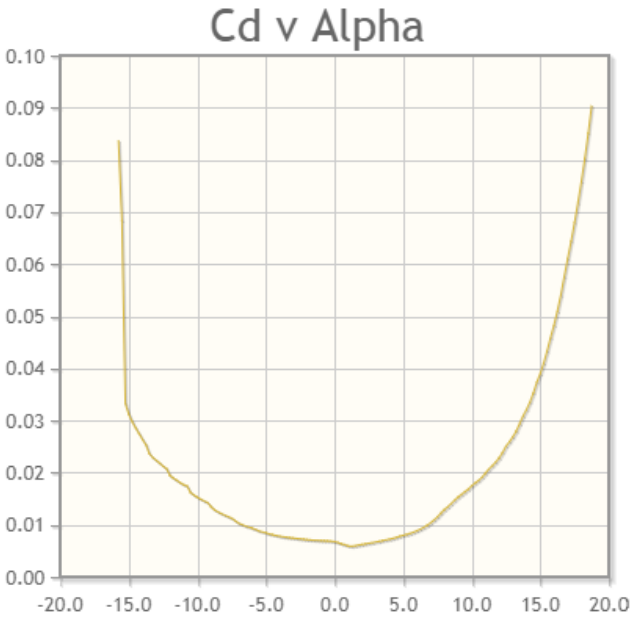

*Figure 22: Drag coefficient for Rey=1*10^6, (www.airfoiltools.com)*

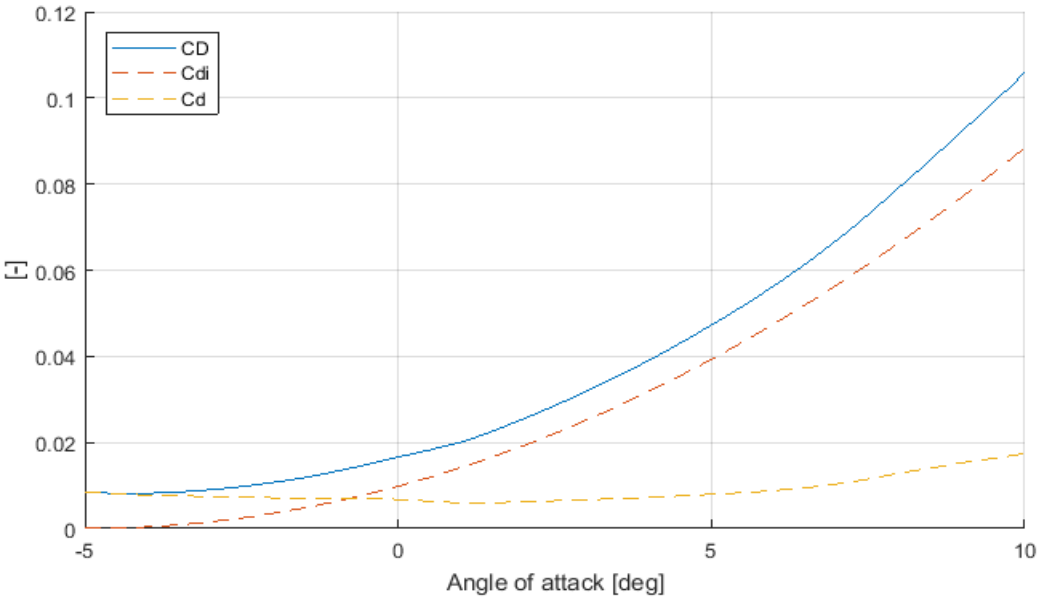

Figure 23: 3D drag coefficient, induced drag coefficient and 2D drag coefficient

The induced drag coefficient and 3D lift coefficient have a lot of influence on the total thrust production. With an estimated free flow angle of 5° an estimate of the lift, induced drag and thrust is made based on the above formulas, the result is shown in Figure 24. As seen the resulting horizontal force coefficient is only positive for small angles of attack. For the highest thrust the optimal angle of attack would be somewhere between 2° and 4°.

The Hull Vane has a constant profile over the entire span and no wingtips. This causes the pressure difference to decrease near the tip and thereby decreasing the lift near the tip. This change in lift will cause extra circulation and vortex shedding, increasing the induced drag. The induced drag for the Hull Vane will therefore be higher than calculated.

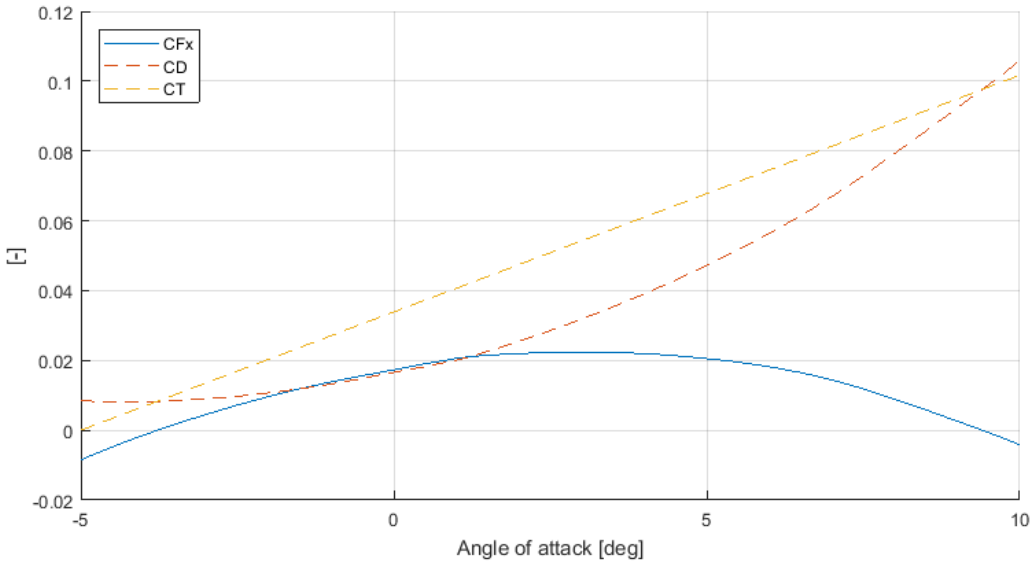

Figure 24: Horizontal force coefficient, 3D drag coefficient and thrust coefficient

2.3.3 ASYMMETRIC VERSUS SYMMETRIC PROFILE

The Hull Vane always uses an asymmetric foil, as the inflow angle is usually from one side. For an oscillating foil the inflow angle can be positive or negative, so the lift can either be positive or negative. For the conditions showed in previous section, the angle of the flow almost never becomes negative to the earth fixed coordinate system (-0.5° in Figure 18). As the lift is perpendicular to the flow, there will only be a very small horizontal force possible from the negative inflow, in these conditions. The delayed stalling and higher lift/drag ratios of the asymmetric profiles provides a big advantage for flows coming from one direction. When the flow direction on the Hull Vane only has an angle of 0.5° to the horizontal probably no thrust can be generated. For the AMECRC#13 in these conditions there would be no advantage to a symmetric foil.

2.4 CONCLUSION LITERATURE REVIEW

In the conclusion the lessons learned from the literature review are summarized.

The first part investigated the working and possibilities of the oscillating foil as a propulsion device. Research showed high thrust coefficients and efficiency coefficients can be achieved, especially when there is no power needed for the heave motion. It also showed that the dynamic Hull Vane is working at a very low Strouhal number, where the oscillating foil will hardly produce a positive thrust. The lift on the dynamic Hull Vane will produce thrust due to the oblique inflow, instead of the changing angle of attack as for the oscillating foil. Different trajectories or phase angles showed little effect on the low Strouhal numbers. The study in oscillating foil principle showed that a control algorithm generating thrust will only be loosely related to the oscillating foil, but more based on optimal Hull Vane angle of attack. Therefore in this research a control algorithm based on the oscillating foil motion was rejected.

The second part investigated the change of flow direction on the Hull Vane. It showed the pitch velocity will have the largest influence on the change of flow direction. And the flow will mostly be from one side.

The third part investigated the performance of the Hull Vane. It showed the Hull Vane will provide the most thrust at a low angle of attack, due to the rapid increase in induced drag. Because the inflow will almost always be from one side onto the dynamic Hull Vane, the use of an asymmetric profile will provide the advantage of a higher stall angle and larger efficiency coefficients. The study of the NACA4412 profile showed optimal thrust production between an angle of attack of 2° and 4°.

Based on the results of the literature review it is decided to not develop an algorithm similar to the oscillating foil control. The operating conditions (oblique inflow and low Strouhal number) of the dynamic Hull Vane make its working principle significantly different from the oscillating foil. The thrust will mainly be created by the oblique inflow and not by the oscillating motion. A control algorithm generating thrust will only be loosely related to the oscillating foil, but more based on optimal Hull Vane angle of attack. Therefore in this research a control algorithm based on the oscillating foil motion is not a goal anymore.

3. METHOD

In this chapter the method used in the research will be explained. From the background of the mathematics used in CFD to the mesh used in the simulations.

3.1 COMPUTATIONAL FLUID DYNAMICS

The simulation of fluid flow in a numerical model is called Computational Fluid Dynamics (CFD). A continuous domain is discretized, by dividing the entire domain in cells. The governing equations can then be solved on the discrete domain. In this chapter a short overview of the fundamentals is given, for further reading there is a multitude of books available, an example is (Tannehill & Anderson, 2013).

3.1.1 FUNDAMENTAL EQUATIONS

The physical models are represented in mathematics by the fundamental laws of fluid mechanics. Two physical rules are the basis for the fundamental equations.

- Conservation of mass
- Conservation of momentum

The conservation of mass leads to the continuity equation (15) which describes the fluid passing through an infinitesimal, fixed control volume. The first term represents the rate of increase of the density of the control volume, while the second term represents the rate of mass flux passing out of the control surface.

$$\frac{\partial \rho}{\partial t} + \nabla \cdot (\rho V) = 0 \tag{15}$$

Because we are mostly interested in water and (relatively) slow air flow, we can assume to have two incompressible fluids. So the density of each fluid element remains constant and is incompressible. For steady airflow with speeds under 100 m/s, the assumption of incompressibility is a good approximation. This reduces the continuity equation to equation (16), where only the divergence of the fluid field is set to zero. This means the net mass flux in and out of an infinitesimal fixed control volume must be equal to zero, no fluid can be created or lost inside the control volume.

$$\nabla \cdot V = 0 \tag{16}$$

The conservation of momentum is described by the momentum equation in (17). The first term represents the rate of change of momentum in the control volume. The second term represents the rate of change of momentum trough convection. The first term on the right is the force on the fluid. Usually the fluid will experience gravity, this means the force is equal to the gravity vector ($f = g$). The final term on the right represents the surface forces on the fluid element. The surface force consist of normal stress and shearing stress.

$$\frac{\partial}{\partial t}(\rho V) + \nabla \cdot \rho VV = \rho f + \nabla \cdot \mathbb{p}_{ij} \tag{17}$$

The momentum equation is often rewritten for a case with a constant viscosity for a Newtonian fluid, as in (18).

$$\rho \frac{DV}{Dt} = \rho f - \nabla p + \mu \nabla^2 V \tag{18}$$

3.1.2 DISCRETIZATION

These continuous equations cannot be solved by a computer directly. Therefore the domain on which we want to do the calculations is discretized. The partial differential equations can now be solved on the finite-difference mesh or grid. In Figure 25 an example is given of a grid representation of a square domain. We can now solve the following equations on the points of this domain. This grid can be extended to a three dimensional time dependent grid. Which is being used in this research.

$$\begin{aligned} u_{i+1,j} &= u(x_0 + \Delta x, y_0) & u_{i-1,j} &= u(x_0 - \Delta x, y_0) \\ u_{i,j+1} &= u(x_0, y_0 + \Delta y) & u_{i,j-1} &= u(x_0, y_0 - \Delta y) \end{aligned} \tag{19}$$

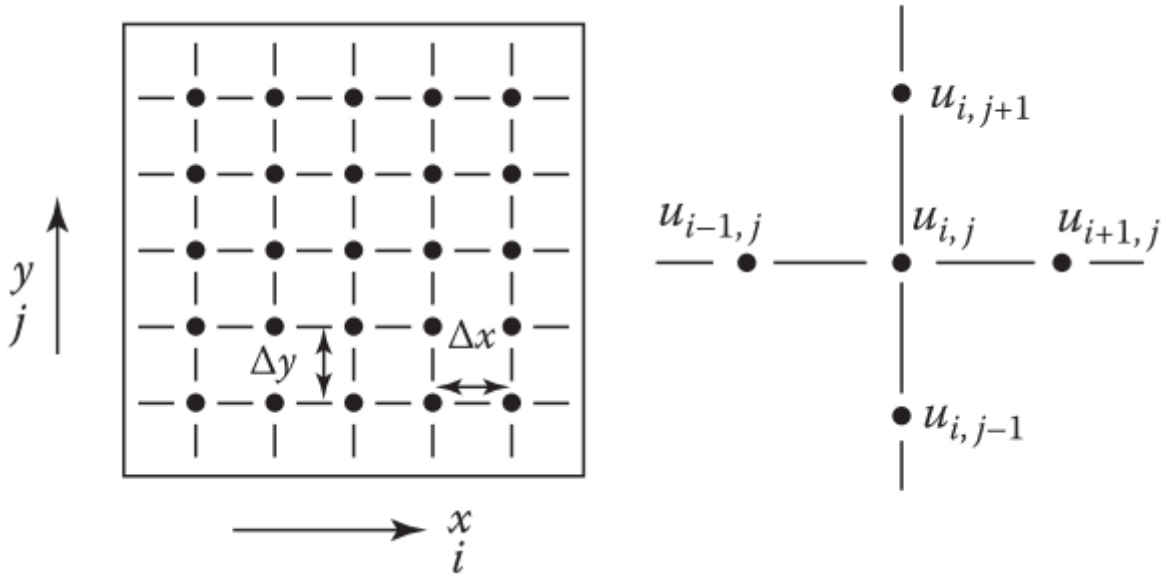

Figure 25: Example of a finite difference grid (Tannehill & Anderson, 2013)

As differential equations consist of derivatives, it is important to have an expression for the derivative on the finite-difference grid. This can be introduced by recalling the definition of the derivative.

$$\frac{\partial u}{\partial x} = \lim_{\Delta x \to 0} \frac{u(x_o + \Delta x) - u(x_0)}{\Delta x} \tag{20}$$

The finite difference approximation can be made more exact when represented by a Taylor series expansion. A Taylor-series expansion around x_0 will have the following form, where $n \to \infty$.

$$u(x_0 + \Delta x) = u(x_o) + \left(\frac{\partial u}{\partial x}\right)_{x_0} \Delta x + \left(\frac{\partial^2 u}{\partial x^2}\right)_{x_0} \frac{(\Delta x)^2}{2!} + \ldots + \left(\frac{\partial^n u}{\partial x^n}\right)_{x_0} \frac{(\Delta x)^n}{n!} \tag{21}$$

From this we can form the forward difference scheme by rearranging.

$$\left(\frac{\partial u}{\partial x}\right)_{x_0} = \frac{u(x_0 + \Delta x) - u(x_o)}{\Delta x} - \left(\frac{\partial^2 u}{\partial x^2}\right)_{x_0} \frac{(\Delta x)^2}{2!} - \cdots \tag{22}$$

When we switch to the notation used in the mesh for a first order approximation we get.

$$\left(\frac{\partial u}{\partial x}\right)_i = \frac{u_{i+1} - u_i}{\Delta x} + T.E. \tag{23}$$

The higher order terms are now part of the Truncation Error (T.E.). This is the difference between the partial derivative and the finite difference representation. Because the terms in the truncation error are dependent of Δx^2 or higher, the error is in the order of Δx. This error is introduced by the fact that Δx cannot go to zero as in equation (20), due to the finite-difference grid. This is just one way to discretize the partial derivative, there is a multitude of methods available all with different tradeoffs. Some may focus on numerical stability, smallest truncation error or computational speed.

3.1.3 TURBULENCE

The complexity of turbulence in flows has been of interest to man for a long time. In Figure 26 a sketch is shown of the turbulence created by an artificial waterfall falling in a puddle. The sketch is made by Leonardo Da Vinci around 1508. He describes the flow as hairs with two motions, one of which is caused by the weight of the hair, the other by the direction of the curls. One part is caused by the principal current, the other is a more a random event.

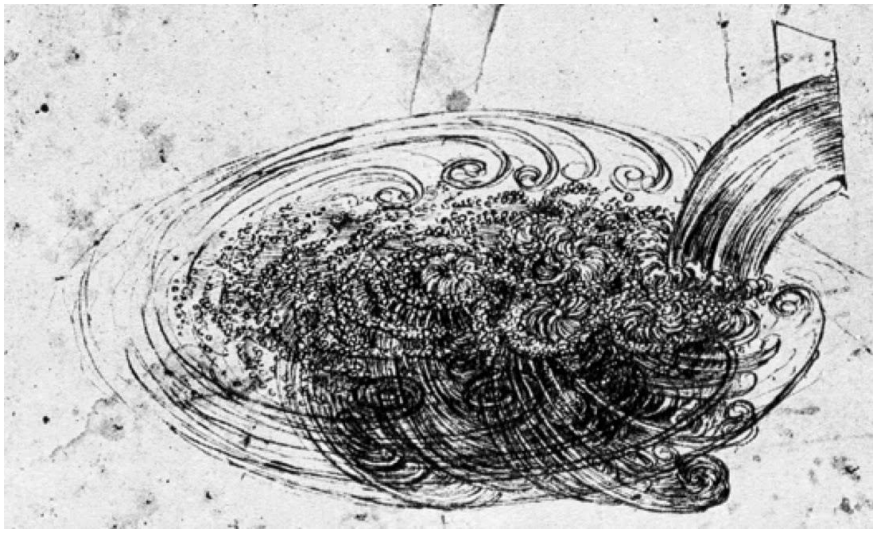

Figure 26: Leonardo Da Vinci`s sketch of turbulence

The sketch and text of Da Vinci show already the understanding of a random or chaos component in a turbulent flow. This random component is very hard to model precisely in CFD, the exact modeling of the process requires a lot of computer power. Precise modeling of the turbulence is possible with a few methods which are shown descending in complexity.

- Direct Navies-Stokes (DNS)
- Large Eddy Simulation (LES)
- Reynolds Averaged Navier-Stokes (RANS)

The DNS solvers solve the full Navier-Stokes equation. As this includes all the effects, it is also the most computational intensive. All the vorticity and eddies in the flow are fully resolved, but this requires a very fine grid to capture all the detail in the flow. A cruder approximation is done by the LES, this only calculates the largest or significant eddies. Small turbulence in the flow field is unresolved. Both methods are mostly used for research and not in practice, as the computation time for the method is too long to be useful. The most used method for practical applications is the RANS method. With the RANS simulation the flow is split up in the mean component and the fluctuating component, as seen in Figure 27. The flow quantity now consists of two parts $u = \bar{u} + \acute{u}$. The time average of the fluctuating component is per definition zero. So the mean is a good representation of the flow. With the continuity equation for an incompressible flow now written as in equation (24), where $\bar{u}_j$ is the averaged flow vector.

$$\frac{\partial \bar{u}_j}{\partial x_j} = 0 \tag{24}$$

And the momentum equation can be changed to equation (25), in which the turbulent stress is contained in $(\tau_{ij})_{turb} = -\rho\overline{\acute{u}_i \acute{u}_j}$.

$$\frac{\partial}{\partial t}(\rho\bar{u}_i) + \frac{\partial}{\partial x_j}(\rho\bar{u}_i\bar{u}_j) = -\frac{\partial\bar{p}}{\partial x_i} + \frac{\partial}{\partial x_j}\left(\mu\left(\frac{\partial\bar{u}_i}{\partial x_j} + \frac{\partial\bar{u}_j}{\partial x_i}\right) - \rho\overline{\acute{u}_i\acute{u}_j}\right) \quad (25)$$

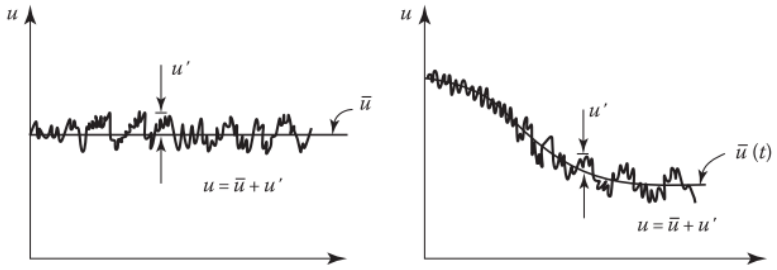

Figure 27: Typical measurement of fluctuating signal (Tannehill & Anderson, 2013)

In a RANS simulation the time fluctuating component is not being solved, therefore the stresses associated with the turbulence are ignored. Turbulence models need to be introduced to account for the turbulent stress. Turbulence models come in two forms, based on the Boussinesq hypothesis or on the Reynolds-stress. Models based on the Boussinesq hypothesis model the turbulent stress based on the eddy-viscosity. The models based on the Reynolds-stress do not assume that the turbulent stress is proportional to the rate of mean strain. According to the ITTC the two-equation models based on the Boussinesq hypothesis are most used and give accurate predictions in ship hydrodynamics (ITTC, 2014). In FINE/Marine™ multiple two-equation models are implemented, for this study the commonly used SST Menter κ-ω is used. This model is recommend by the best practices of NUMECA and is described in the NUMECA theoretical manual (NUMECA, 2013).

3.2 MESH

As explained in 3.1.2 the calculations can only be done on a discrete domain. Therefore the entire domain is discretized in the mesh. The mesh includes the entire flow field, the ship and the Hull Vane. In this section the steps of the mesh making process used by Hexpress are explained.

3.2.1 DOMAIN

As in an experiment in the towing tank, there are boundaries to our numerical domain. The boundaries need to be sufficiently far to not be of influence on our result, the same way a towing tank needs to be wide and deep enough. A numerical domain has the advantage that it can be mirrored in a symmetrical plane for symmetrical simulations. The simulation in this research is symmetrical on the xz-plane, so the ship and domain can be mirrored and only the positive y-axis is part of the simulation. The origin of the coordinate system is at the transom at the waterline, as seen in Figure 28.

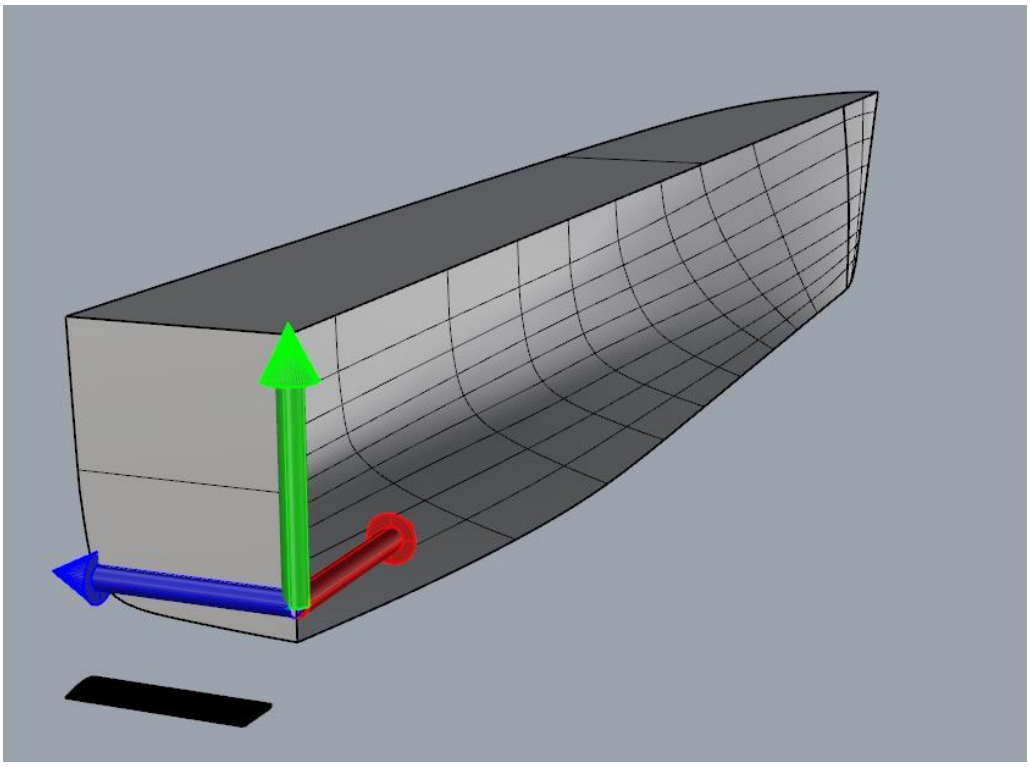

Figure 28: Definition of coordinate system

The size of the domain is set to the standards used by Van Oossanen.

- In front of the ship the domain is extended for one ship length and behind the ship there are four ship lengths (depending on the speed of the ship). The total length of the domain is six times the ship length.
- In the y-direction the domain consists of two times the ship length for the half domain.
- In the z-direction there is half a ship length above the origin and two ship lengths below the origin.

The question is of course if this domain is big enough to avoid any effects from the boundaries. Although no definitive answer to this can be given without studying different domain sizes, we can compare it to recommendations and previous work to get an indication. The ITTC recommends a minimum of one ship length distance from the ship to all boundaries (ITTC, 2014). So the minimum domain size recommendations of ITTC are met. The standards of Van Oossanen can also be compared to standards set by other companies involved with numerical computations. A large study comparing multiple different discretization methods of the free-surface is done by researchers from CNRS (Centre National de la Recherche Scientifique), CWI (Centrum Wiskunde & Informatica), MARIN (Maritime Research Institute Netherlands) and NMRI (National Maritime Research Institute), uses a domain size of -2.5L<x<3L, 0<y<2L and -1.5L<z<0.5L. The overall size of the domain is comparable to the standards at Van Oossanen. In Table 2 the three different standards are compared, as seen the standards of Van Oossanen meet the minimum standards of ITTC and are close to the standards of the reference study. In comparison to most towing tanks the computational domain is also larger in z and y direction, so it is reasonable to assume an undisturbed flow condition along the x-axis in the domain.

Table 2: Comparison of different domain standards

	ITTC	Reference	Van Oossanen
X aft of ship	1	2.5	4
X front of ship	1	2	1
y max	1	2	2
Z min	1	1.5	2

3.2.2 INITIAL MESH

The domain can now be divided in cells for the initial mesh. The initial mesh represents the largest possible cell size to be obtained in the mesh. In later steps, the mesh is refined near areas of interest. The initial mesh based on the standards of Van Oossanen and is 25x8x10 and can be seen in Figure 29.

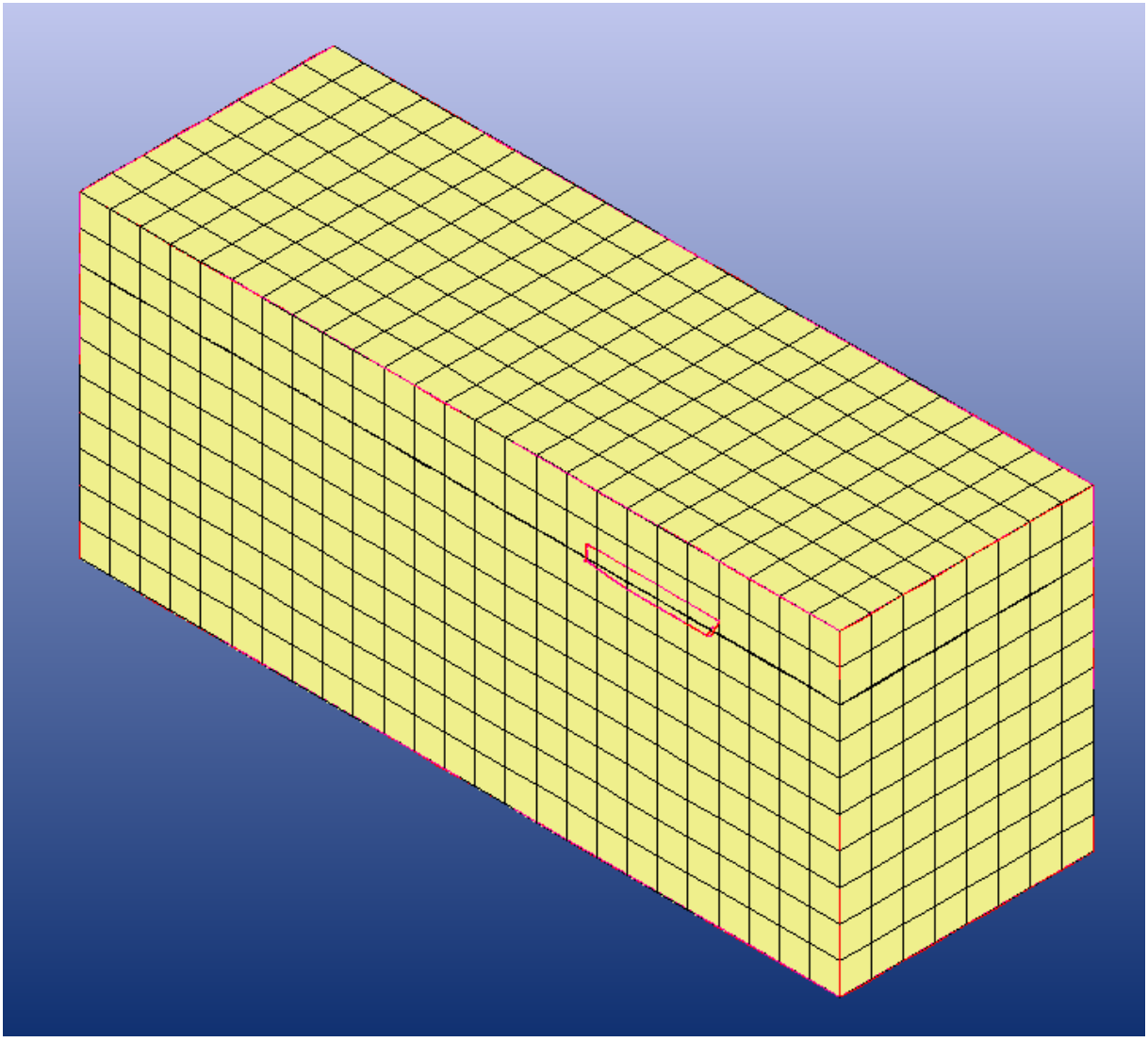

Figure 29: Initial mesh (25x8x10)

3.2.3 ADAPT TO GEOMETRY

The initial mesh is too coarse to describe any geometry, therefore it is refined near surfaces to capture the detail of the geometry. An example of this process can be seen in Figure 30. One refinement corresponds to dividing the cell by two in each direction, thereby splitting each cell in eight smaller cells. The uniform refinement in all directions is not necessary for all surfaces, therefore the aspect ratio of the cells is also controlled. For example on the top and bottom of the Hull Vane, along the y-axis the cells are 4 times larger than along the x-axis. The number of refinements along each surface are specified in Table 3.

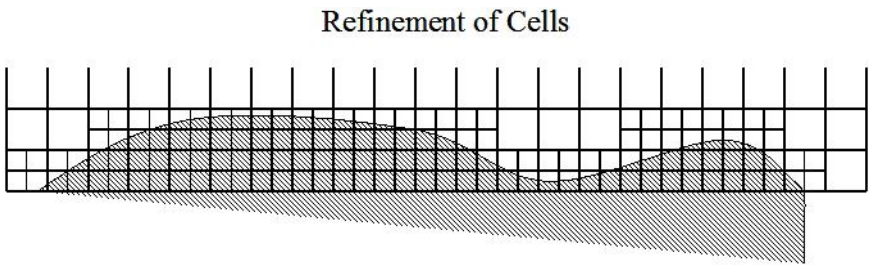

Figure 30: Refinement example, from NUMECA manual

Table 3: refinements used on different surfaces

Surface	Refinements
Deck	5
Hull	6
Transom	6
Bow	7
Free-surface	8
Free-surface kelvin	8
Hull Vane bottom	9
Hull Vane top	9
Hull Vane tip	10
Hull Vane leading edge	12
Hull Vane trailing edge	12

The number of refinements are based on the experience at Van Oossanen and are related to the initial mesh settings, as a more detailed initial mesh would need less refinements. A fine mesh is used around the Hull Vane as this is an area with very small radii. An example of these refinements can be seen in Figure 31. Additional refinements are also used at the free-surface to accurately capture the waves. This band of refinements needs to be able to capture the entire wave, so it is extended in z-direction by the height of the wave. The waves of the ship also need to be accurately captured, therefore additional refinements are used inside the Kelvin angles of the ship. Inside the Kelvin angles the aspect ratio is also constrained so the propagation of the waves can be accurately captured. Outside the Kelvin angles and behind the ship the aspect ratio is larger.
Large jumps in cell size are to be avoided, therefore the refinements gradually diffuse trough the domain. As a standard the refinement diffuses trough four extra cells. This diffusion is shown around the Hull Vane in Figure 32.

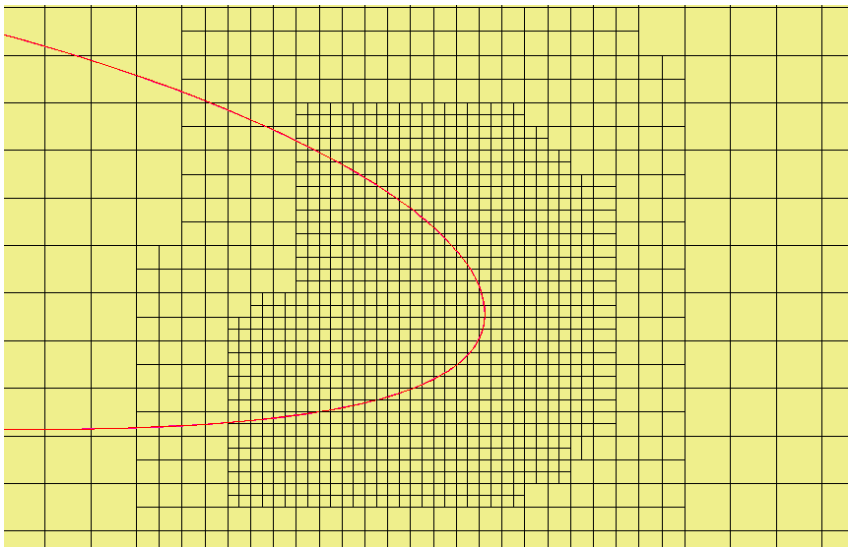

Figure 31: Refinement around leading edge of the Hull Vane

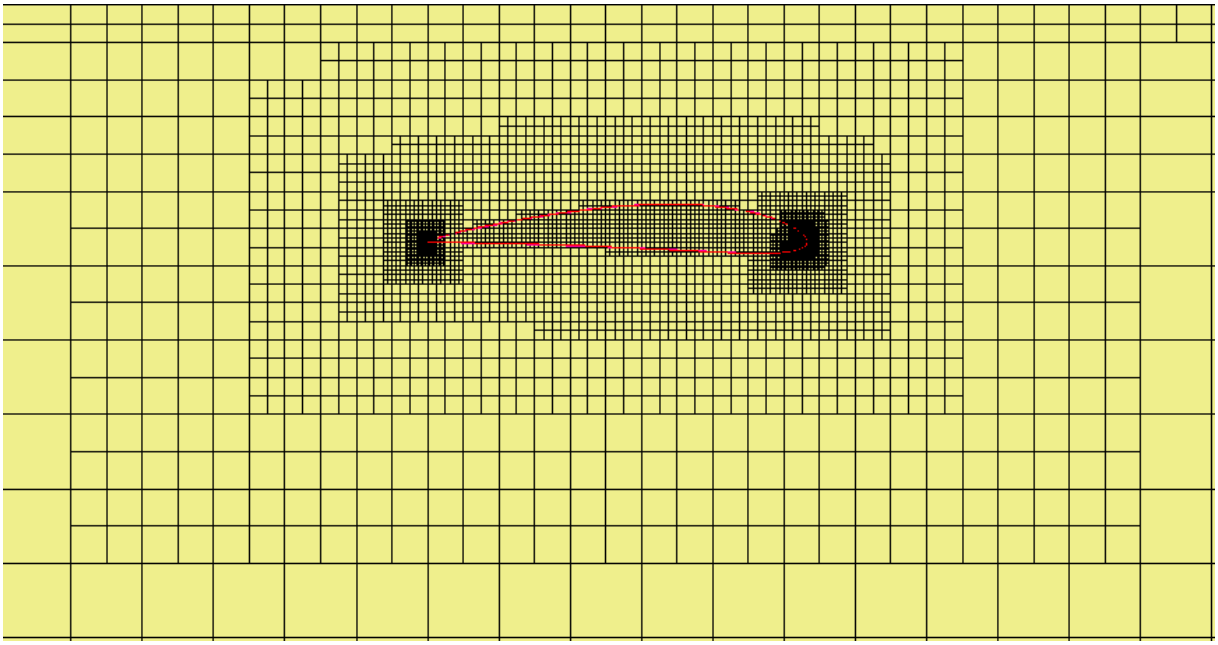

Figure 32: Refinement diffusion around Hull Vane

3.2.4 SNAP TO GEOMETRY

As seen in Figure 31, mesh still doesn't describe the geometry. In the snapping process the staircase mesh is adapted to fit the geometry. The algorithm makes sure that every surface is described by a multitude of cells and all sharp corners are covered by a cell vertex. The grid generator will create additional cells where it cannot follow the geometry. In Figure 33 the sharp corners of the trailing edge of the Hull Vane are fully preserved, and the leading edge curve is as good as possible described by the deformed cells. The zoom level in Figure 33 is not the same for the trailing and leading edge pictures, the actual cell sizes at trailing and leading edge are equal.

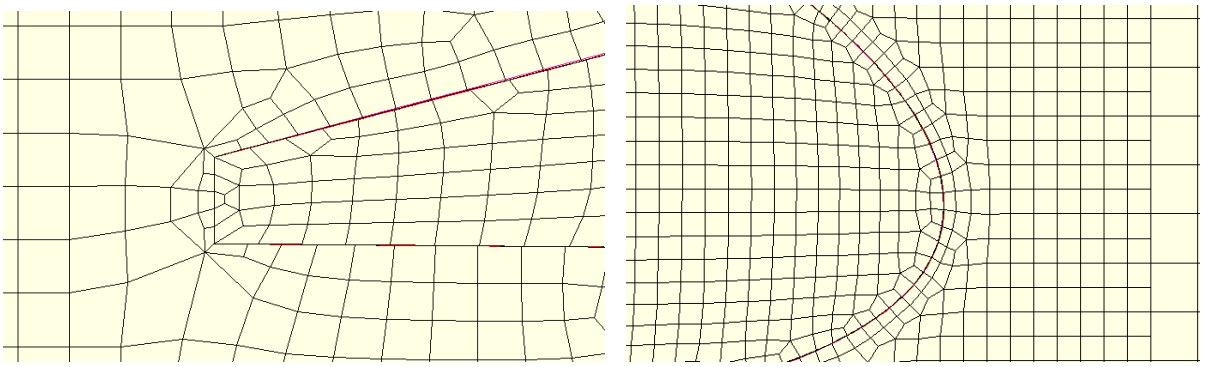

Figure 33: Snapping of mesh to trailing edge and leading edge

3.2.5 OPTIMIZATION

The snapping to the geometry may lead to cells being twisted, negative or concave. This will lead to stability problems in the simulation. These cells are a result of the unstructured meshing approach. When enough refinements are used, HEXPRESS can optimize the mesh and get rid of all the concave, twisted or negative cells. At the end of the optimization step the mesh is free of these cells.

3.2.6 VISCOUS LAYERS

Any viscous flow over a plate will have some form of a boundary layer. In the boundary layer there is a steep gradient of the velocity at the normal to the plate. To accurately model this steep velocity profile extra cells are introduced near the wall. These high aspect ratio cells will capture the velocity gradient in the boundary layer. The number of viscous cells inserted in the viscous layers is based on the local cell size and the gradient of the velocity profile. HEXPRESS automatically calculates the appropriate amount of viscous layers needed. There are no viscous layers inserted at the deck, as it is expected to be dry. On all the other surfaces viscous layers are inserted. The amount of viscous layers is dependent on the local cell size, because at some point the local cell size will already be fine enough. The viscous layer cells are increasing in size away from the surface, as the velocity gradient is less steep there. In Figure 34, the viscous layers on the hull are shown and it can be seen that a lot of high aspect ratio cells are added. Where the original cells were mostly square, the cells are now flat and long. While the velocity gradient perpendicular to the hull is more constant, less fine cells are needed in the direction along the hull.

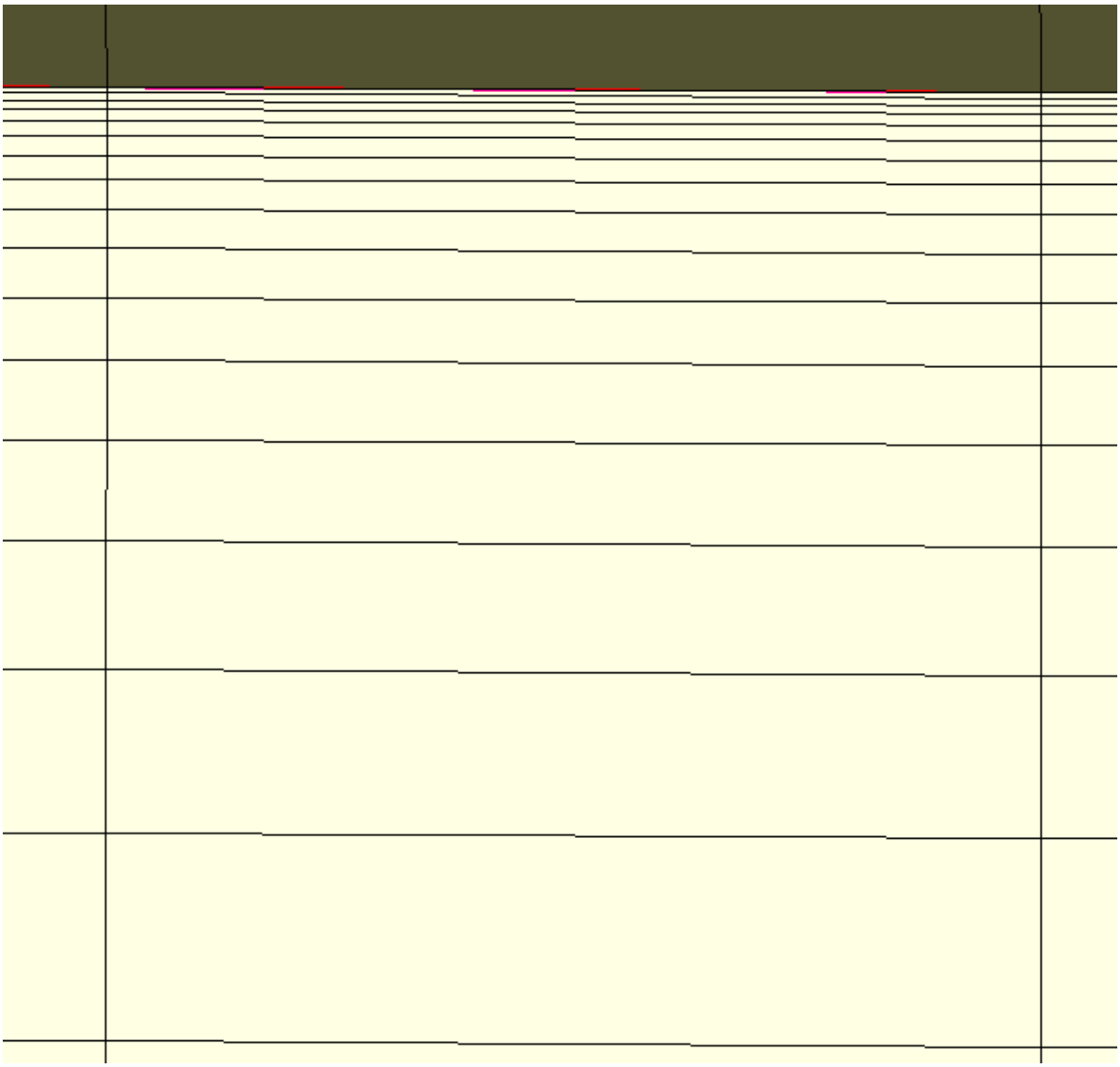

Figure 34: Viscous layers under hull

3.2.7 MESH QUALITY

The results of the simulation will depend on the quality of the mesh, but this is hard to quantify. The concave, twisted and negative cells are removed in the optimization process, so the mesh is valid for computation. One of the ways to measure the quality is to look at the orthogonality of the mesh. The orthogonality describes the minimum angle of one of the faces of the cell. If the orthogonality is 90 degrees the cell is orthogonal, which means all sides have an angle of 90 degrees. This does partly shows the quality of the mesh, although a mesh with cells with a low orthogonality doesn't always produce inaccurate results, as the solver is built to handle unstructured meshes. Cells with very low orthogonality (under 10 degrees) can cause instabilities in the simulation, so they should be avoided. The orthogonality of the mesh is calculated by HEXPRESS and an example of these results is shown in Figure 35. As seen there are no cells with an orthogonality below 10 degrees and most of the cells are above 80. The cells with the lowest orthogonality are at the bow, where the curvatures in different directions makes it hard for the mesh to adapt to the surface. A solution could be to add extra refinements to this area, but as this will not crash the simulation nor influence an important local flow field (for example the trailing edge of the Hull Vane) the effect of these cells is not significant.

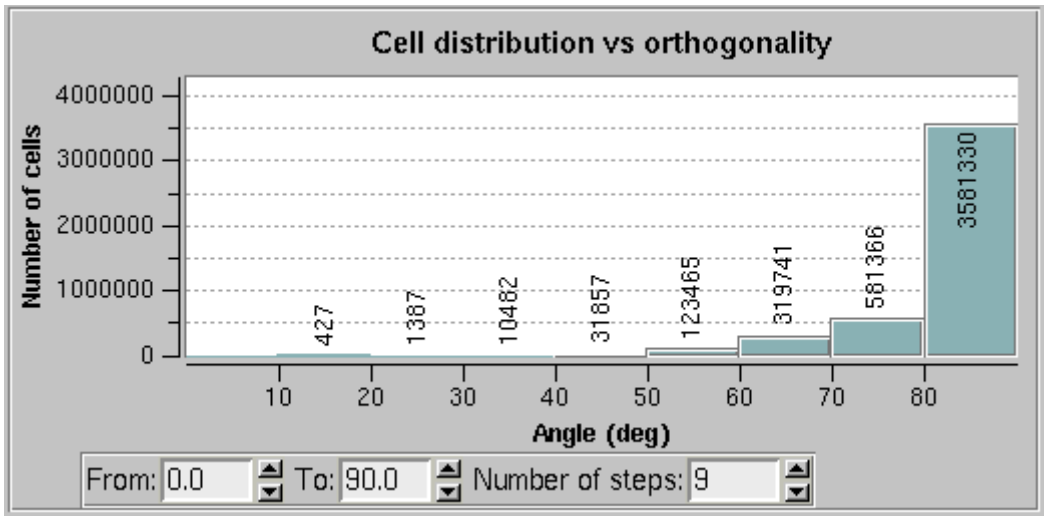

Figure 35: Orthogonality of mesh

3.3 EULER FLOW VERSUS RANSE

The RANSE simulations are computationally intensive. The use of a potential code is considered in the introduction, this would greatly speed up the computation time and would allow for more simulations. In the optimization stage this would provide extra data, and the final configuration could then be validated using RANSE simulations. In this chapter a comparison is made between Euler flow calculations and RANSE calculations on a static Hull Vane, this will show the relevance of the Euler simulations.

As the added wave resistance and the lift of the Hull Vane are pressure based phenomena, the effect of a Hull Vane may be represented accurately with an Euler flow. The Euler flow does not simulate the viscosity of the fluid, thereby also neglecting the boundary layer and the wake. As the Hull Vane is near or in the wake, maybe even more in waves, this would influence the results of the simulations. The significance of this is researched to check if the Euler model would be valid for initial computations.

A comparison is made between RANSE simulations and Euler flow simulations. The same simulation settings are used for both simulations. In the mesh the extra refinement layers that would normally account for the boundary layer are removed, which saves a significant amount of cells and thus computing time. The simulation is done on the AMECRC#13 sailing at Froude 0.6 (25.38 knots) in one meter head waves with a wave length equal to the ship length. The comparison is done in waves because the research is aimed at resistance and ship motions in waves. The advantage and disadvantage of both methods will be taken into account into for the comparison as it would be in the research. This is not an absolute comparison between the methods, but a comparison in how they would be used in this research with their respective advantages and disadvantages for this research.

A comprehensive analysis of the results is given in appendix B. The Euler simulations proved to simulate the ship motions fairly accurate, but in the resistance prediction there is a difference when comparing the pressure resistance. Therefore all results of the Euler simulations would need to be verified with a RANSE simulation. For the Euler simulation the extra refinement in the viscous layer around the hull was removed, this saved a significant amount of cells in the mesh. The computation was done on the same amount of cores, and was for both still within a reasonable amount of cells per cores. This made sure that any difference in computation time was caused by the amount of cells and the simulation, not by difference in cores or a bottleneck in communication between cores. With this setup the Euler simulation took around 70% of the time of the RANSE simulation. The difference in computing was deemed to be not enough to justify the difference in the result. Especially when validation on the Euler simulations increases the total amount of runs.

3.4 TEST MATRIX

To answer the main research question, it is important to choose representative wave frequencies and speeds. The combination of wave frequencies and boat speeds need to be elaborate enough to show the concept in a wide range of situations, but shouldn't be excessively more than needed. In this section the combination of wave frequencies and boat speeds is discussed. The test conditions are determined based on the bare hull.

3.4.1 SHIP SPEED

For the chosen ship speeds, a balance needs to be found between efficiency of the Hull Vane and a practical ship speed. The Hull Vane is developed for higher speeds, as its working principle depend on pressure differences. Therefore the Hull Vane is usually more effective in reducing resistance at higher speeds. High speeds also increase the encounter frequency, although this is academic research the circumstances should be realistic. The amount of time a ship will sail in certain conditions depends on the operating profile. No operating profile is defined in this research, but the conditions should be reasonable for the ship and area. Previous research on the AMECRC#13 done by Van Oossanen showed large resistance reduction between Froude numbers of 0.3 to 0.5 (15% to 30%) (Uithof, Hagemeister, Bouckaert, van Oossanen, & Moerke, 2016). This means the Hull Vane worked efficiently at these speeds. The speeds are also reasonable for this ship. As a base velocity Froude 0.4 was chosen.

As the effectiveness of the Hull Vane is dependent of ship speed, so is the effectiveness of the dynamic Hull Vane. As this research needs to show the effect of the dynamic Hull Vane multiple speeds are investigated. Therefore it is chosen to also do simulations at speeds of 0.3 and 0.5 Froude. This shows the effect the Hull Vane in a broader range of speeds, without looking at the details at low and very high speeds.

3.4.2 WAVE FREQUENCY

The wave encounter frequency will dictate the frequency of the ship motions and therefore the Strouhal number. The ship and water interaction can be modeled as a damped mass vibration system, with a natural frequency and transfer function. The transfer function will show the (linearized) response of the ship to the waves. In order to have a result that will clearly show the effect of the dynamic Hull Vane, the simulations will need to be at an encounter frequency that shows a clear response. Therefore the RAO (response amplitude operator) of the ship is calculated using the strip theory software MAXSURF Motions.

An extensive description of strip theory given in (Journée & Adegeest, 2003). The hull shape is imported in MAXSURF motions and the hydrodynamic parameters are calculated. For the distribution of the mass the default settings are used. The inertia around the x-axis (roll) is calculated as in equation (26).

$$\boldsymbol{I_{xx}} = \boldsymbol{k_{xx}}^{\boldsymbol{2}} * \boldsymbol{\Delta} \tag{26}$$

The moment of inertia for the pitch and yaw motion are calculated in a similar manner. The radius of gyration is unknown as there is no weight distribution for the ship. Commonly used assumptions for these are: $k_{xx} = 40\%\, Boa$, $k_{yy} = 25\% Loa$ and $k_{zz} = 25\% Loa$.

The RAO of the heave and pitch motion are calculated for multiple speeds and frequencies. As strip theory linearizes the motions this result is validated with CFD RANSE calculations. Both results are not exact measurements and will have an uncertainty, but if they are qualitatively similar, the frequencies to be tested can be based on this result. The result can be seen in Figure 36. The lines are the RAO`s as calculated by MAXSURF Motions and the points are the RAO`s calculated over 10 waves. Although there is a difference in the amplitude at the high and low frequencies, the peak lies around the same point. For the experiments we don't need to be at exactly the natural frequency, but we just need to know its approximate position. These results provide enough information to define the frequencies to be tested.

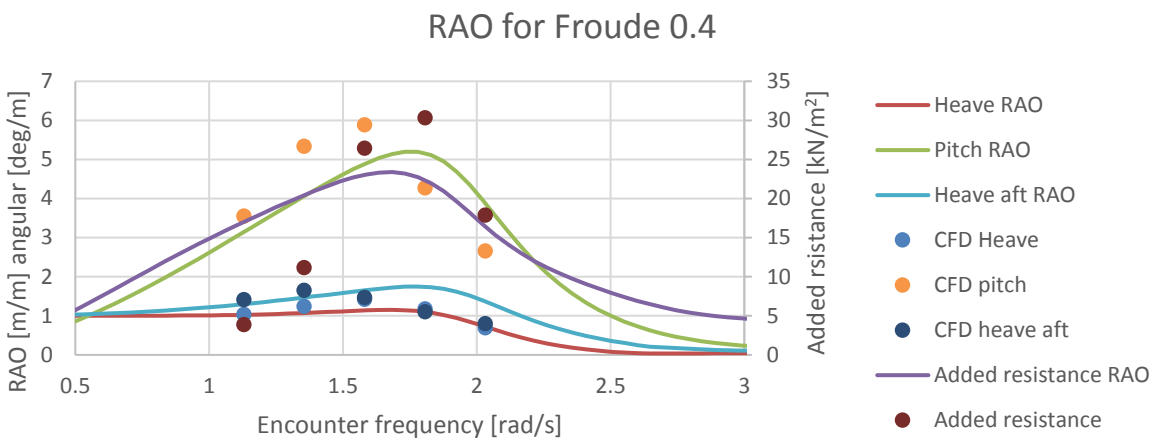

Figure 36: RAO calculated with strip theory and CFD

Based on the results of Figure 36 the base encounter frequency is chosen to be 1.75 rad/s. This is close to the natural frequency and large motions on the ship are therefore to be expected. This will either give enough reason to damp the motion, or will impose a large vertical movement which can generate thrust. This base frequency is chosen for the reduction of ship motions as well as for the thrust generation. At an encounter frequency of 1.75 rad/s large ship motions and added wave resistance can be expected.

As the dynamic Hull Vane uses the frequency of the ship, it is also tested on frequencies different from natural frequencies. This ensures that the dynamic Hull Vane also works on different frequencies, and that the control scheme can adapt to different frequencies. It could also show its effectiveness in a variety of conditions. The lower and higher frequency are chosen as 1.25 and 2.25 rad/s. This ensures a broad range of frequencies where there is still a significant pitching motion, but where it is definitely next to the natural frequency. In Table 4 the speeds and encounter frequencies are shown, according to the Global Wave Statistics these wave frequencies are not uncommon for the North Sea or open oceans.

Table 4: Speeds and frequencies used for testing

Speeds (Froude)	Speeds (knots)	Encounter frequencies (rad/s)
0.30	12.92	1.25
0.40	17.22	1.75
0.50	21.53	2.25

Not all combinations of ship speed and wave frequency are tested. In Table 5 the test matrix is shown, a base wave frequency and ship speed is chosen, from where alternate situations are tested. So the response to different encounter frequencies is only tested for one speed, and different speeds are only tested based on the base encounter frequency. The higher and lower speeds will show the effect of the decrease or increase of the lift on the Hull Vane, while the different wave frequencies will test the effectiveness with less ship motions, and the effectiveness of the algorithm at different frequencies.

Table 5: Test matrix

Encounter frequency / ship speed	1.25 (rad/s)	1.75 (rad/s)	2.25 (rad/s)
0.30 (Froude)		X	
0.40 (Froude)	X	X	X
0.50 (Froude)		X	

For both control schemes it is assumed that some tuning is necessary before a good result is achieved. Therefore, it is expected that multiple runs are necessary for testing. The whole test matrix also needs to be repeated for the static Hull Vane.

3.5 UNCERTAINTY ASSESSMENT

The quality of any study can be assessed by the uncertainty interval of the answer. It gives the reader an indication of the confidence that can be assumed of the answer. Usually this implies a validation of the experiment with an exact solution, or repeating tests to eliminate random variables. This is a problem for numerical studies. The equations that are solved are exact, repeating the experiment doesn't show any uncertainty. If the same numerical simulation is done twice, the result will be the same. The sources of errors that are present in a numerical hydrodynamic study are listed by many sources, for example (Ferziger & Peric, 2002) (ITTC, 2011). These errors can be split up in multiple sources, which are now discussed in descending relative importance.

First of all are the modeling errors. In the simulation we try to capture the physics of moving water in equations. A DNS simulation could simulate all the physics involved in this process, but this is a very computationally expensive method and not used for practical applications. Usually it is relied on turbulence models for estimating the influence of the turbulence. Although these models have proved to be reliable, it doesn't include the physics of reality. Other sources of errors might be in the model or the domain. In reality the model could have a different trim, so we are making assumptions about the weight distribution. Additionally, the domain is restricted to boundaries. Therefore the simulation setup differs from reality and the solution of the real flow differs from the exact solution of the mathematical model. The effect of these differences are known as the modelling errors.

A second error comes from the calculation on a finite difference grid. By transferring the continuous domain to a finite difference domain we inherently introduce errors. From a simulation point of view, ideally the mesh would consist of infinitesimal cells and an infinite amount of cells. However this would lead to infinite computation times. Therefore the mesh is of a finite size. The difference between the exact solution of the governing equations and the exact solution of the discrete approximation is known as the discretization error. As this error is in every calculation on a mesh, there are methods available to estimate this error. This will be done in section 3.6.

The non-linear set of equations is solved iteratively and this iteration process has to be stopped at some point. The error that is left after the iterations is known as the iteration error and it is defined as the difference between the fully converged solution and the iterative solution of the discretized equations. The iteration error should be one order lower than the discretization error. This is done by using enough nonlinear iterations.

The machines running the simulation can handle a limited amount of digits. By rounding off the solution to the equations, the machine introduces the round of error. For a double-precision machine, calculations are done with 16 digits. Usually this is several orders smaller than the iterative error.

A final error can be introduced by programming errors or bugs. It is the responsibility of the developer of the software to eliminate these errors. Usually this is done by validating the code with experiments or cases for which the exact solution is known. FINE/Marine™ has been extensively validated by the developer and studies comparing different software packages. Therefore it is assumed that there are no programming errors left.

3.6 GRID REFINEMENT STUDY

For most CFD simulations no exact or experimental solution is known, so the results cannot be validated with an exact solution. The goal of this grid refinement study is to calculate the uncertainty of the leading source of errors, such that the bandwidth of the solution is known. As the round-off error is insignificant and the iteration error can be checked and reduced to an insignificant level, the modeling error and the discretization error are left. A modeling error can lead to results that don't represent the physical situation that was supposed to be modelled, and are controlled by the one doing the simulation. This report needs to be detailed enough to convince the reader that the modeling errors are in a reasonable range. Then only the discretization error is left and the uncertainty of this should be calculated. The uncertainty of the discretization error is calculated with a grid refinement study as described in (Eça & Hoekstra, 2014). The method estimates the discretization error based on a series of geometrically similar grids. The discretization error should become smaller as the size of the cells in the grid is reduced, this would be a better approximation of a continuous domain. The grid refinement study starts with the creation of the series of grids, after which the convergence of the simulations over the cell size can be shown.

3.6.1 GRID GENERATION

The generation of geometrically similar grids on an unstructured mesh is nearly impossible. The result will be a mesh with slightly different geometry and grid quality. The differences in the similarity of the grids will result in scatter in the convergence of the data. Therefore, more than three different grid sizes should be used to see if the solution is actually converging. During the creation of the grids extra attention is paid to ensure similar grids as much as possible. Although it is very hard to quantitatively measure the quality of a grid, several quantities of the grids are compared to check how similar they are.

The cell size varies throughout the grid, therefore a typical cell size (h_i) is defined that is representative for the cell size through the entire grid.

$$\boldsymbol{h_i = \sqrt[3]{\frac{V_\Omega}{N_i}}} \tag{27}$$

In equation (27 V_Ω is defined as the volume of the entire domain and N_i is the number of cells of the grid. The refinement factor is now defined as:

$$\boldsymbol{r_i = \frac{h_{i+1}}{h_i}} \tag{28}$$

Ideally, the systematically refined grids should cover a large range of grid refinement ratios, however this is limited by practical constraints. Preferably one would start with the coarsest possible grid, and refine it systematically by a grid refinement ratio of 2. In this way no interpolation is done between the different grids, and the vertices of the original grid can stay at the same place. This would provide the least amount of scatter in the convergence study. However due to the three dimensional domain this would lead to 8 times the amount of cells for each refinement. This is infeasible if multiple refined grids are to be created, therefore it was chosen to look for achievable refined grids, while still respecting the geometry.

As a baseline the standard of Van Oossanen is chosen, as this already defines areas in which multiple refinements are needed for an accurate solution. The size of the cells is varied by controlling the size of the initial grid. In this way the distribution of the cells to the different surfaces is kept similar as best as possible. The process of creating the grid is the same as described in section 3.2. The insertion of the viscous layers is kept the same for all the grids, as this process is not dependent on the size of the grid. For the coarse grids it does give very high aspect ratio cells, as the thickness of the cells is the same but the longitudinal size of the cells has changed a lot. In Table 6 an overview is given of the different grids. The medium setting is the standard initial grid of Van Oossanen, from this setting coarser and finer grids have been made. Although the initial grid size was doubled the amount of cells isn't divided by 8. The diffusion of the fine cells caries through the entire domain and also influences the outer cells. As the trailing and leading edge of the Hull Vane have a very small but important geometry, special attention was paid to capturing this part of the geometry. The coarsest grid was just able to capture the geometry of the Hull Vane.

Table 6: Grid series

	Initial grid	Number of cells	Typical cell size	Refinement ratio to fine grid
Coarsest	3,1,1	1,268,463	1.4352	1.8909
Coarser	6,2,2	1,877,283	1.2594	1.6593
Coarse	12,4,5	3,547,381	1.0187	1.3421
Medium	25,8,10	4,650,055	0.9308	1.2263
Fine	50,16,20	8,576,132	0.7590	1.0000

For all five grids a side view of the hull with the free surface and a side view of the Hull Vane are shown below in Figure 37 to Figure 46. As seen the coarsening is mainly near the hull as the cells on the edge are of a similar size. The figures do not show the boundary of the domain, for the fine mesh the boundaries consisted of smaller cells. Figure 42 with the Hull Vane on the coarsest mesh, shows the importance of enough cells to describe the geometry. The coarsest mesh has only one cell for the trailing edge and makes relatively sharp corners on the leading edge. Therefore, the mesh is not exactly geometrically similar, and caution is needed when interpreting the result of the grid refinement study.

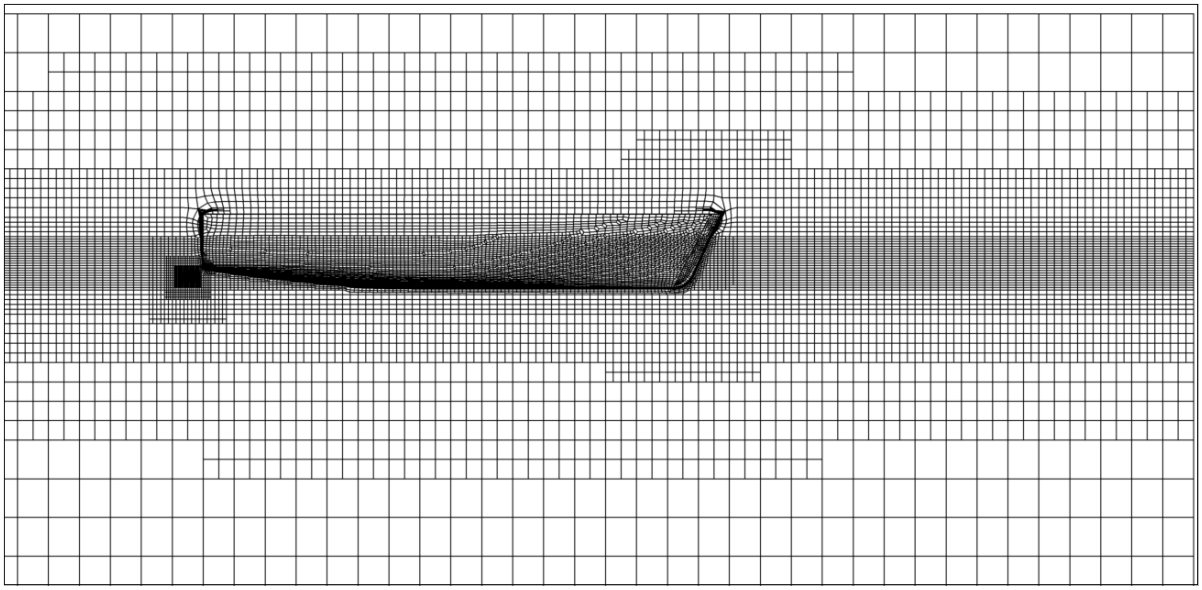

Figure 37: Overview of coarsest grid

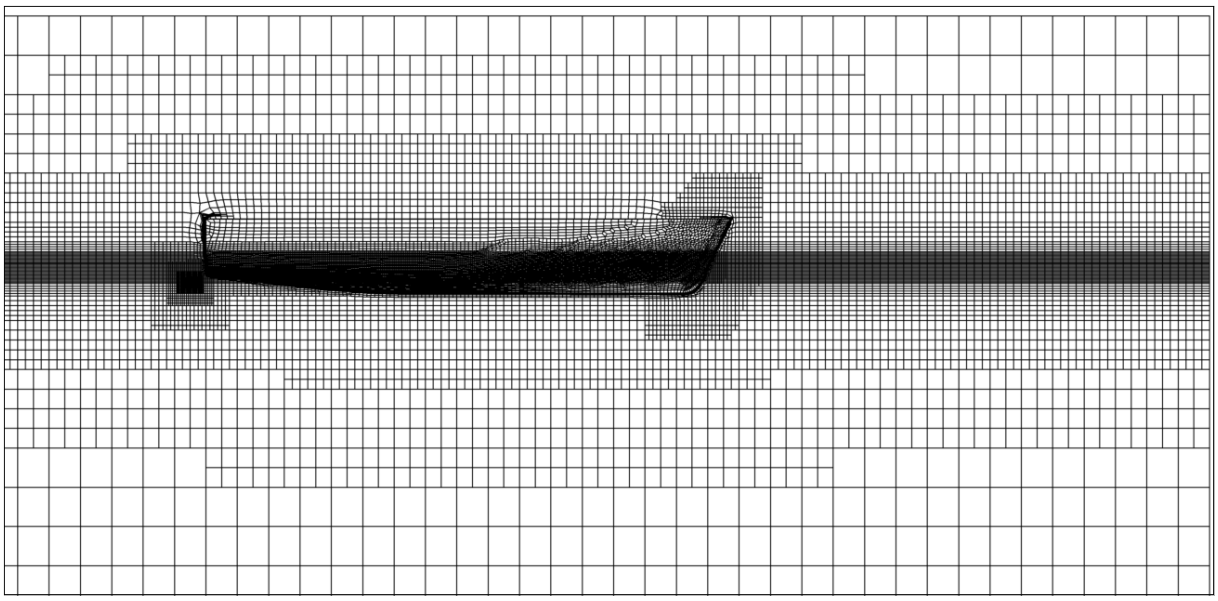

Figure 38: Overview of coarser grid

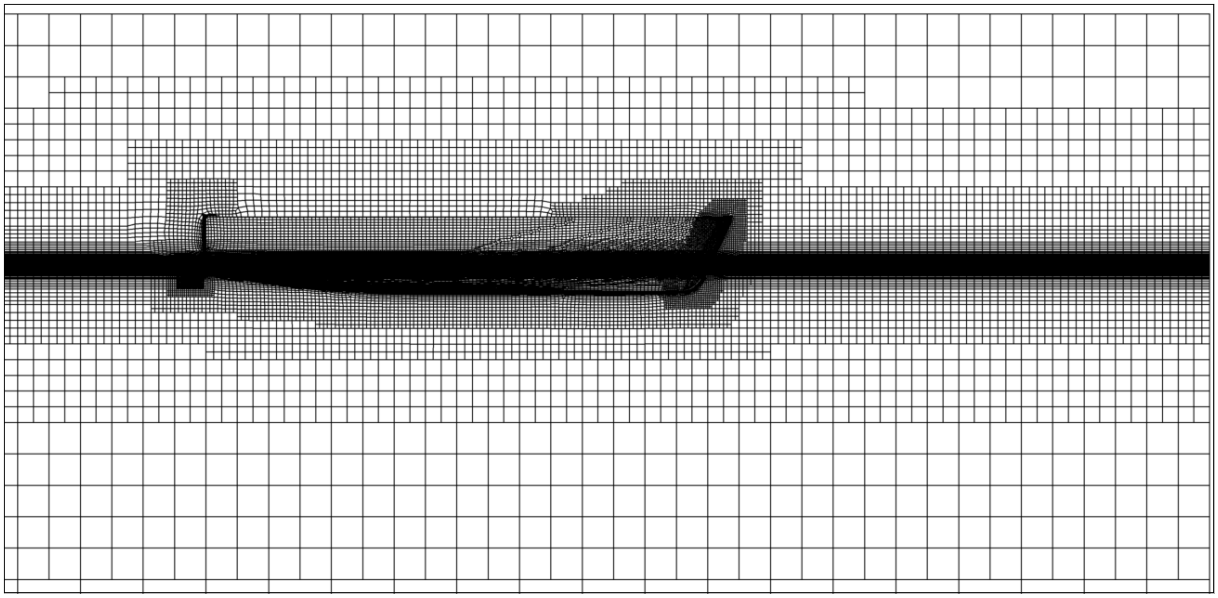

Figure 39: Overview of coarse grid

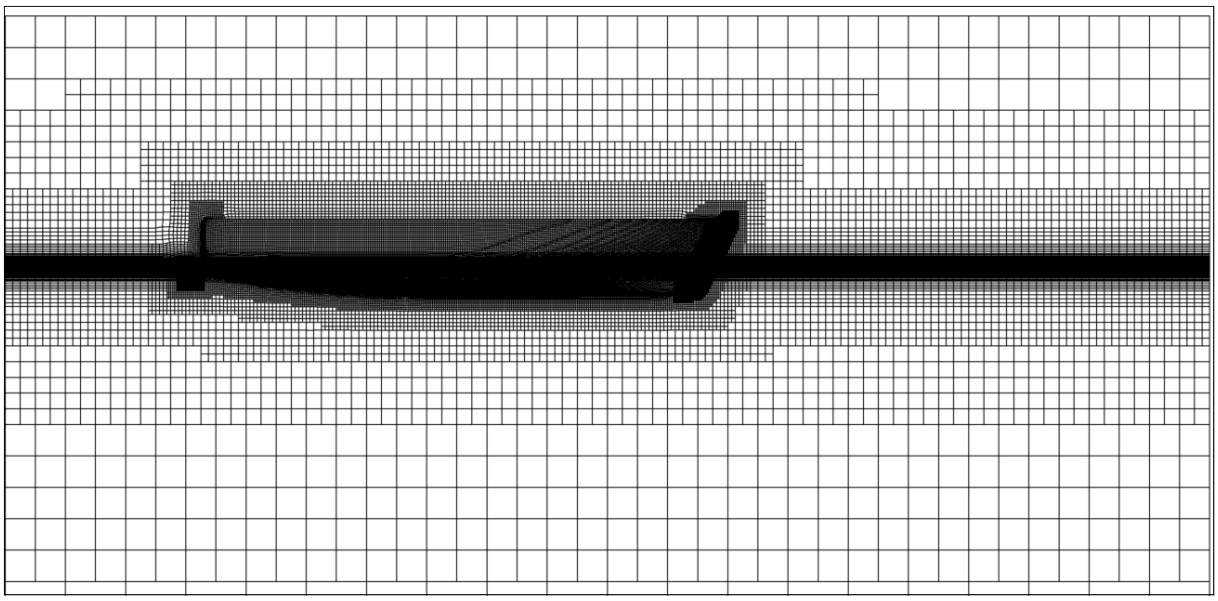

Figure 40: Overview of medium grid

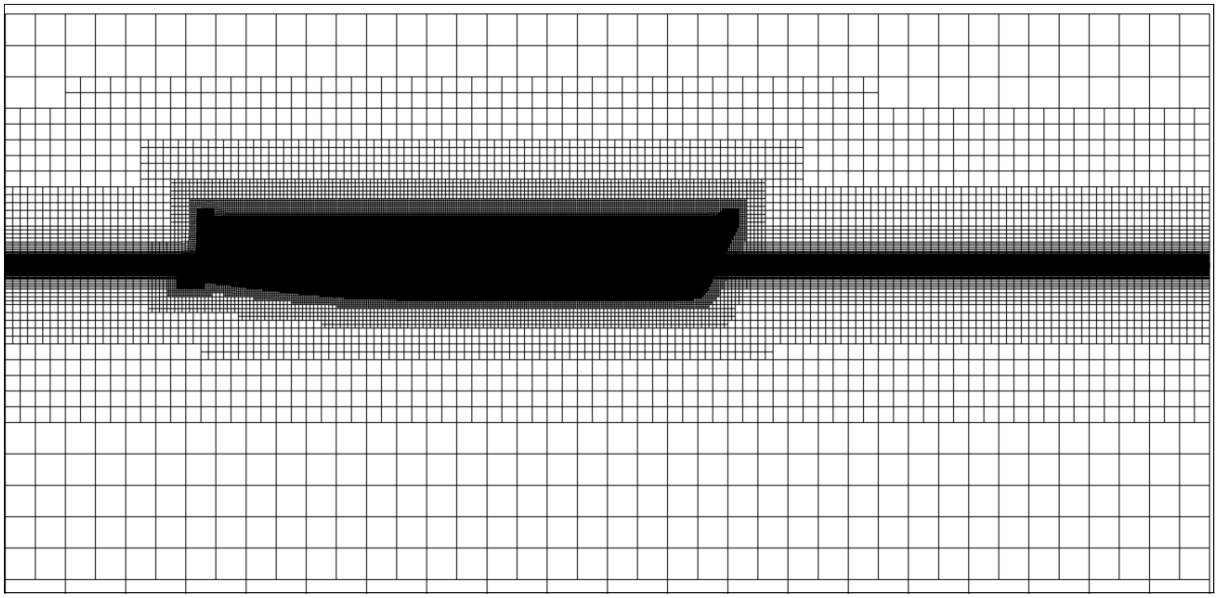

Figure 41: Overview of fine grid

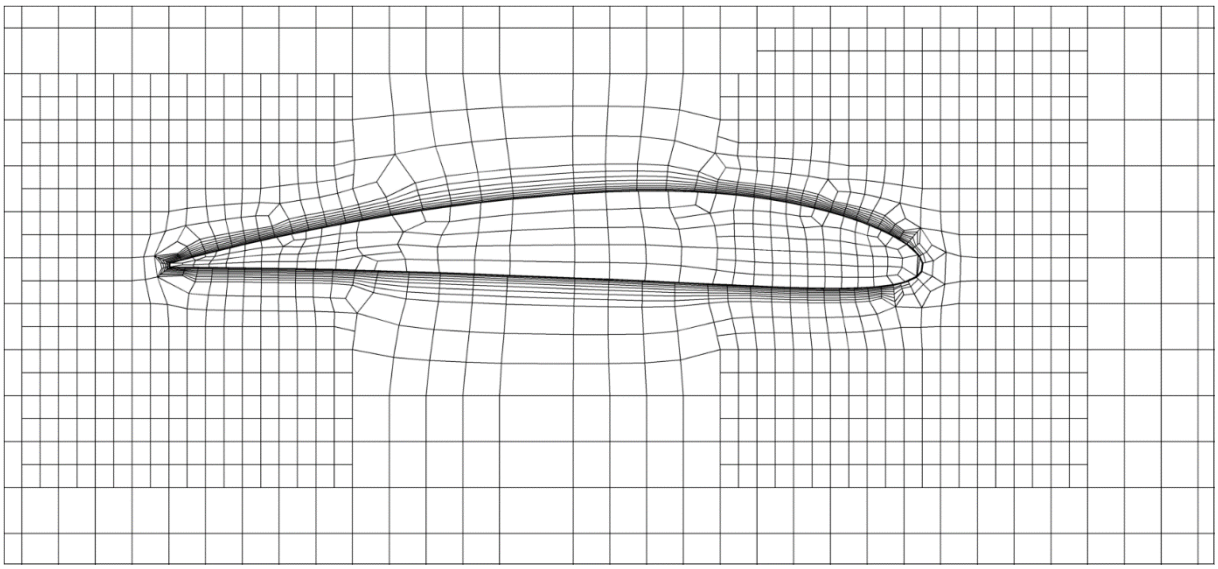

Figure 42: Hull Vane on coarsest grid

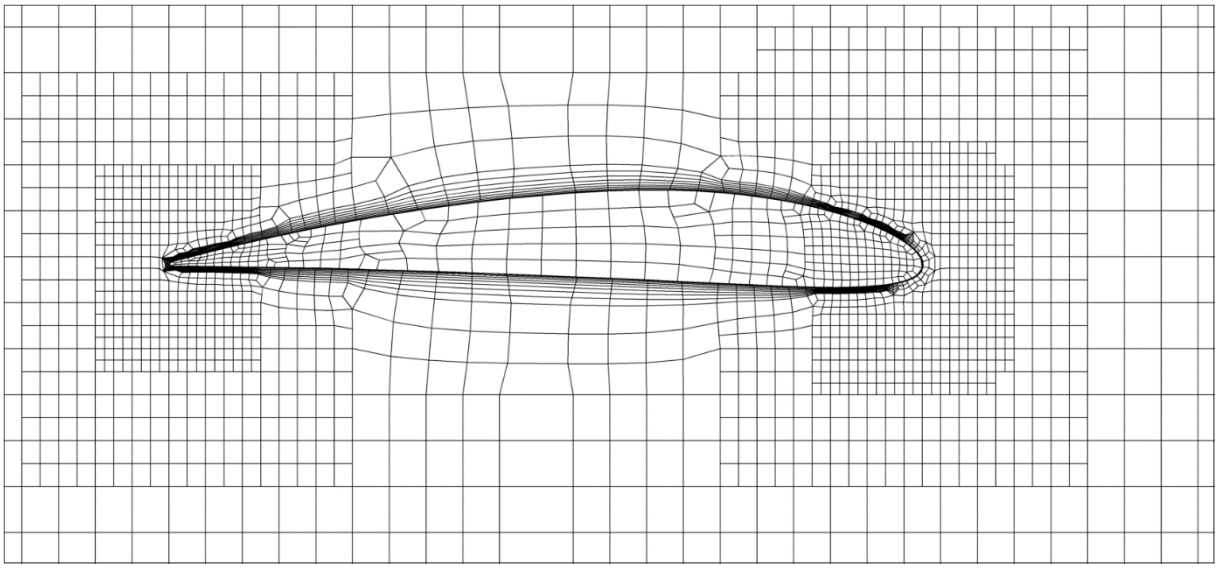

Figure 43: Hull Vane on coarser grid

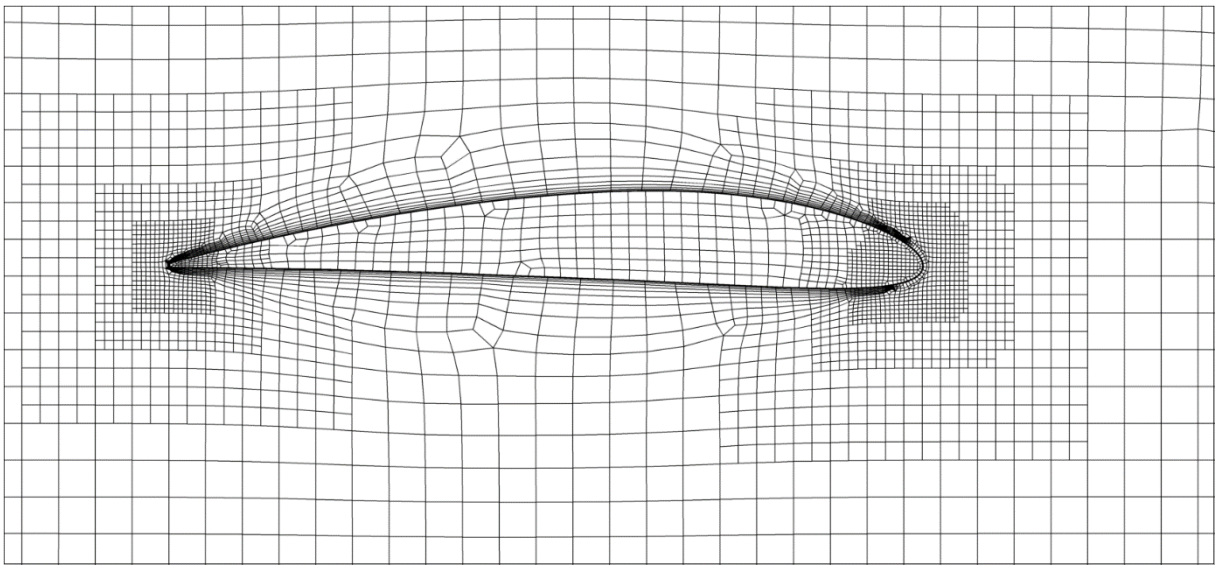

Figure 44: Hull Vane on coarse grid

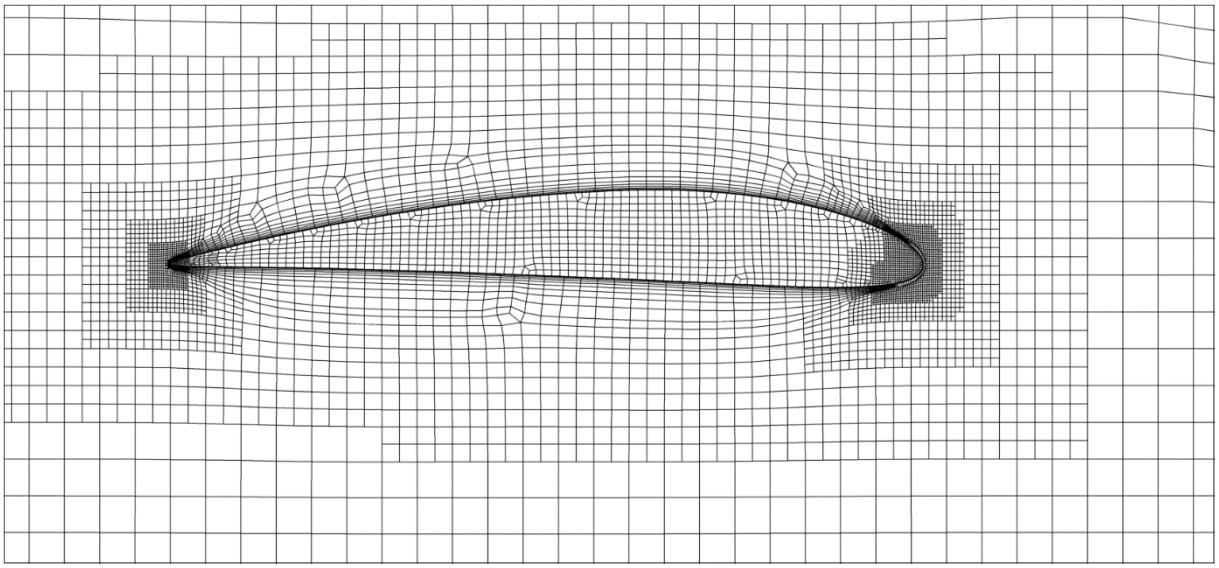

Figure 45: Hull Vane on medium grid

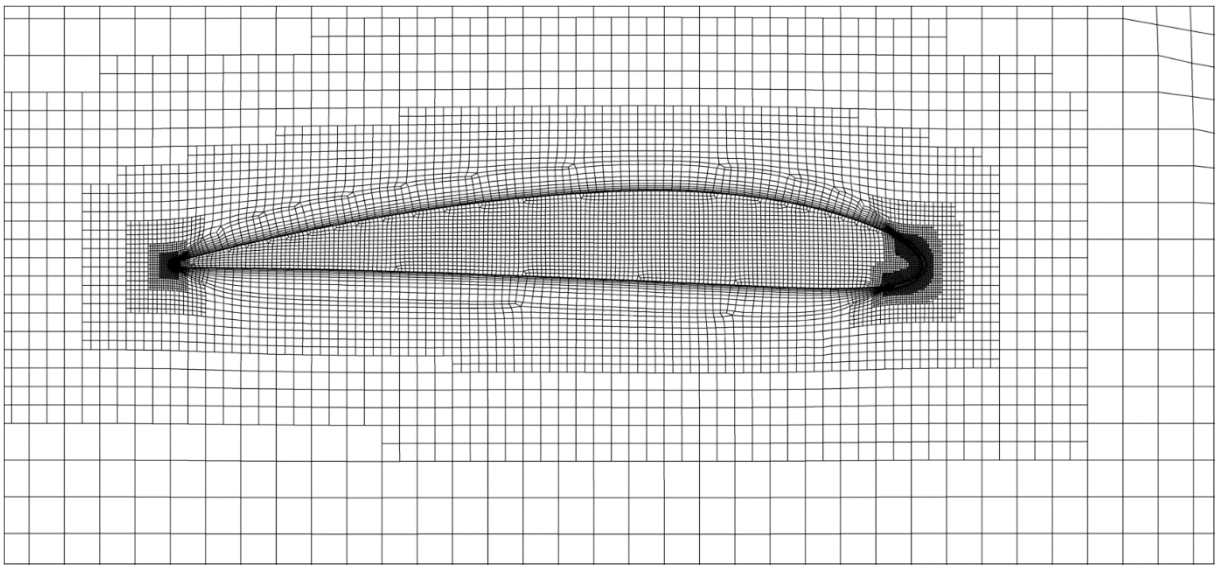

Figure 46: Hull Vane on fine grid

After this visual comparison of the different grids, a quantitative comparison of the different grids is made by looking at the distribution of orthogonality, aspect ratio and expansion ratio of the different grids.

In Figure 47 the orthogonality distribution of the five different grids is shown. The orthogonality is defined as the smallest angle between two surface normals of one cell. Very low orthogonality angles can lead to stability problems, but are sometimes insurmountable. The distribution in Figure 47 shows that the distribution of the orthogonality is mostly similar between the grids. The minimum angle was lower in the coarsest grid, because the bigger cells had to be stretched further to snap to the geometry, especially near small details in the geometry such as the trailing edge of the Hull Vane

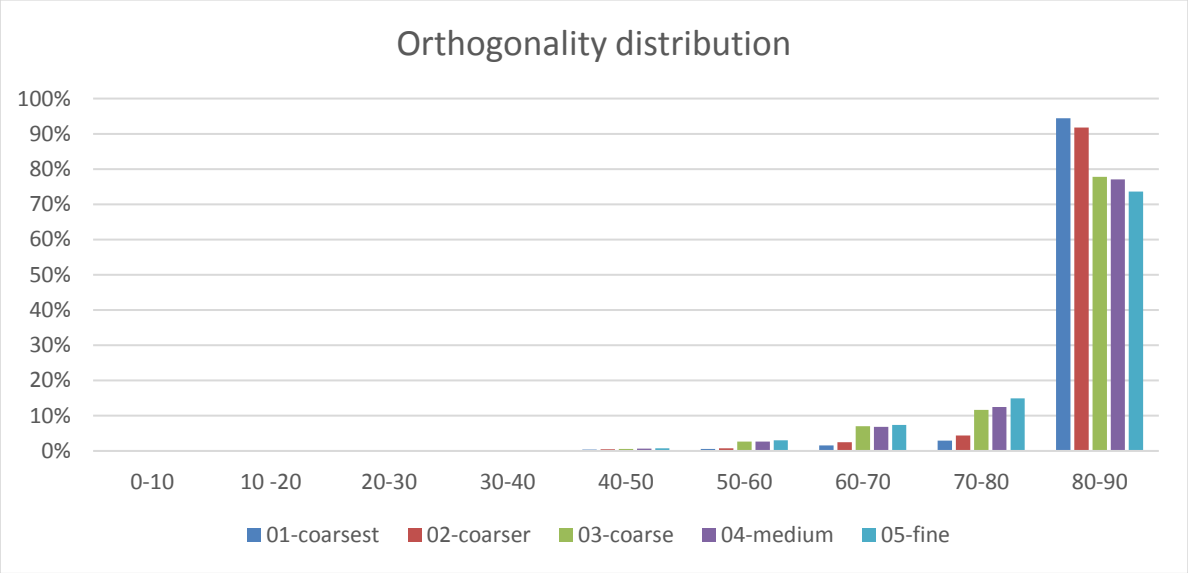

Figure 47: Orthogonality distribution for the different grids

In Figure 48 the distribution of the aspect ratio of the different grids is shown. The aspect ratio is calculated as the largest difference between the three dimensions of the cell. Usually aspect ratio of the cells is kept within reasonable bounds, but for example in the viscous layer high aspect ratio cells are expected. Mainly because there is one dominant flow direction in these cells, over which there is no rapid change. About the distribution the same thing can be said as for the visual inspection of the different grids, although there are similarities they are not exactly equivalent. This again will have influence on the scatter in the convergence diagram.

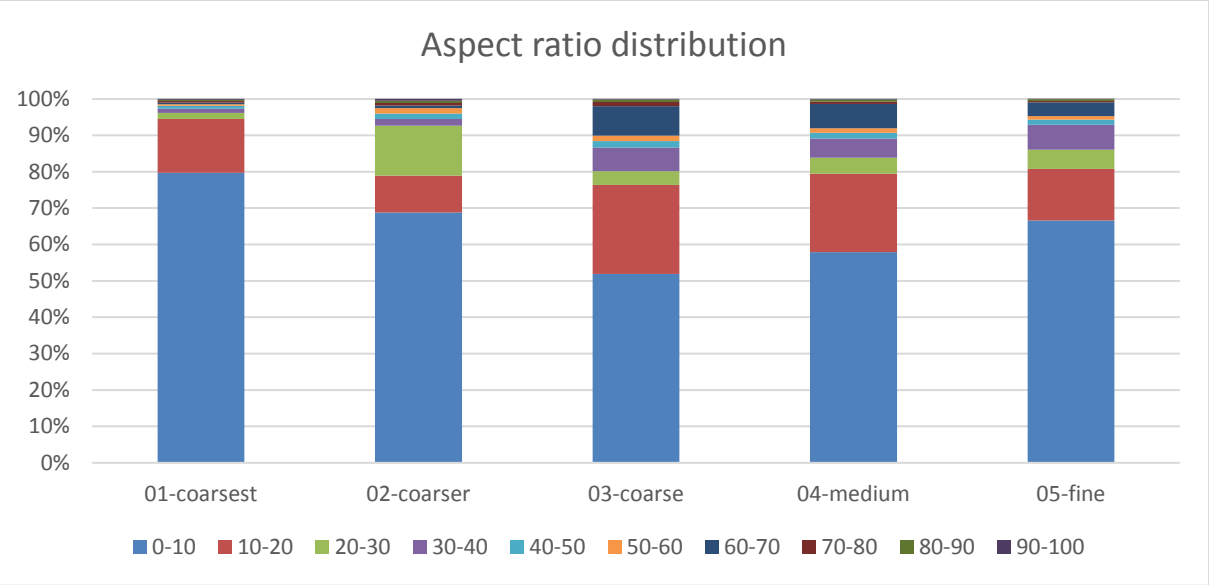

Figure 48: Aspect ratio distribution

Finally the expansion ratio of the grids are compared. The expansion ratio is defined as the largest size difference between two adjacent cells. In Figure 49 the distribution of this expansion ratio is shown for the five different grids. Most cells have an expansion ratio near 1 or near 2, which is caused by the diffusion rate throughout the grid. Because of the same diffusion rate on the different grids, the distribution of the expansion ratio is similar on the different grids.

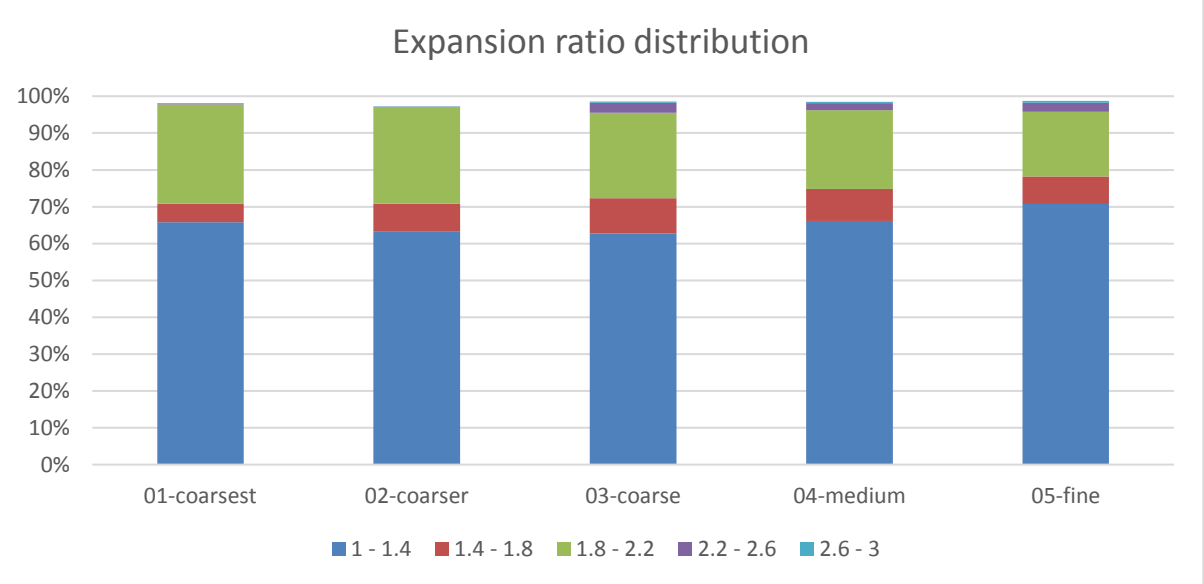

Figure 49: Expansion ratio distribution

In this section it has been tried to give some visual and quantitative description of the similarity of the grids. The comparison showed some similarity of the grids. As expected from an unstructured mesh the resulting mesh cannot be exactly similar and this will give some scatter in the result.

3.6.2 ERROR ESTIMATION

The full procedure proposed by Eca and Hoekstra involves many steps, Tao Xing and Frederick Stern give a good overview of the method, which is shown in Figure 50. First the grid convergence is determined based on equation (29. This assumes the error is a function of a constant α, the typical cell size of the grid h_i and the grid convergence factor p. Any integral or local flow quality can be described by ϕ_i, for which ϕ_0 is an estimate of the exact solution.

$$\epsilon_\phi \cong \delta_{RE} = \phi_i - \phi_0 = \alpha h_i^p \tag{29}$$

The goal is to find a function that describes the convergence with a minimal error. Therefore a minimum is sought for the least squares error estimation of equation (29), by solving for the minimum of equation (30). This is a weighted version where extra weight is added to the finer solutions based on a linear distribution. It is assumed that the finer simulations will result in a more accurate solution.

$$S_{RE}(\phi_0, \alpha, p) = \sqrt{\sum_{i=1}^{n_g} W_i * (\phi_i - (\phi_0 + \alpha h_i^p))^2} \tag{30}$$

According to the method, if the grid convergence factor is positive and larger than 2, there are two error estimators to choose from. A grid convergence factor with a higher order then the discretization method would be impossible, therefore the calculated grid convergence factor is replaced by 1 or 2.

$$\delta_1 = \alpha h_i \tag{31}$$

$$\delta_2 = \alpha h_i^2 \tag{32}$$

From these error estimators the one with the smallest standard deviation is used. Following the method as shown in Figure 50, the simulations showed a grid convergence factor over 2 and a standard deviation lower than a data range perimeter $\Delta_\phi = \frac{max(\phi_i) - min(\phi_i)}{n_g - 1}$, therefore the uncertainty can be calculated with equation (33) and a safety factor (F_s) of 3.

$$U_\phi(\phi_i) = F_s\epsilon_\phi(\phi_i) + \sigma + |\phi_i - \phi_{fit}| \quad (33)$$

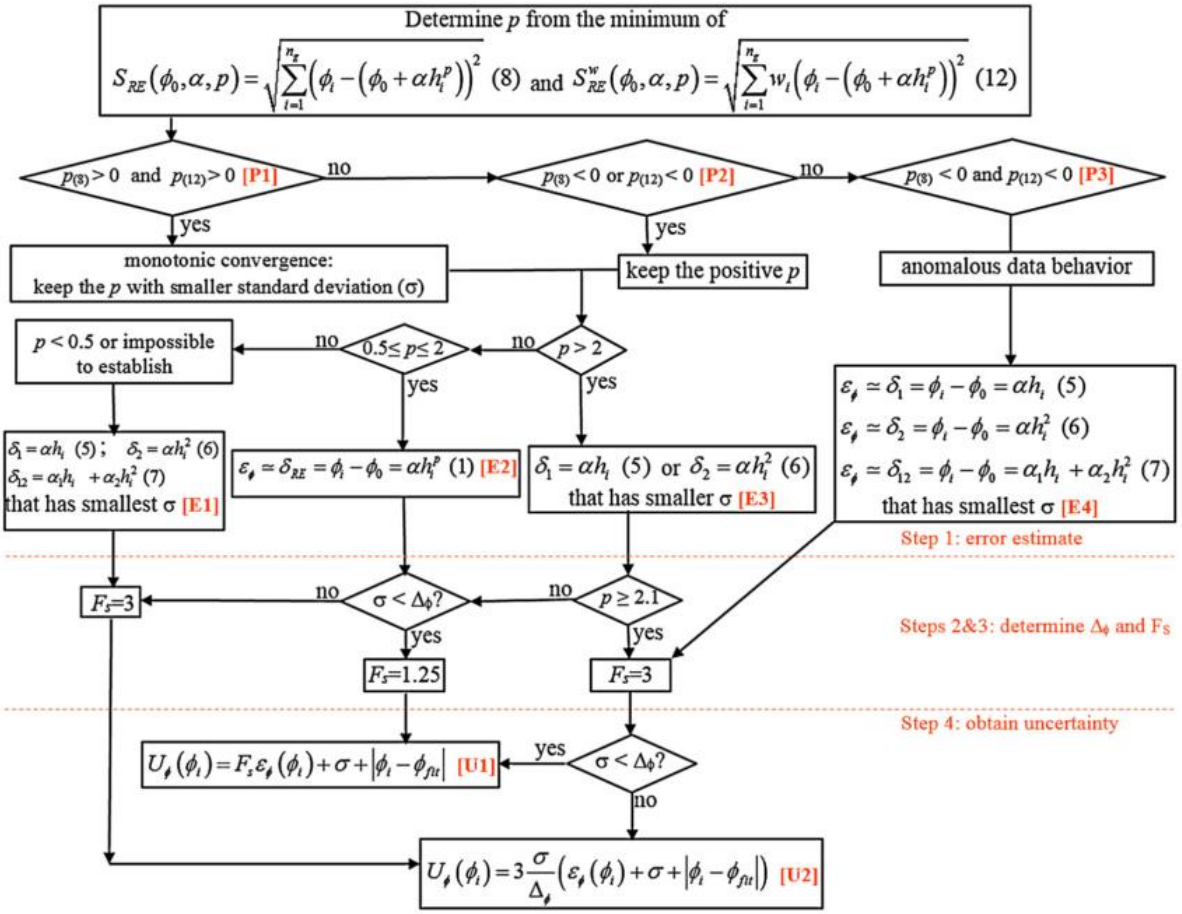

Figure 50: Overview of grid refinement method (Xing & Stern, 2015)

The calculated grid convergence was around 6. This is much higher than the order of the discretization method (AVLSMART for momentum and turbulence equation: third order combined with first order, BRICS for free surface: second order). A grid convergence factor (p) larger than the order of the discretization scheme, would underestimate the produced error. Therefore the method suggests using a defined order of convergence. The lowest standard deviation was found with the error estimator of equation (32, which uses a convergence factor of 2. The numerical results of this uncertainty study are shown in Table 7 and a visual interpretation can be found in Figure 51. The variables for the fitted curve are: $\alpha = 1.0181 * 10^3, \phi_0 = 5.6119 * 10^4$.

Table 7: Results of grid refinement study

Grid	h_i [-]	φ_i [kN]	U_φ [kN]	U_φ [%]
Coarsest	1.4352	58.430	6.870	11.76
Coarser	1.2594	57.740	5.216	9.03
Coarse	1.0187	56.644	4.066	7.18
Medium	0.9308	57.064	3.056	5.36
Fine	0.7590	56.947	2.366	4.15
Estimated solution	0	56.119	0	0

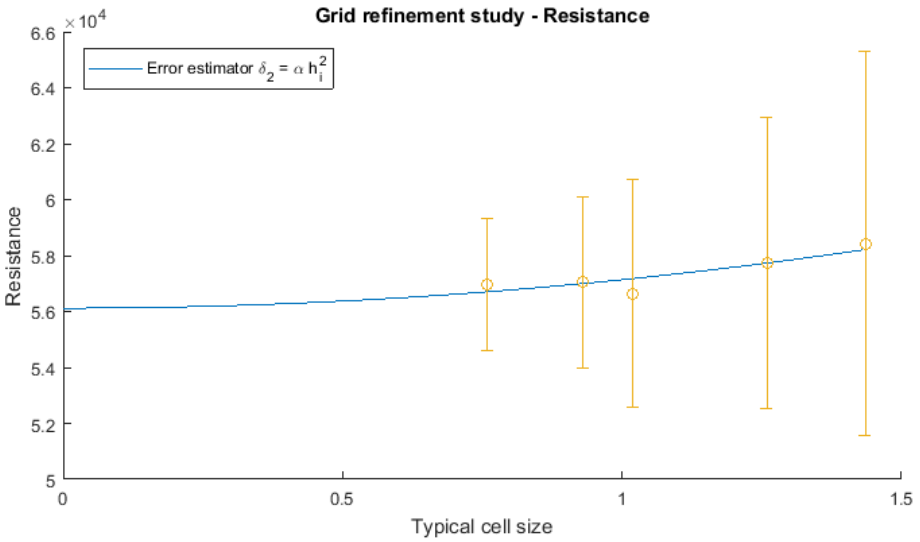

Figure 51: Grid refinement study on resistance

The calculated discretization uncertainty for the finest and medium grid is $\pm 4.15\%$ and $\pm 5.36\%$ respectively. Before the question arises what would be sufficient accuracy for the research, a critical note needs to be added to be added to the method. The grid refinement study assumes the only thing changing is the size of the cells. For structured grids this is difficult, for unstructured grids this is practically impossible. For grids to be fully geometrically similar each cell would need to be divided in eight cells. This leads to unrealistically large grids and is therefore impossible for this research. A grid triplet is needed for the estimate of the grid convergence, which would lead to a multiplication of 64 times the smallest grid. Although care has been taken in making the grids similar, the quantification of the geometric similarity showed significant differences between the grids. This probably results in scatter which can have positively or negatively affected the uncertainty estimation. So the result should not be used as an absolute value, more as an indication.

Furthermore most of the discretization schemes are of third order (turbulence equation, momentum equation), while the error is estimated with a second order error estimator. The error produced by the second and third order schemes will be between a combination of second and third order. A second order error estimator will overpredict the error and a third order error estimator will under predict the error. Because there is already a safety factor (of 3!) present, it could make more sense to under predict the error. Therefore a third order error estimator is proposed in equation (34). The system and uncertainty is calculated in a similar way as for the second order error estimator. The results of this study are shown in Table 8 and Figure 52.

$$\delta_3 = \alpha h_i^3 \quad (34)$$

Table 8: Grid refinement study with third order error estimator

Grid	h_i [-]	φ_i [kN]	U_φ [kN]	U_φ [%]
Coarsest	1.4352	58.430	5.957	10.20
Coarser	1.2594	57.740	4.076	7.06
Coarse	1.0187	56.644	2.771	4.89
Medium	0.9308	57.064	1.902	3.33
Fine	0.7590	56.947	1.345	2.36
Estimated solution	0	56.119	0	0

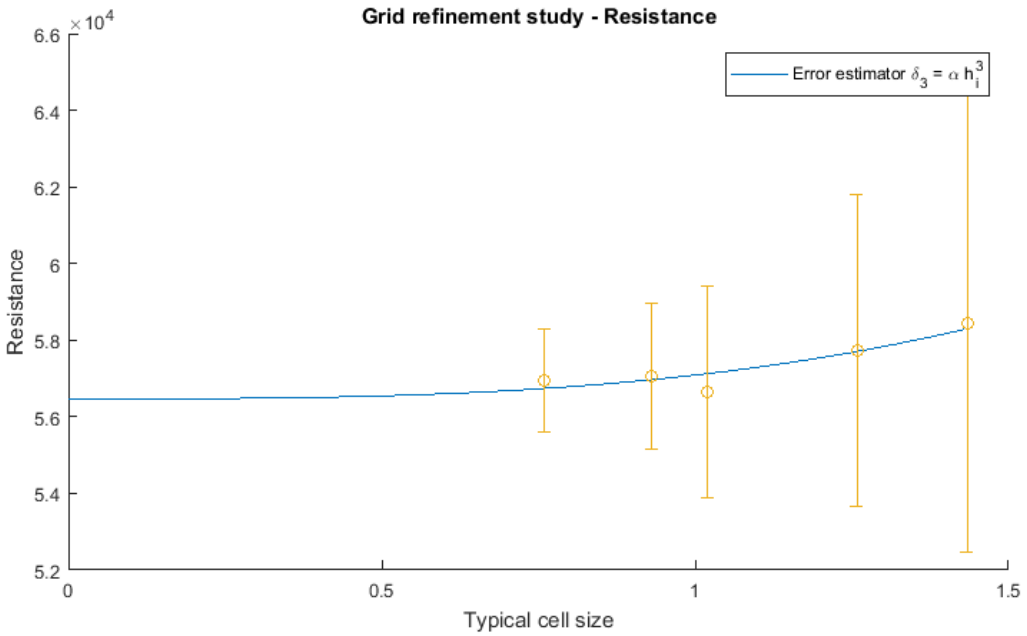

Figure 52: Grid refinement study based on third order error estimator

The estimated uncertainty of the simulation is significantly reduced. It is hard to say which of these methods is correct. The original paper only uses a second order method and does not mention a third order error estimator. However the use of the third order discretization schemes in the simulation suggests the use of a third order error estimator. This method still only provides an indication of the numerical uncertainty, as in this research it is impossible to only vary the grid size.

4. CONTROL STUDY

This section describes the different algorithms that have been tried and the criteria that led to the final algorithm. For all algorithms the goal, working principle, results and conclusion are discussed. The algorithms are tested at Froude 0.40 with 1 meter waves at an encounter frequency of $\omega_{enc} = 1.75\,{}^{rad}/_{s}$ unless stated otherwise. All dynamic Hull Vane runs are continued for 5 wave encounters, and the average will be taken over the last 3 wave encounters. As the sailing ship in waves is an unsteady process, the analysis is mostly done with video. Stills of the videos will be shown in this report. The videos are made by postprocessing the results with multiple Python scripts.

Four algorithms have been designed for various goals.

- Reduce pitch motion by control on pitch acceleration.
- Keeping a constant angle of attack based on the pitching velocity.
- Maximizing the thrust on the Hull Vane by a controlling on optimal angle of attack.
- Reduce pitching motion based on pitching velocity.

In this chapter the algorithms are tested and the results are analysed. Before starting the algorithm design a short pre study is done, to measure the operating conditions (lift/drag) of the dynamic Hull Vane. This is shown in appendix C.

4.1 CONTROL ON PITCH ACCELERATION

The added wave resistance of a ship is related to the relative motion of the ship to the water and the motion of the ship (Blok, 1993). If the dynamic Hull Vane can minimize the ship motion, the added resistance that is caused by the ship motion will also be reduced. Reduction of the pitch motion can be achieved by controlling the lift of the Hull Vane.

As explained in section 2.3.3 the flow on the Hull Vane will usually have a positive vertical component, therefore positive lift on the Hull Vane will produce thrust, and negative lift will produce extra drag. This ‘pulling’ force on the Hull Vane will create extra drag and displacement. For this algorithm to decrease the total resistance, the additional drag of the Hull Vane will need to be smaller than the added wave resistance component it reduces. This could add additional resistance and is inefficient with the asymmetric profile. Therefore this algorithm will focus on reducing the pitch motion by only producing a positive vertical force. As a consequence only the bow up motion can be actively dampened. During the bow down motion the algorithm can only try to minimize the lift.

4.1.1 SETUP

The algorithm will increase the angle of attack of the dynamic Hull Vane when the ship is accelerating bow up. When the ship is accelerating bow down the dynamic Hull Vane will be put in a neutral position. A schematic representation of this algorithm is given in Figure 53. This will minimize the pitch motion of the ship within the boundary conditions of the defined maximum and minimum angles.

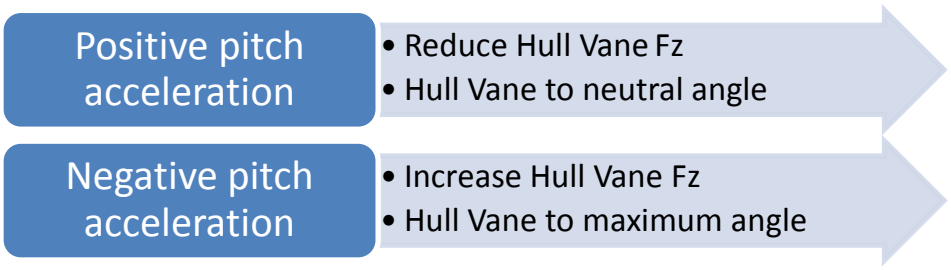

Figure 53: overview of resistance reduction algorithm based on pitch control

The maximum angles of the Hull Vane to the ship are manually set and the velocity of the Hull Vane is limited to a realistic level (36 $^{deg}/_{s}$). To check the influence of the minimum and maximum angle, several simulations with different parameters are run. The angles are defined in the ship axis system, with the same orientation as the global axis system. A neutral setting of 4° indicates a 4° angle to the ship with the leading edge down, a maximum of -7° is a 7° angle of the Hull Vane to the ship with the leading edge up.

4.1.2 RESULTS

In Table 9 the results are shown for different limits on the maximum angles of the dynamic Hull Vane. It shows that a significant reduction in pitch motion is possible, while there is little influence on the total resistance.

Table 9: overview of dynamic Hull Vane results with a variation in control parameters

	$\overline{R_{total}}$ [kN]	$\overline{R_{total}}$ [%]	$\overline{F_x^{HV}}$ [kN]	$\overline{F_x^{HV}}$ [%]	$\hat{\theta}$ [deg]	$\hat{\theta}$ [%]
Static	118.34	0%	10.58	0%	2.26	0%
N=4° M=-3°	118.49	0.1%	10.69	1.1%	2.05	-8.9%
N=4° M=-7°	117.57	-0.7%	8.49	-19.7%	1.91	-15.8%
N=4° M=-10°	117.55	-0.7%	5.93	-43.9%	1.75	-21.5%
N=10° M=-7°	118.09	-0.2%	6.43	-39.1%	1.66	-25.2%

With the higher limits the dynamic Hull Vane is able to further increase and decrease the lift, which gives more possibility to control the pitching of the ship. When optimizing this control algorithm up to 25% reduction of pitch amplitude is possible, while the total resistance is similar. The increased lift decreases the thrust on the Hull Vane, because the drag of the Hull Vane is increased. As shown in the literature study (section 2.3.2) the Hull Vane produces the most thrust for a relatively low angle of attack. This is confirmed by this iteration on the dynamic Hull Vane, when the lowest limits are set the thrust on the Hull Vane is the largest.

A good algorithm will not only work at the natural frequency, but will also show effect at other frequencies. To verify that the working principle of this algorithm is not only effective at one wave condition, a second simulation is done at an encounter frequency of $\omega_{enc} = 2.25\,^{rad}/_{s}$. This frequency is well away of the natural frequency of the ship, so the ship motions are significantly lower. At the higher frequency the ship motions will cause a smaller part of the added wave resistance, and a larger part will be caused by the difference in relative surface elevation.

The results of the two wave conditions are shown in Table 10. The comparison is done with moderate settings of the previously tested variation(N=4° M=-7°), to check for robustness instead of limits.

Table 10: Comparison for one algorithm in two different conditions

N=4° M=-7°	$\overline{R_{total}}$ [kN]	$\overline{R_{total}}$ [%]	$\overline{F_x^{HV}}$ [kN]	$\overline{F_x^{HV}}$ [%]	$\hat{\theta}$ [deg]	$\hat{\theta}$ [%]
$\omega = 1.75\,^{rad}/_{s}$	117.57	-0.7%	8.49	-19.7%	1.91	-15.8%
$\omega = 2.25\,^{rad}/_{s}$	102.85	1.2%	7.27	-27.0%	0.61	-21.5%

4.1.3 ANALYSIS

As seen, the reduction in ship motion does not result in a significant reduction of the total resistance. The damping of the ship motions should lead to a decrease in added wave resistance, if it is caused by the ship motions. Therefore the resistance of the hull is compared to the flat water resistance of the hull and shown in Table 11. Now an analysis can be made of the added wave resistance.

Table 11: Comparison of added wave resistance

	$\overline{R_{total}}$ [kN]	$\overline{F_x^{HV}}$ [kN]	$\overline{R_{hull}}$ [kN]	$\overline{R_{AW}}$ [kN]	R_{AW} [%]	$\hat{\theta}$ [%]
Flat water	91.93	8.82	100.75	0		
Static	118.34	10.57	128.92	28.167	0%	0%
N=4° M=-3°	118.49	10.69	129.19	28.44	1.0%	-8.9%
N=4° M=-7°	117.57	8.49	126.06	25.32	-10.1%	-15.8%
N=4° M=-10°	117.55	5.93	123.49	22.74	-19.3%	-21.5%
N=10° M=-7°	118.09	6.43	124.52	23.78	-15.6%	-25.2%

Only the resistance of the hull is compared, so a decrease of thrust on the Hull Vane does not lead to an increase in added wave resistance. A change in mean pitch angle could also lead to a change in resistance, but as the different mean pitch angle is also a result of the waves or the control algorithm this is included in the added wave resistance. The reduction in added wave resistance caused by a change in mean trim cannot be extrapolated to higher waves. The results show a significant decrease in added wave resistance, comparable to the decrease in ship motions. If the added wave resistance caused by the ship motions would be a larger portion of the total resistance, the reduction in ship motions could lead to a larger decrease in the total resistance.

The comparison of added wave resistance is also done for the higher encounter frequency and shown in Table 12. Since the encounter frequency is higher than the natural frequency of the ship, the ship motions and added resistance are significantly lower. The algorithm shows it can dampen a larger percentage of the ship motions. Since the maximum and minimum angles of the dynamic Hull Vane are the same, the amplitude in vertical force is similar. It is not the same as the other wave condition because the angle of attack changes more when the vertical velocity is larger. The range in lift is relatively larger to the smaller motion, therefore it has a larger potential to damp the motions. In other words, the range in lift is relatively larger compared to the wave exciting forces. The relative reduction in wave added resistance is slightly larger, so the ship motions still cause a significant part of the added wave resistance. The total resistance has been increased, since the absolute reduction in added wave resistance is lower than the change in thrust on the Hull Vane.

Table 12: Added resistance for two different wave conditions

N=4° M=-7°	$\overline{R_{total}}$ [kN]	$\overline{R_{total}}$ [%]	$\overline{R_{hull}}$ [kN]	$\overline{R_{AW}}$ [kN]	$\overline{R_{AW}}$ [%]	$\hat{\theta}$ [deg]	$\hat{\theta}$ [%]
$\omega = 1.75\,{}^{rad}/_{s}$	117.57	-0.7%	126.06	25.32	-10.1%	1.91	-15.8%
$\omega = 2.25\,{}^{rad}/_{s}$	102.85	1.2%	110.12	9.368	-13.6%	0.61	-21.5%

In Figure 54 an overview of some simulation quantities is shown, for an algorithm with a neutral setting of 10° and a maximum angle of -7°. The figure shows a comparison between the static Hull Vane (red) and dynamic Hull Vane (blue) for: pitch, heave, Hull Vane angle to horizontal, Hull Vane vertical force, Hull Vane horizontal force and total resistance. The mean and difference between highest and lowest of three wave periods (white parts) is shown in text. The measured force on the Hull Vane includes heavy oscillations, this is caused by the numerical method. To make the control easier and avoid overshoot, the rotational velocity of the Hull Vane is limited. This allows for high accelerations, which results in peaks in the force signal on the Hull Vane. It is assumed these oscillations have a negligible effect on the mean over multiple periods.

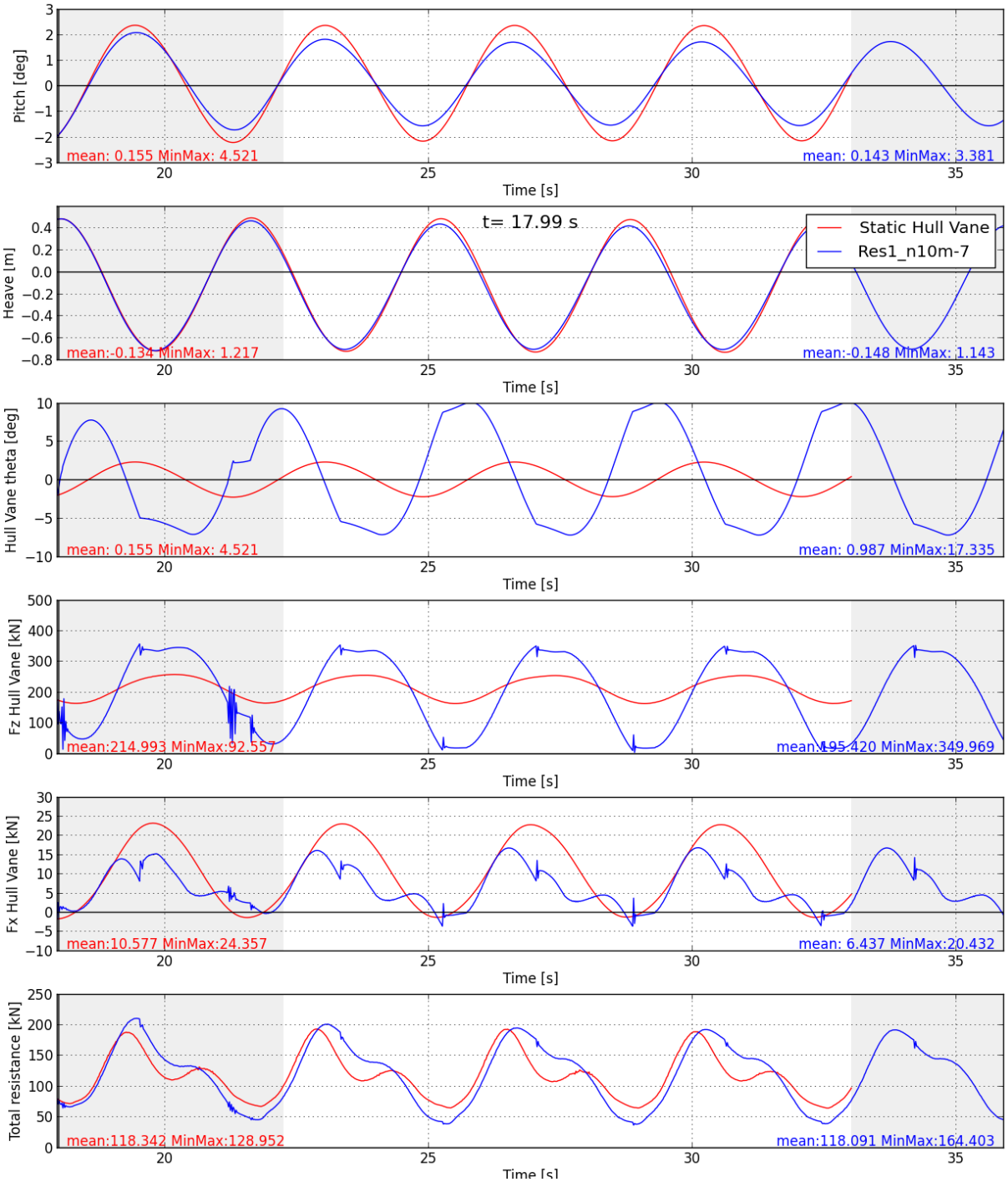

Figure 54: overview of simulation quantities for neutral=10° max=-7°

For the total resistance a period can be observed where the ship with a static Hull Vane has a lower resistance and a period where the ship with static Hull Vane has a higher resistance. At these instances the reduction of ship motions leads to a difference in resistance. Part of this can be explained by the change in thrust on the Hull Vane (5-15 kN), but a larger part is caused by the different resistance of the hull (25-40 kN). The simulations showed that the resistance difference increases when the motions are damped more.

The effect of the induced drag can be seen when the dynamic Hull Vane has the lowest angle of attack, for example at 25.5 seconds in Figure 54. Here the dynamic Hull Vane produces almost no lift and consequentially almost no thrust. The static Hull Vane does produce a significant amount of lift, and some of that will produce thrust. But due to the induced drag the net thrust force is around zero, equal to the dynamic Hull Vane. The lift in these instances can be used for motion control of the ship, but not for thrust, therefore a larger vertical flow component would be necessary.

For this control algorithm the streamlines relative to the Hull Vane are shown in Figure 55 and Figure 56 at t=27 seconds. The streamlines of relative velocity to the Hull Vane make it possible to see how the angle of attack changes when the Hull Vane has vertical velocity. At this instance the ship has a pitch acceleration bow up, which is counteracted by increasing the lift on the Hull Vane. The 7 degree angle relative to the ship results in approximately 5 degree angle to the horizontal. The dynamic Hull Vane has a 7 degree higher angle of attack than the static Hull Vane, which results in about 100 kN extra lift as shown in Figure 54. This extra lift is caused by the higher pressure difference, and the effect of this can also be seen at the free surface of Figure 55 and Figure 56.

In the same figure it can be seen that when the ship is accelerating bow down, the dynamic Hull Vane almost reduces the lift to zero. This is the maximum influence the dynamic Hull Vane can have on the bow down motion of the ship without creating a negative lift. A maximum angle of 10 degrees backwards relative to the ship is also tried, but this led to separation at the top of the foil, unsteady lift and large resistance on the Hull Vane.

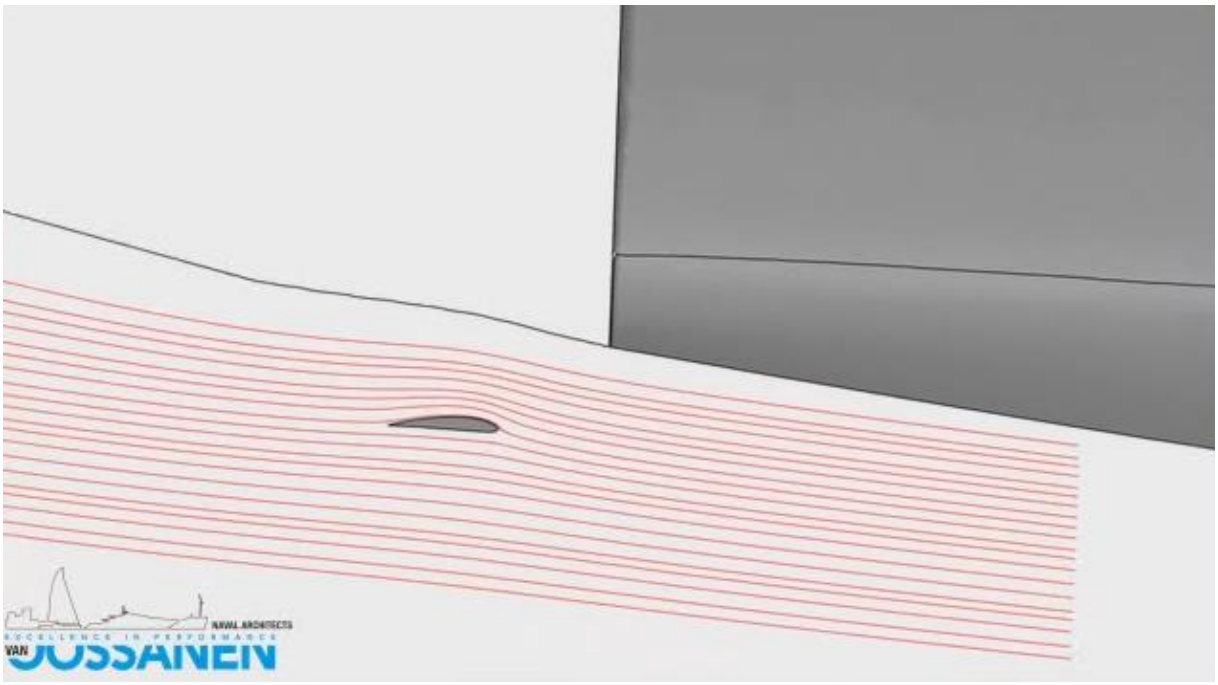

Figure 55: Streamlines relative to static Hull Vane at t=27

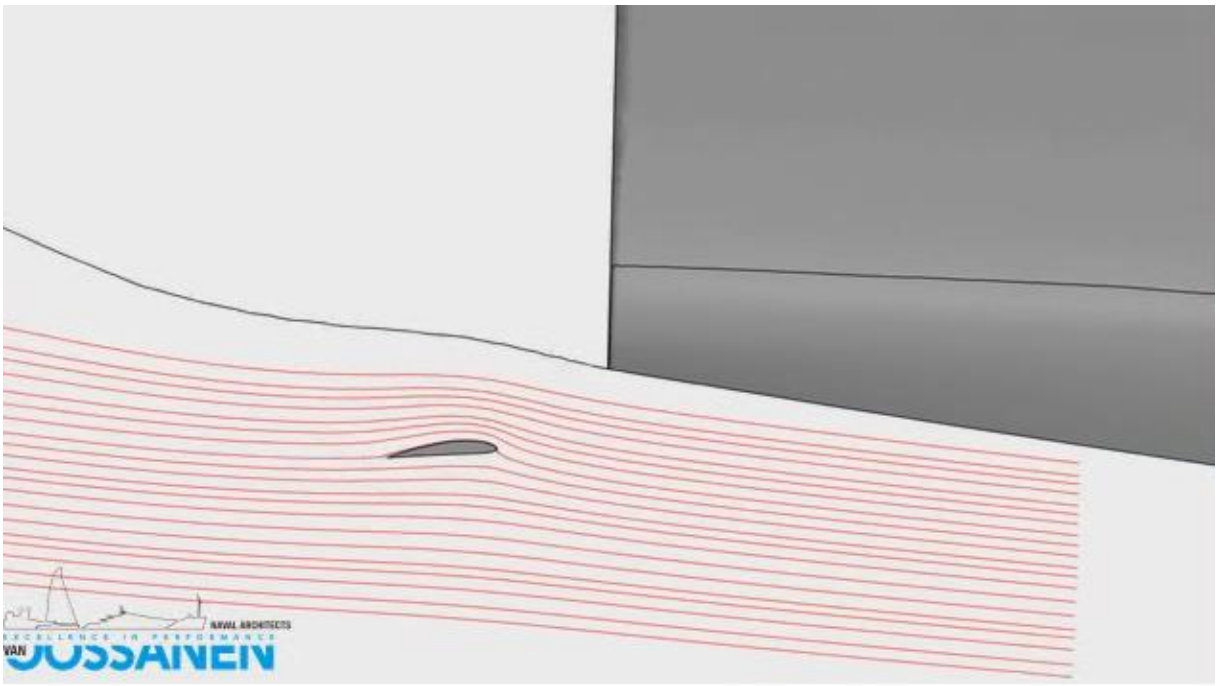

Figure 56: Streamlines relative to dynamic Hull Vane at t=27

4.1.4 CONCLUSION

With a control algorithm based on the pitch acceleration of the ship, the ship motions and added wave resistance can be reduced significantly for the two tested wave conditions. The penalty is a decrease in thrust on the Hull Vane which cancels out the gain in reduced added wave resistance. The influence on total resistance is therefore negligible for these wave conditions. When the added wave resistance is a larger part of the total resistance and a similar reduction of ship motions can be achieved, the total resistance might be reduced.

While optimizing this algorithm, different settings have been tested. These showed that the damping of ship motions can be increased by allowing larger limits on the maximum Hull Vane angles. An optimum can be found depending on the demands and limits of the ship and crew.

4.2 CONSTANT ANGLE OF ATTACK BASED ON SHIPMOTION

The literature review in section 2.2.4 showed that the vertical motion of the Hull Vane had the largest influence on the change of angle of attack. A control algorithm is designed based on this movement to see if the dynamic Hull Vane can have a constant angle of attack. In practice this could be used to have a constant lift on the Hull Vane. This control algorithm would also be the basis for a control like the oscillating foil, as it is based on equation (3) with a constant angle of attack. This algorithm will also check if the angle of attack can be estimated with the pitch velocity of the ship. If this algorithm can keep a constant angle of attack, it can be adjusted to have an angle of attack variation as requested for the oscillating foil (although this is not a goal anymore).

4.2.1 SETUP

For this algorithm the change in angle of attack is based solely on the vertical velocity of the Hull Vane caused by pitch velocity. The vertical velocity of the Hull Vane is calculated with the pitch velocity of the ship as in equation (35.

$$V_{Z_{HV}} = (X_{HV} - LCG)\dot{\theta}_{ship} \quad (35)$$

The change in angle of attack is then calculated with equation (36). This change is applied relative to the pitch angle of the ship.

$$\alpha_n = atan2\left(\frac{V_{Z_{HV}}}{V_x}\right) \quad (36)$$

With this algorithm the dynamic Hull Vane will follow the change in angle of attack as calculated by the pitch velocity. If the prediction of change in angle of attack can be based on the pitch velocity as shown in section 2.2.4, the Hull Vane will now have a constant angle of attack.

4.2.2 RESULTS

In Table 13 an overview of the results of this control algorithm are shown. As seen the total resistance, added wave resistance and ship motions are increased. The average thrust on the Hull Vane is not increased and the increase in pitch amplitude will have increased the added wave resistance, as shown in the prestudy in appendix C.

Table 13: overview of results of angle of attack estimator

	$\overline{R_{total}}$ [kN]	$\overline{R_{total}}$ [%]	$\overline{R_{hull}}$ [kN]	$\overline{R_{AW}}$ [kN]	$\overline{R_{AW}}$ [%]	$\hat{\theta}$ [deg]	$\hat{\theta}$ [%]
static	118.342	0%	128.92	28.17	0%	2.26	0%
AOA estimator	121.37	2.6%	129.63	28.88	2.5%	2.5	12.4%

4.2.3 ANALYSIS

The goal of this algorithm was to keep a constant angle of attack, which would result in a constant lift on the Hull Vane. The same simulation quantities as before are plotted in Figure 57, which include the vertical force on the Hull Vane. The amplitude of the vertical force is slightly lower for the dynamic Hull Vane but still around 40 kN. This means the angle of attack is not kept constant by the algorithm, but changes with an amplitude of around 2° (as in Figure 70). The largest change in angle of attack might be caused by the vertical motion, but the total change in angle of attack can't be predicted by this.

The reason for the difference between the theory from section 2.2.4 and the practice in this section, might be explained by the difference in ship motions with and without Hull Vane. The measurements of change in angle of attack form paragraph 2.2.4 were done without a Hull Vane, what resulted in larger ship motions (≈20%) and therefore a larger change in angle of attack caused by the vertical velocity. The angle of attack should be measured for a ship moving similar to a ship with a dynamic Hull Vane, but the measured flow field should be undisturbed. This could give a better basis for an algorithm based on ship motions, but would be an iterative process.

Further tuning could be done to increase the precision of this method. This would be arbitrary tuning not based on the initial theory. Based on the results and the questionable physical background, the optimization of this algorithm is not continued. This also ends the investigation into the use of the oscillating foil principle, since the ship motions cannot be used for a valid estimation of the angle of attack.

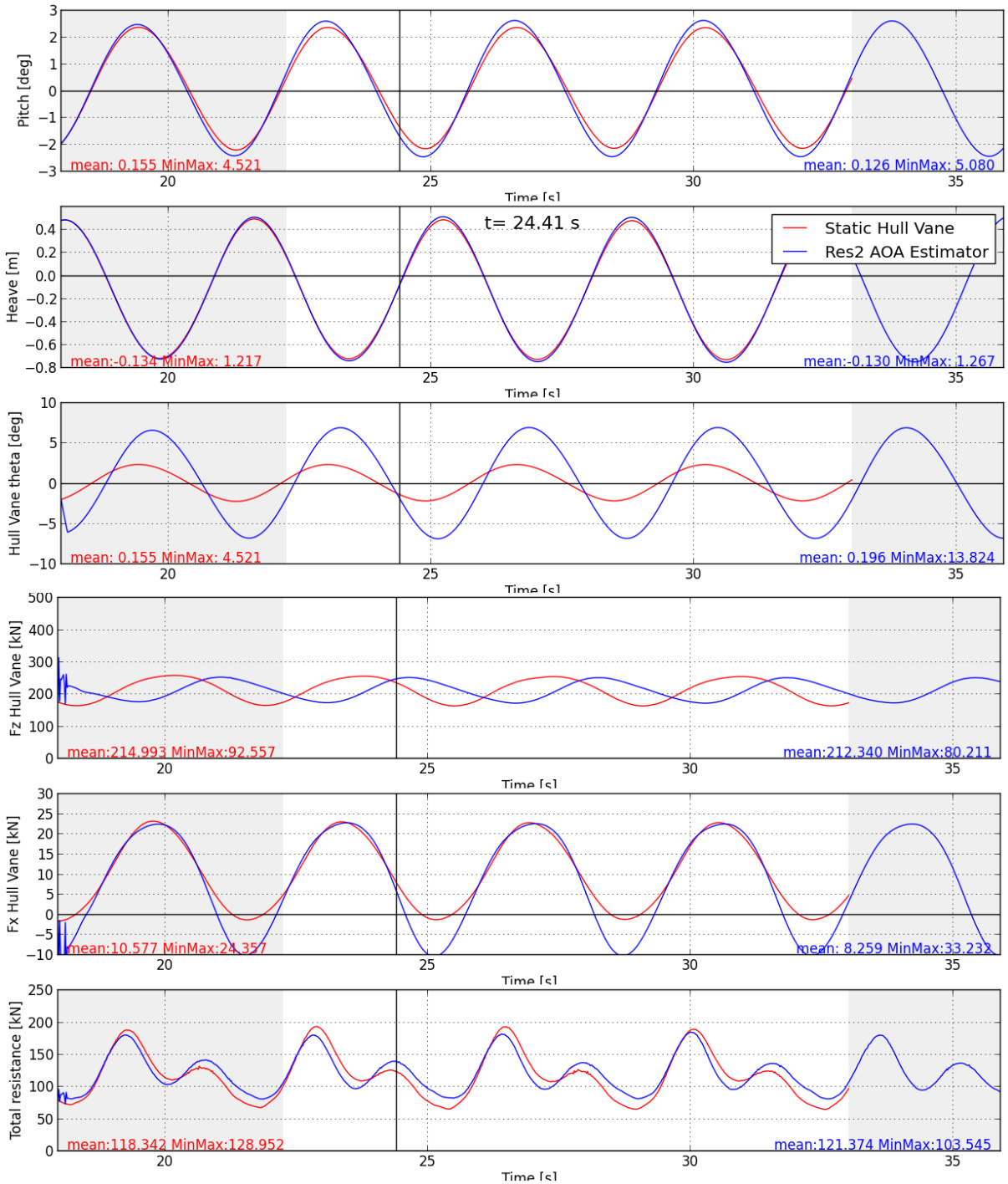

Figure 57: overview of simulation quantities for control based on angle of attack estimation

4.2.4 CONCLUSION

In theory, a control algorithm based on a estimation of the change in angle of attack could be able to keep a (relative) constant angle of attack during the waves. The literature review suggested that the largest change in angle of attack is caused by the vertical motion of the Hull Vane. This control algorithm was based on a estimation on the change of angle of attack due to the vertical velocity. The algorithm slightly lowered the variation in vertical force, but not nearly enough to call it a constant angle of attack. The control based on ship motions is not sufficient for creating a constant angle of attack, therefore it is also not sufficient for using it as control for the oscillating foil principle.

4.3 MAXIMUM THRUST

The previous algorithms focussed on motion reduction or a constant angle of attack on the Hull Vane. This algorithm will focus on a maximum thrust on the Hull Vane based on the 3D lift theory as explained in paragraph 2.3.2.

4.3.1 SETUP

In paragraph 2.3.2 an optimal angle of attack to get maximum thrust was calculated for a free stream angle of 5°. This theoretical optimal angle of attack can be calculated for every free stream angle. When the free stream angle is known, the dynamic Hull Vane can go to the defined optimal angle of attack. With the current algorithm the free stream angle is estimated based on the measured vertical force. The lift coefficient is calculated as in equation (37), and based on the lift coefficient the current angle of attack is calculated as in equation (38). The vertical force is not equal to the lift but dependent of the free stream angle, this will be fixed with one additional iteration. The first approximation of the free stream angle is then used to calculate the lift based on the measured horizontal and vertical force. This iterated lift is then again used to calculate the lift coefficient.

$$C_L = \frac{F_z}{0.5 * \rho * v^2 * S} \tag{37}$$

From the lift coefficient we can estimate the angle of attack as in equation (38). This equation is based on rewriting equation (12). The measured lift coefficient the 2D lift coefficient and the 2D zero angle of attack lift coefficient are respectively expressed by: C_L, C_l, C_{l0}. The 2D lift coefficients are determined in 2.3.1.

$$\alpha = \frac{1}{C_l} * \left(C_L * \frac{AR + 2}{AR} - C_{l0} \right) \tag{38}$$

Combined with the current angle of the dynamic Hull Vane the flow angle to the horizontal can be calculated. To test this method a flat water simulation is done in which the ship is fixed and the angle of the Hull Vane is varied from 5° to -15°. For angles of attack between 0° and 7° the estimated flow angle was within a spread of 1°. This range of relative error seems reasonable, in comparison to the control precision of an actual dynamic Hull Vane. This is a relative error of the method, the absolute error of this method could not be estimated from this. The absolute error could be calculated with the information about the flow field, but would be different per wave condition and ship speed, therefore it would require extensive tuning.

In Figure 58 the calculated optimal angle of attack and the linear approximation for the control are shown. Based on the estimated flow angle and this linear approximation an optimal angle of attack is calculated, as in equation (39).

$$\boldsymbol{\alpha_{opt} = -5 + 1.4 * \gamma_{free}} \quad \textbf{(39)}$$

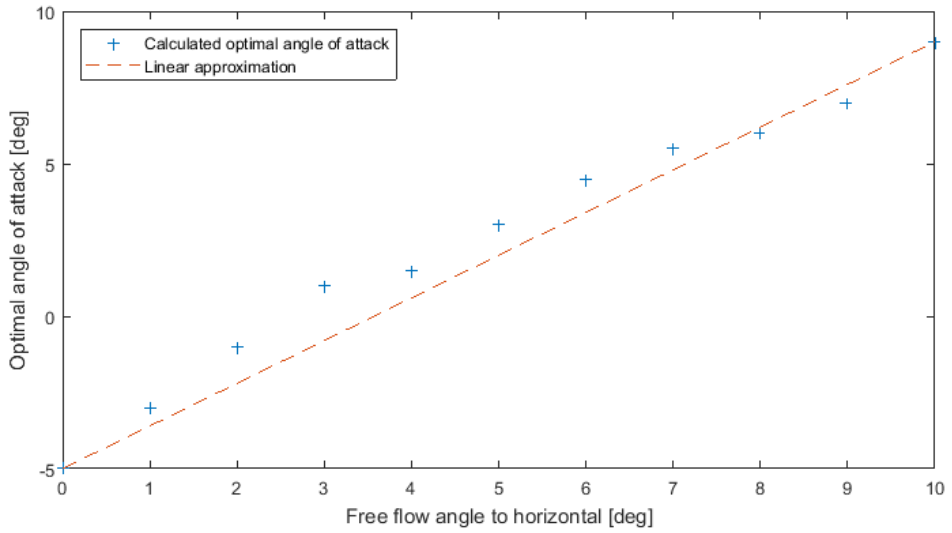

Figure 58: Linear approximation of optimal angle of attack

The change in Hull Vane angle is now based on the measured vertical force. As seen in previous algorithms, a sudden change in Hull Vane angle leads to a peak in the forces on the Hull Vane. The numerical method will always output peaks in the force measurement for sudden changes in Hull Vane acceleration, which makes the control unstable. The oscillations in the vertical force are filtered out by taking a five point derivative over the average of the previous six points and extrapolating this to the current measurement. So the next Hull Vane angle is not actually based on the current measurement but on a extrapolation of the previous six points. A schematic representation of this filtering is shown in Figure 59, in which the stars represent the average value of two measurements as in equation (40). The fifth order derivative and extrapolation are shown in equation(41). No investigation into the performance of multiple filtering algorithms has been done, this method proved sufficient for an initial estimate of the performance of this control algorithm.

$$\boldsymbol{f^{i^*} = \frac{f^i + f^{i-1}}{2}} \quad \textbf{(40)}$$

$$f^{0^*} = f^{-1^*} + 1.5 * \left(\frac{25}{12} * f^{-1^*} - 4 * f^{-2^*} + 3 * f^{-3^*} - \frac{4}{3} * f^{-4^*} + \frac{1}{4} * f^{-5^*}\right) \quad (41)$$

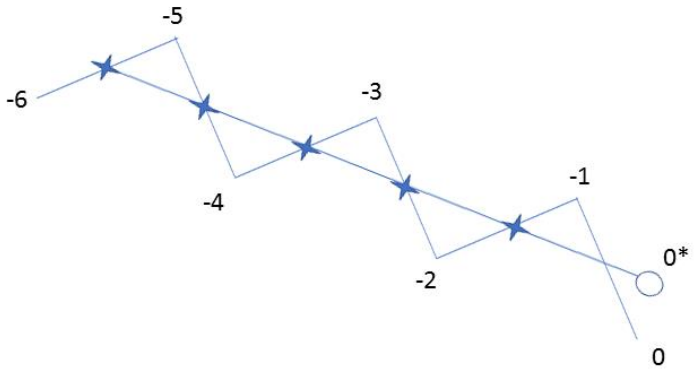

Figure 59: Schematic representation of the five point average derivative

4.3.2 RESULTS

In Table 14 an overview of the results of this algorithm is shown. It shows that the mean thrust of the Hull Vane has decreased with this algorithm. The total resistance is slightly reduced while the pitch motion is slightly increased. The decrease in total resistance could also be caused by the change in mean pitch angle of the ship, which is 0.1° higher with the dynamic Hull Vane. The goal of this algorithm was to maximise the thrust on the Hull Vane but it did not succeed. This algorithm was also tested at an encounter frequency of $\omega_{enc} = 2.25\,{}^{rad}/_{s}$, as shown in Table 15 it gave a similar result.

Table 14: Overview of results of maximum thrust algorithm

	$\overline{R_{total}}$ [kN]	$\overline{R_{total}}$ [%]	$\overline{F_x^{HV}}$ [kN]	$\overline{F_x^{HV}}$ [%]	$\hat{\theta}$ [deg]	$\hat{\theta}$ [%]
static	118.342	0%	10.58	0%	2.26	0%
Max thrust	117.57	-0.6%	8.33	-21.2%	2.34	+3.7%

Table 15: Overview of results of maximum thrust algorithm, at $\omega_{enc} = 2.25\,{}^{rad}/_{s}$

	$\overline{R_{total}}$ [kN]	$\overline{R_{total}}$ [%]	$\overline{F_x^{HV}}$ [kN]	$\overline{F_x^{HV}}$ [%]	$\hat{\theta}$ [deg]	$\hat{\theta}$ [%]
static	101.645	0%	9.952	0%	0.76	0%
Max thrust	100.625	-1.0%	8.558	-14.0%	0.82	+5.7%

4.3.3 ANALYSIS

In Figure 60 an overview of the simulation quantities is shown. Despite the filtering there is still an oscillation of up to 40kN in the vertical force of the Hull Vane. Since the angle of the Hull Vane is based on this signal there can be oscillations on the angle of the Hull Vane to. The signal of the angle of the Hull Vane seems smooth in this figure, only zoomed in to individual time steps the difference in acceleration can be observed. The oscillations in measured vertical force are higher than the oscillations in Hull Vane angle, the filtering cuts away most of the oscillations. Since the oscillations in Hull Vane are limited, it is assumed these oscillations have no significant effect on the average of the system.

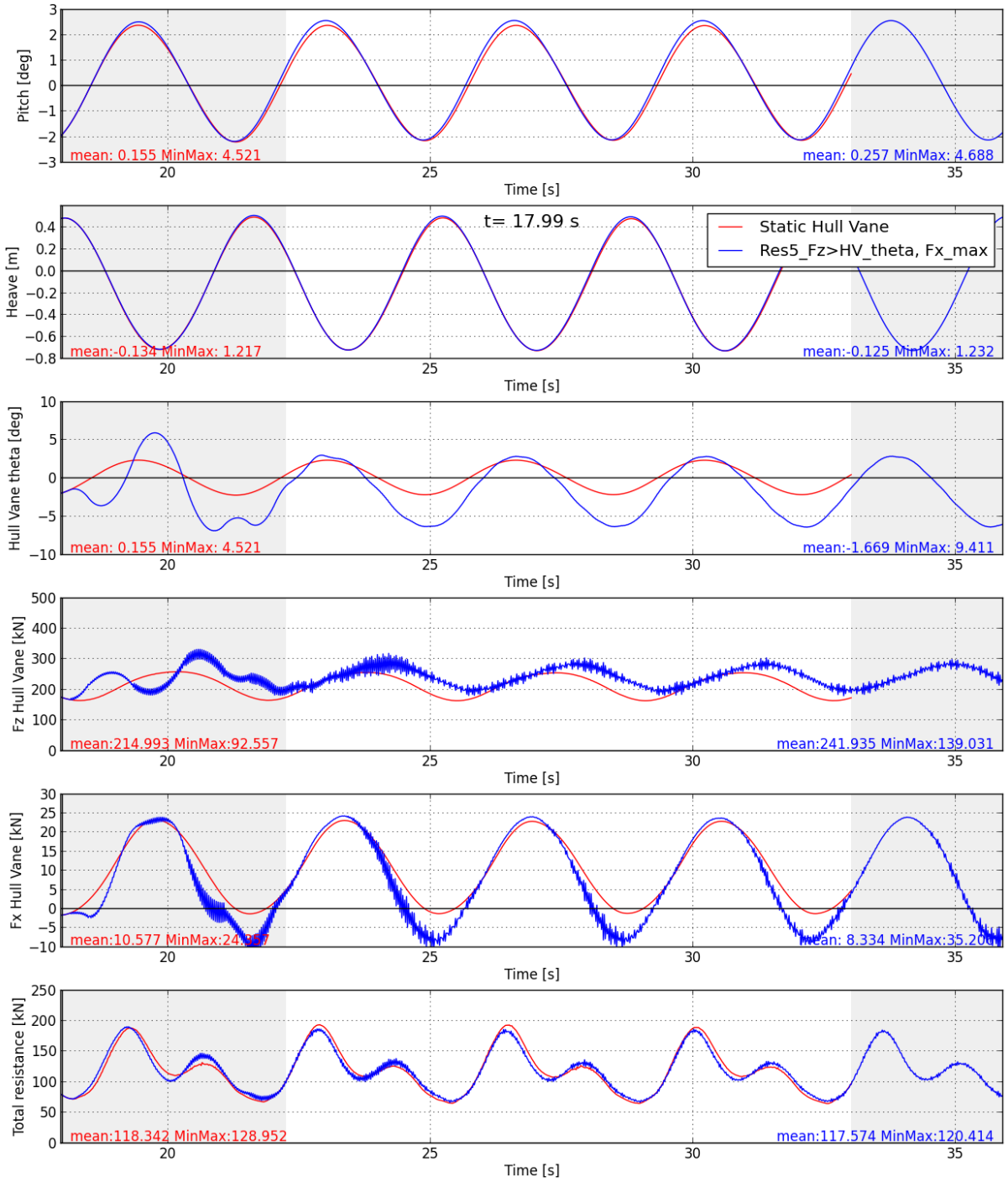

Figure 60: Overview of simulation quantities for maximize thrust algorithm

This algorithm focusses on maximum thrust production of the Hull Vane, but still has a lower mean thrust then the static Hull Vane. Several factors influence the position of the dynamic Hull Vane and the error could be a summation of those. The estimation of the angle of attack showed a reasonable accuracy for moderate Hull Vane angles (0°-7°). Within these boundaries, the lift is fairly linear with the angle of attack, and the approximation will only have about a 1° relative error. Near the boundaries, the lift will become more non-linear and the linear estimation will not accurately predict the angle of attack. Equation (38) assumes an elliptical circulation distribution, which is impossible for a square foil. A second source of error is in the calculation of the optimal angle of attack. One of the coefficients in the induced drag coefficient is the “planform efficiency factor”, which is assumed to be 0.7 in paragraph 2.3.2. This assumption influences the induced drag coefficient and the optimal angle of attack.

4.3.4 CONCLUSION

This section showed an algorithm which should produce maximum thrust on the dynamic Hull Vane. The control was based on a measurement of lift forces on the Hull Vane, this meant filtering was necessary to get a stable control. The result did not show an improvement in thrust of the Hull Vane and only a marginal reduction in total resistance. The combined errors between theory and practice make the method not precise enough. Further tuning could improve this method but from this first estimation it is clear that no large gains in thrust are possible when compared to the static Hull Vane. A foil that would produce less induced resistance at high angles of attack could benefit from this algorithm, when tuned accordingly.

4.4 VERTICAL VELOCITY DAMPING

The first algorithm showed potential for motion damping with little influence on the total resistance. Based on the previous results a new algorithm is designed which combines several elements of the previous algorithms. Since the previous algorithms showed potential in motion reduction, this algorithm will focus on motion reduction. The first algorithm showed the best motion reduction, but with a method which would require tuning. The second method has the most physical basis, as velocity is directly linked to a change in relative flow direction, but the control method didn't show any motion or resistance reduction. The last algorithm showed that no large increase in thrust on the Hull Vane is possible with the current foil. This control algorithm will continue with the relative flow direction change as calculated with the second algorithm, but will use it to minimize the ship motions as in the first algorithm.

4.4.1 SETUP

The change in angle of attack (α_n) is calculated in the same way as for the second algorithm (equation (35) and (36). The difference is in the control that is applied based on this angle of attack change, which is based on equation (42). When the ship is pitching bow up (negative pitching velocity), the Hull Vane has a negative vertical velocity and its angle of attack will increase. With this algorithm the dynamic Hull Vane will then further increase the angle of attack by a factor $\boldsymbol{s}$. An offset can be given by a factor $\boldsymbol{n}$. These parameters give control over the average and amplitude of the lift.

$$\boldsymbol{\theta_{HV} = -s * \alpha_n + n} \quad \textbf{(42)}$$

The bow up pitching of the ship will cause an increase in angle of attack and an increased lift on the Hull Vane, this will dampen the pitching motion. Since the vertical component in the flow velocity increases, the lift will have a larger forward component. This means the induced drag will be compensated by a larger horizontal component in the lift. A similar reasoning applies when the ship is pitching bow down. The flow will be more horizontal and the algorithm will turn the Hull Vane towards it, further reducing the angle of attack. With the decrease in lift the bow down pitching moment is decreased, while also decreasing the induced drag.

4.4.2 RESULTS

A study is done to investigate the effect of the parameters $\boldsymbol{s}$ and $\boldsymbol{n}$. The neutral setting and angle amplitude are varied in multiple steps. The results of the neutral angle variation can be seen in Table 16. The goal of this variation in neutral angle is to check the influence of a different neutral settings on the mean lift in waves and the influence on the ship. A positive $\boldsymbol{n}$ is an offset leading edge down, similar to the ship coordinate system.

Table 16: overview of results of neutral angle variation

	$\overline{R_{total}}$	$\bar{\theta}$ [deg]	$\hat{\theta}$	$\overline{F_z^{HV}}$ [kN]	$\widehat{F_z^{HV}}$ [kN]	$\overline{F_x^{HV}}$ [kN]
Static	118.34 [kN]	0.155	2.26°	214.99	46.24	10.58
S=0.5 n=2	+0.1%	0.067	-15.0%	184.46	112.55	10.24
S=0.5 n=0	-1.9%	0.183	-14.6%	215.16	111.10	9.55
S=0.5 n=-2	-2.5%	0.295	-13.9%	244.53	109.50	8.01

The results show that this control algorithm provides good control over the mean lift and the amplitude of the lift. When varying the neutral setting the mean lift is changed systematic, while the amplitude is approximately constant. This shows that the relation between angle of attack and lift is almost linear for small angles as seen in the theory. The mean pitch angle is also slightly increased, while the mean Hull Vane thrust has decreased. The decrease in resistance is probably caused by the increased mean pitch angle, which is consistent with the result of the pre study in C. I. For a better comparison of decrease in resistance it would be fair to compare the algorithms with an offset to a static Hull Vane with a neutral offset. On the other hand, this static offset can also be a part of the advantages of the dynamic Hull Vane, since it can be varied with different speeds. While the static Hull Vane is designed at one angle for all speeds. To not further complicate the results, the comparison is done with a static Hull Vane without neutral offset. Based on this result it is decided to continue with a neutral angle of 0°, because the results are similar and this is most in line with the current Hull Vane design.

The second variation is done for the pitch angle amplitude, to control the generated lift by the Hull Vane and with that the possible motion damping. When there is a larger variation in Hull Vane angle, the amplitude of lift variation will also increase. This results in a larger influence on the pitch motion. For the highest pitch angle variation the neutral setting is changed to -2° to avoid excessive negative angles of attack. The results of this variation are shown in Table 17. It is clear that with the larger amplitude in the lift force the pitching can be damped more.

Table 17: overview of result of pitch angle amplitude variation

	$\overline{R_{total}}$	$\bar{\theta}$ [deg]	$\hat{\theta}$	$\overline{F_z^{HV}}$ [kN]	$\widehat{F_z^{HV}}$ [kN]	$\overline{F_x^{HV}}$ [kN]
Static	118.34 [kN]	0.155	2.26°	214.99	46.24	10.58
S=0.5 n=0	-1.9%	0.183	-14.6%	215.16	111.10	9.55
S=0.75 n=0	-1.7%	0.186	-19.3%	213.28	133.52	8.41
S=1 n=0	-1.3%	0.187	-23.6%	211.07	153.90	7.01
S=1.5 n=0	+0.3%	0.183	-30.9%	205.91	188.33	4.20
S=2 n=-2	+3.4%	0.242	-35.3%	218.47	211.37	-1.41

The results of this algorithm are verified for one other wave condition. The variation of $\boldsymbol{s}$ is repeated for an encounter frequency of $\omega_{enc} = 2.25\,{}^{rad}/_{s}$. The results are shown in Table 18.

Table 18: overview of results of pitch angle amplitude variation for $\omega_{enc} = 2.25\,{}^{rad}/_{s}$

	$\overline{R_{total}}$	$\overline{\theta}$ [deg]	$\widehat{\theta}$	$\overline{F_z^{HV}}$ [kN]	$\widehat{F_Z^{HV}}$ [kN]	$\overline{F_x^{HV}}$ [kN]
Static	102.65 [kN]	0.271	0.61°	210.20	30.35	9.95
S=0.5 n=0	+0.3%	0.289	-8.3%	214.23	64.97	9.60
S=0.75 n=0	+0.3%	0.288	-11.1%	213.77	77.12	9.31
S=1 n=0	+0.7%	0.086	-13.8%	213.43	89.12	8.97
S=1.5 n=0	+1.6%	0.285	-19.1%	212.55	111.96	8.22

The second wave condition shows a similar trend in reduction of pitch motion when there is a larger amplitude in the lift. The relative damping of the pitch motion is smaller for the same algorithm settings, since the lift amplitude is smaller. This difference is caused by the lower vertical velocity of the Hull Vane for smaller movements.

4.4.3 ANALYSIS

The same analysis of the added wave resistance is made as for the first algorithm, the results are shown in Table 19.

Table 19: Overview of added wave resistance

	$\overline{R_{total}}$ [kN]	$\overline{F_x^{HV}}$ [kN]	$\overline{R_{hull}}$ [kN]	$\overline{R_{AW}}$ [kN]	$\overline{R_{AW}}$ [%]	$\widehat{\theta}$ [%]
Flat water	91.93	8.82	100.75	0		
Static	118.34	10.57	128.92	28.167	0%	0%
S=0.5 n=0	116.08	9.55	125.66	24.90	-11.6%	-14.6%
S=0.75 n=0	116.29	8.41	124.71	23.96	-15.0%	-19.3%
S=1 n=0	116.79	7.01	123.89	23.14	-17.8%	-23.6%
S=1.5 n=0	118.68	4.20	122.88	22.214	-21.5%	-30.9%
S=2 n=2	122.38	-1.40	120.98	20.23	-28.3%	-35.3%

The relation between pitch motion, added wave resistance and total resistance is comparable to the first algorithm. The reduction of added wave resistance is similar to the thrust loss of the Hull Vane. At the natural frequency the ship motions cause a large part of the added wave resistance (Blok, 1993). At other frequencies the damping of the ship motions will cause less reduction in added wave resistance. In Table 20 the added wave resistance is shown for an encounter frequency of $\omega_{enc} = 2.25\,{}^{\mathrm{rad}}/_{\mathrm{s}}$.

Table 20: overview of added wave resistance for $\omega_{enc} = 2.25\,^{rad}/_{s}$

	$\overline{R_{total}}$ [kN]	$\overline{F_x^{HV}}$ [kN]	$\overline{R_{hull}}$ [kN]	$\overline{R_{AW}}$ [kN]	$\overline{R_{AW}}$ [%]	$\hat{\theta}$ [%]
Flat water	91.93	8.82	100.75	0		
Static	101.65	9.96	111.60	9.37	0%	0%
S=0.5 n=0	101.91	9.60	111.50	10.75	-0.9%	-8.3%
S=0.75 n=0	102.00	9.31	111.30	10.55	-2.7%	-11.1%
S=1 n=0	102.37	8.97	111.342	10.59	-2.4%	-13.8%
S=1.5 n=0	103.31	8.22	111.52	10.77	-0.7%	-19.3%

The results agree with the theory that at this encounter frequency the ship motions cause a smaller portion of the added wave resistance. The damping of the ship motions reduces the added wave resistance by a smaller amount. In Figure 61 the same simulation quantities are shown for settings s=1 n=0.

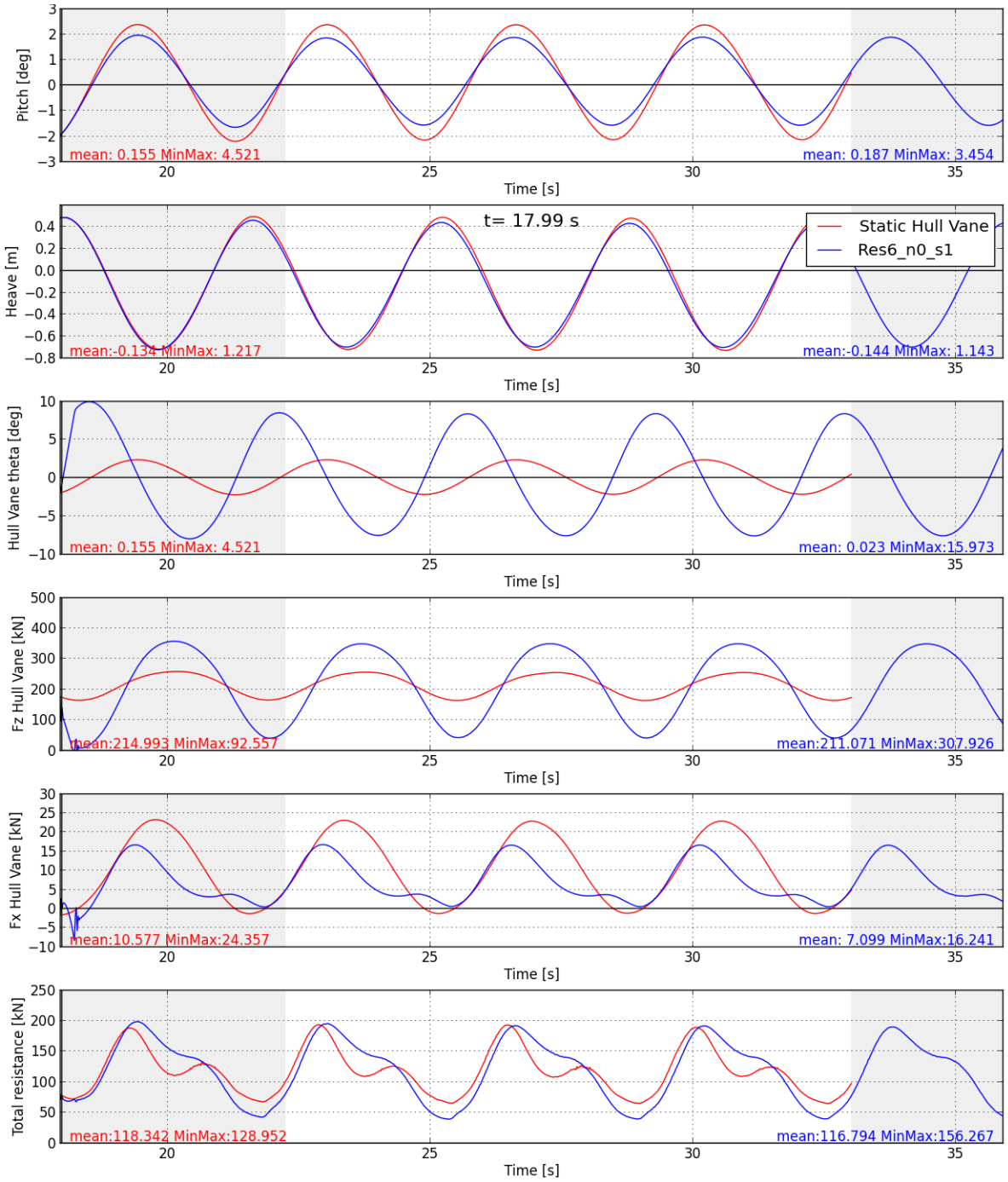

Figure 61: overview of simulation quantities for vertical velocity damping

Also for this algorithm the total resistance of the ship with dynamic Hull Vane varies above and below the resistance of the static Hull Vane. To get a better understanding of what is happening at these moments a plot of the difference in resistance distribution is shown in Figure 62. This resistance difference is at 20 seconds for s=1 and n=0, when the hull with static Hull Vane has a dip in the resistance and the ship is pitched bow down.

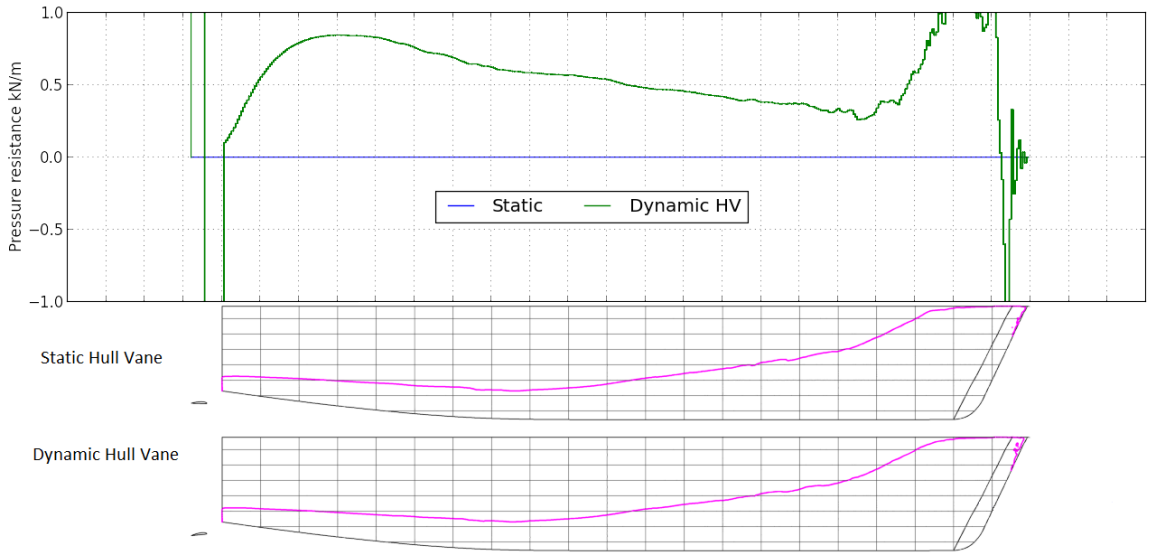

Figure 62: Pressure difference over hull

As seen the hull with a dynamic Hull Vane has a higher pressure resistance over its entire length. Large peaks are visible at the end of the ship as the dynamic Hull Vane has a different angle of attack.

Four explanations are found for the difference in resistance.

- The difference in pitch angle of the ship will change the normal direction of the bottom and thereby the resulting force caused by the pressure.
- The different pitch angle will also mean the draft of the vessel is different, so the static pressure distribution is different.
- The larger motions of the undamped system will require more energy, this could lead to a larger resistance at instances with high acceleration.
- The different heave of the ship will change the displacement. The lift on the Hull Vane also influences the heave, this can reduce the mean and instantaneous resistance.

Together these effects will cause a change in resistance, and it is hard to quantify them or look at them separately. For the situation shown in Figure 62 there was a difference in pitch of 0.2°. The difference in resistance on the hull at this moment is 32kN. Distributed over the hull this gives an average pressure difference of 0.64 kN/m.

4.4.4 CONCLUSION

With a control algorithm based on the pitch velocity good control over the mean and maximum lift is achieved. By changing the offset and the pitch amplitude of the Hull Vane the mean and amplitude of the lift can be tuned to the operating profile of the ship. This makes the control algorithm very suitable for motion reduction in practical applications. The resulting decrease in added wave resistance was not significantly larger than the loss in thrust on the Hull Vane.

4.5 COMPARISON

In this chapter several control algorithms have been tested and the results have been analyzed. The results showed the dynamic Hull Vane with a good control scheme has great potential for reducing the ship motions. For this ship the reduction in added wave resistance was not enough to significantly reduce the total resistance. The literature review already suggested the induced drag becomes significant at larger angles of attack, and the thrust will be largest for small angles of attack. The experiments confirmed this, because no increase in thrust could be achieved by a control algorithm specifically made for thrust. The most successful algorithms are focused on pitch reduction in two similar ways.

- Control on pitch acceleration with defined maximum angles
- Control on pitch velocity with a scalable amplitude of Hull Vane angle

To determine the efficiency of both algorithms we compare the pitch reduction they achieve with a similar amplitude of vertical force in the Hull Vane. In Table 21 a comparison between the different control algorithms is shown. The chosen algorithms have a similar mean and amplitude for the lift, the main difference is in the phase angle of the lift.

Table 21: Comparison between different control algorithms

	$\overline{R_{total}}$ [%]	$\widehat{F_Z^{HV}}$ [kN]	$\overline{F_z^{HV}}$ [kN]	$\hat{\theta}$ [%]
N=4° M=-7°	-0.7%	125	224.67	-15.8%
S=0.75 n=0	-1.7%	133.52	213.29	-19.3%
N=10° M=-7°	-0.2%	174.99	195.42	-25.2%
S=1 n=0	-1.3%	153.97	211.07	-23.6%

As seen in the table the algorithm based on pitch velocity provides better motion reduction for a slightly larger amplitude in lift variation for the smaller angles. At the larger angles the motion reduction of algorithm based on acceleration is slightly better, but has a larger lift amplitude. For both situations the algorithm based on pitch velocity manages to reduce the total resistance the most. The first variation of both algorithms is compared for an encounter frequency of $\omega_{\text{enc}} = 2.25\,{}^{\text{rad}}/_{\text{s}}$ in Table 22.

Table 22: Comparison between different control algorithms for $\omega_{enc} = 2.25\,{}^{rad}/_{s}$

	$\overline{R_{total}}$ [%]	$\widehat{F_Z^{HV}}$ [kN]	$\overline{F_z^{HV}}$ [kN]	$\hat{\theta}$ [%]
N=4° M=-7°	1.2%	115	222.71	-21.5%
S=0.75 n=0	0.3%	77.06	213.78	-11.1%

As seen, the algorithm based on acceleration creates a bigger amplitude in lift and sequentially manages to damp a larger percentage of the ship motions. The maximum defined angles of the first algorithm, gives it a larger angle of attack than the algorithm based on pitch velocity. For the algorithm based on pitch velocity the angle of attack of the Hull Vane is proportional to the change caused by the vertical velocity. So when the ship motions are smaller the algorithm will damp less.

Although both algorithms showed a reduction in ship motion, the algorithm based on pitch acceleration proved it is more efficient at small pitch angles. However, the reduction of ship motions for small pitch angles is less important for most ships. The algorithm with minimal and maximal angles might also cause trouble in irregular waves, since there will be short periods in which the acceleration is changing. The algorithm based on pitch velocity is less effective for small pitch angles, but will be more robust in irregular waves. The more physical basis of this algorithm and the easy tuning make it more suitable for use in practice. Therefore this algorithm (s=1, n=0) is chosen to be validated in more wave conditions and speeds. This is not necessarily the "optimal" algorithm, but a viable candidate that can be easily adopted to work on any ship.

4.6 CONTROL PERFORMANCE

The chosen control algorithm (s=1, n=0) is tested for the previously stated test matrix (section 3.4) to verify whether it works in multiple conditions.

4.6.1 PERFORMANCE IN DIFFERENT WAVE CONDITIONS

The control algorithm should work for more than one sea state. Therefore the performance of the algorithm is tested in four additional sea states. The results of this are shown in Table 23. The results are relative to the static Hull Vane in that condition.

Table 23: Performance of control algorithm in different wave conditions

	$\overline{R_{total}}$ [%]	$\hat{\theta}$	$\hat{\theta}$ [%]	$\overline{F_z^{HV}}$ [kN]	$\overline{F_x^{HV}}$ [%]
Fn=0.30 $\omega_{enc} = 1.75\,^{rad}/_{s}$	+0.2%	1.63°	-18.5%	113.66	-36.5%
Fn=0.40 $\omega_{enc} = 1.25\,^{rad}/_{s}$	+2.3%	1.81°	-13.4%	119.18	-18.9%
Fn=0.40 $\omega_{enc} = 1.75\,^{rad}/_{s}$	-1.3%	1.73°	-23.6%	153.97	-23.6%
Fn=0.40 $\omega_{enc} = 2.25\,^{rad}/_{s}$	+0.9%	0.67°	-13.7%	89.29	-9.9%
Fn=0.50 $\omega_{enc} = 1.75\,^{rad}/_{s}$	+0.2%	1.55°	-28.4%	178.35	-29.9%

A couple of things can be noted about the results.

- At low speed the dynamic Hull Vane produces less lift and consequentially gives less control over the ship motions.
- For the medium speed and low frequency the amplitude of the lift is also lower. For this case it is caused by the lower vertical speed, since the amplitude of the motion is comparable to the medium frequency but the lower frequency causes a lower vertical velocity.

- The medium frequency was the original natural frequency, but the amplitude of the motion is now smaller than for the low frequency. The control algorithm can produce more lift with the higher frequency and faster motion, and dampens more of the motion. This means the natural pitching frequency of the ship shifted.

- For the highest frequency the movement has become very small, therefore the vertical velocity is lower again and the lift amplitude becomes lower.

- At the highest speed the lift on the Hull Vane is larger and provides more control over the pitch motion.

It is clear that when the thrust of the Hull Vane is similar to the added wave resistance caused by the ship motions, there is no reduction of total resistance possible by reducing the ship motions. The loss of thrust on the Hull Vane is then greater than the reduction of the added wave resistance of the ship.

4.6.2 PERFORMANCE IN DIFFERENT WAVE HEIGHTS

So far the performance of the algorithm has only been checked for waves of 1.0 meter height. In this paragraph results of simulations in 0.5 & 2 meter waves are discussed. In the smaller waves the motions of the ship will be less, so the flow on the Hull Vane will also change less. With the larger waves the ship motions will be larger, and the potential lift on the Hull Vane will reach its limit. This will also limit the damping potential of the Hull Vane. These simulations are again done at a speed of Fn=0.40 and the encounter frequency equal to the natural frequency $\omega_{enc} = 1.75\,{}^{rad}/_{s}$. The ship motions in 2 meter waves are expected to submerge the bow of the ship. To reduce these non-linearities the freeboard of the ship is increased by 2 meters. The non-linear iterations of the solver are increased from 8 to 16 to achieve a second order reduction of the residuals between every time step. An overview of the pitch amplitude and added wave resistance is given in Figure 63, quadratic and linear trendlines are drawn for the added wave resistance and pitch amplitude respectively. The results agree with the theory that for small waves the ship motions increase linear and the added wave resistance with the second order wave height. Interestingly the added wave resistance does decrease, but relatively less than the reduction in pitch motion. This agrees with the theory that only a portion of the added wave resistance is caused by the ship motion (Pinkster, 1980).

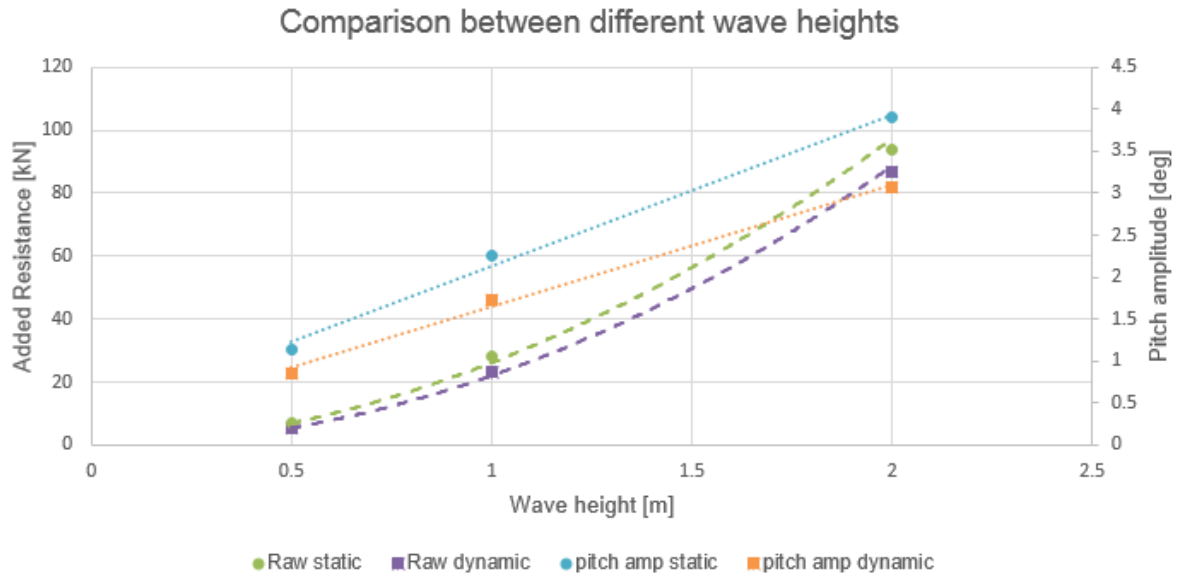

Figure 63: Comparison of ship motions and added wave resistance between different wave heights

For all wave heights the dynamic Hull Vane achieved a reduction of the ship motions and resistance. In Table 24 the numerical values are shown. It shows that the reduction in added wave resistance does not cause a reduction in total resistance. The relative reduction in pitch motion decreases because there is a limit in potential lift on the Hull Vane at this speed.

Table 24: Overview of algorithm results for different wave heights

Fn=0.40 $\omega_{enc} = 1.75\ ^{rad}/_{s}$	$\overline{R_{total}}$	$\hat{\theta}$	$\hat{\theta}$	$\widehat{F_Z^{HV}}$ **[kN]**	$\overline{F_x^{HV}}$ **[%]**
H = 0.5 [m]	-0.4%	0.86°	-24.8%	160.91	-10.8%
H = 1.0[m]	-1.3%	1.73°	-23.5%	307.80	-32.7%
H = 2.0 [m]	+1.3%	3.07°	-21.3%	542.98	-85.4%

5. CONCLUSION

Based on the literature review several control algorithms are designed and tested. In this section the results will be summarized and discussed.

5.1 CONCLUSION

In the introduction the main research question was defined as:

Can a dynamic version of the Hull Vane on the AMECRC#13 reduce the ship motions in head waves, and/or reduce the total resistance by generating thrust using the vertical motion of the stern?

The goal was to design a control algorithm for the dynamic Hull Vane that would reduce the ship motions. Or increasing the thrust on the Hull Vane by using the oscillating foil principle and thereby reducing the total resistance of the ship. The following sub questions provided the necessary information for answering the main question.

The first sub question focusses on the oscillating foil and how it is related to the dynamic Hull Vane. The literature review showed that an oscillating foil can achieve a high propulsive efficiency coefficient (≈60%) and that a small part of this power is used for the pitch control (≈20%). This platform of efficiency applies for Strouhal numbers of 0.2-0.8. However, the Strouhal number at which the dynamic Hull Vane would operate is at 0.05-0.2. This showed that the flow will only be from one side and the oblique inflow will be more important than the oscillating motion. This makes the working principle of the dynamic Hull Vane too different from the oscillating foil, and means no control algorithm will be based on this.

The second sub question discussed how the flow direction varies in waves behind the ship. It showed how the pitch velocity and the accompanying vertical velocity of the Hull Vane are the biggest cause for change in the angle of attack. During the testing of the control algorithms the numerical experiments showed that this is different for an actively damped ship.

The third sub question focused on the operating characteristics of the Hull Vane and the NACA4412 profile. It showed that when evaluating the foil with 2D theory a large angle of attack is beneficial. But in case of a 3D wing, the induced resistance limits the thrust production and the optimal angle of attack is much lower.

This information was used to design several control algorithms, which answered the main research question. The study showed how a control algorithm based on the pitch velocity of the ship was successful in reducing the ship motions in 1 meter waves, while little influence on the total resistance was found. It proved very difficult to achieve an increase in the thrust on the Hull Vane. This would only be possible with arbitrary tuning not based on the theory. The control algorithm for ship motion reduction was tested in different wave conditions and managed to reduce the ship motions between 13.8% and 28.4%. With the reduction in wave motions, the added wave resistance was consequently reduced. The absolute decrease in added wave resistance was similar to the loss of thrust on the Hull Vane, resulting in no significant change in total resistance. The simulations in 0.5 meter waves and 2 meter waves showed similar results to the 1 meter waves. The reduction of pitch motion amplitude was between 21.3% and 24.8%. This resulted again in no significant change in total resistance.

The two parts of the main question can now be answered. The literature review showed that the dynamic Hull Vane operates under different conditions than a thrust producing oscillating foil. The tested algorithms showed that the thrust on the Hull Vane can only be marginally increased and will require arbitrary tuning. The simulations also showed that the lift of the Hull Vane can be used to dampen the ship motion. The use of the Hull Vane to reduce the ship motions had no conclusive effect on the total resistance of the ship.

5.2 RECOMMENDATIONS

In this study several control algorithms for a dynamic Hull Vane are tested. The results showed potential for motion damping, but the tested operating conditions were limited. Before a working product can be released several extra factors will need to be researched.

- The current algorithm was tested with CFD in regular waves. In practice a wavefield will be irregular and this is the wave condition an algorithm will have to work in. To make sure an algorithm will work in practice it will have to be tested in irregular waves, either in CFD or in a towing tank.

- In following waves the ships can also experience a significant pitching motion. Although this research focused on head waves, the performance of this algorithm in following waves would also be of interest in a practical application.

- The dynamic Hull Vane was able to create a large lift force. When the dynamic Hull Vane is split in two parts, this could also be used for roll reduction.

- The movement of the dynamic Hull Vane will require power. Although it is significantly less than an oscillating foil, this will increase the total required power of the ship.

- So far it was assumed that no adjustments to the foil or struts were necessary for the movement of the Hull Vane. A mechanical design should be made to check if the foil and struts can have a similar shape.

- In this research no practical limitations of the struts was taken into account. A full structural design of the dynamic Hull Vane needs to be made. The effect of the struts on the performance of the Hull Vane should be included.

- The dynamic Hull Vane will put a larger stress on the struts. The new strut design should take into account the larger forces and larger amplitude of the forces.

- The thrust production of the dynamic Hull Vane was limited by the induced resistance. The thrust of the dynamic Hull Vane could benefit from well-designed struts or wing tips.

- Many companies specialize in control of fins or other motion dampening devices. An experienced company (e.g. Naiad) could also design a control algorithm for the dynamic Hull Vane. This would be an interesting comparison to the control algorithm designed by the author.

BIBLIOGRAPHY

Abbott, I. H., & Von Doenhoff, A. E. (1959). *Theory of Wing Sections.*

Belibassakis, K., & Filippas, E. (2015). Ship propulsion in waves by actively controlled flapping foil. *Applied Ocean Research*.

Bergsma, F., & Moerke, N. (2013). *CFD Calculations for a 40m Inland Vessel with O-Foil Propulsion.*

Blok, J. J. (1993). *The Resistance Increase of a Ship in Waves.*

Bouckaert, B., Uithof, K., Moerke, N., & Van Oossanen, P. G. (2016). *Hull Vane® on 108m Holland-Class OPVs: Effects on Fuel Consumption and Seakeeping.*

Delaurier, J. D. (1993). An Aerodynamic Model for Flapping-Wing Flight. *Aronautics Journal*.

Eça, L., & Hoekstra, M. (2014). A Procedure fot the Estimation of the Numerical Uncertainty of CFD Calculations Based on Grid Refinement Studies. *Journal of Computational Physics*.

Esfahani, J. A., Barati, E., & Karbasian, H. R. (2013). Comperative Investigations in the Effect of Angle of Attack Profile on Hydrodynamic Performance of Bio Inspired Foil. *Journal of Naval Architecture and Marine Engineering*.

Ferziger, J., & Peric, M. (2002). *Computational Methods for Fluid Dynamics.*

ITTC. (2011). Uncertainty Analysis in CFD Verification and Validation.

ITTC. (2014). Practical Guidelinges for Ship CFD Applications. *Recommended Procedures and Guidelines.*

ITTC. (2014). Recommended Procedures and Guidelines - Practical guidelines for ship resistance CFD. 7.5-03-02-04.

Journée, J., & Adegeest, L. (2003). Theoretical Manual of Strip Theory Program " SEAWAY for Windows " .

Mattheijssens, J., Marcel, J. P., Bosschaerts, W., & Lefeber, D. (2012). Oscillating Foils for Ship Propulsion. *WIT Transactions on Ecology and the Environment*.

Mattheijssens, J., Marcel, J., Bosschaerts, W., & Lefeber, D. (2012). Oscillating Foils for Ship Propulsion. *WIT Transactions on Ecology and the Environment*.

NUMECA. (2013). *Theoretical Manual.*

Pinkerton, R. (1938). *The Variation With Reynolds Number of Pressure Distribution over an Airfoil Section.*

Pinkster, J. A. (1980). *Low frequency second order wave exciting forces on floating structures.*

Politis, G., & Politis, K. (2012). Biomimetic propulsion under random heaving conditions, using active pitch control. *Journal of Fluids and Structures*.

Qing, X., & Wei, L. (2010). Numerical Investigation of Angle of Attack Profile on Propulsion Perfomance of an Oscillating Foil. *Computers and Fluids*.

Read, D. A., & Trantafyllou, M. (2001). *Oscillating Foils for Propulsion and Maneuvering of Ships and Underwater Vehicles.*

Read, D. A., Hover, F. S., & Triantafyllou, M. S. (2002). Forces on Oscillating Foils for Propulsion and Maneuvering. *Journal of Fluids and Structures*.

Schouveiler, L., Hover, F. S., & Triantafyllou, M. S. (2005). Performance of Flapping Foil Propulsion. *Journal of Fluids and Structures*.

Tannehill, J., & Anderson, D. (2013). *Computational fluid dynamics and heat transfer.*

Uithof, K., Bouckaert, B., Van Oossanen, P. G., & Moerke, N. (2016). The Effects of the Hull Vane® on Ship Motions of Ferries and ROPAX Vessels.

Uithof, K., Hagemeister, N., Bouckaert, B., van Oossanen, P. G., & Moerke, N. (2016). A systematic comparison of the influence of the Hull Vane®, interceptors, trim wedges and ballasting ont he performance of the 50m AMECRC series #13 patrol vessel. *Warship 2016: Advanced Technologies in Naval Design, Construction & Operation*.

Uithof, K., Moerke, N., Van Oossanen, P. G., Van Oossanen, P., & Zaaijer, K. S. (2014). An Update on the Development of the Hull Vane®., (p. 11).

Wackers, J., Koren, B., Raven, H., van der Ploeg, A., Starke, A., Deng, G., . . . Ohashi, K. (2011). Free-Surface Viscous Flow Solution Methods for Ship Hydrodynamics. *Archives of Computational Methods in Engineering*.

Xiao, Q., & Liao, W. (2010). Numerical Investigation of Angle of Attack Profile on Propulsion Performance of an Oscillating Foil. *Computer & Fluids*.

Xing, T., & Stern, F. (2015). Comment on "A Procedure for the Estimation of the Numerical Uncertainty of CFD Calculations Based on Grid Refinemetn Studies". *Journal of Computational Physics*.

A. SHIP DIMENSIONS

AMECRC #13		
Displacement	493.6	t
Volume (displaced)	481.565	m^3
Draft at AP	2.564	m
Draft Amidships	2.564	m
Draft at FP	2.564	m
Immersed depth	2.564	m
WL Length	50	m
Beam max extents on WL	8.338	m
Wetted Area	431.445	m^2
Max sect. area	15.498	m^2
Waterpl. Area	331.739	m^2
Prismatic coeff. (Cp)	0.621	
Block coeff. (Cb)	0.451	
Max Sect. area coeff. (Cm)	0.73	
Waterpl. area coeff. (Cwp)	0.796	
LCB length	22.278	from zero pt. (+ve fwd) m
LCF length	20.627	from zero pt. (+ve fwd) m
LCB %	44.556	from zero pt. (+ve fwd) % Lwl
LCF %	41.253	from zero pt. (+ve fwd) % Lwl
Length:Beam ratio	5.997	
Beam:Draft ratio	3.252	
Length:Vol^0.333 ratio	6.379	

B. EULER THEORY

The flat water resistance of the AMERCR#13 has already been calculated for multiple speeds by Van Oossanen. The results are shown in Figure 64. The percentage of the resistance components to the total resistance are shown as the striped lines. Because the pressure resistance is around 80% of the total resistance the Euler simulation should be able to produce an accurate result.

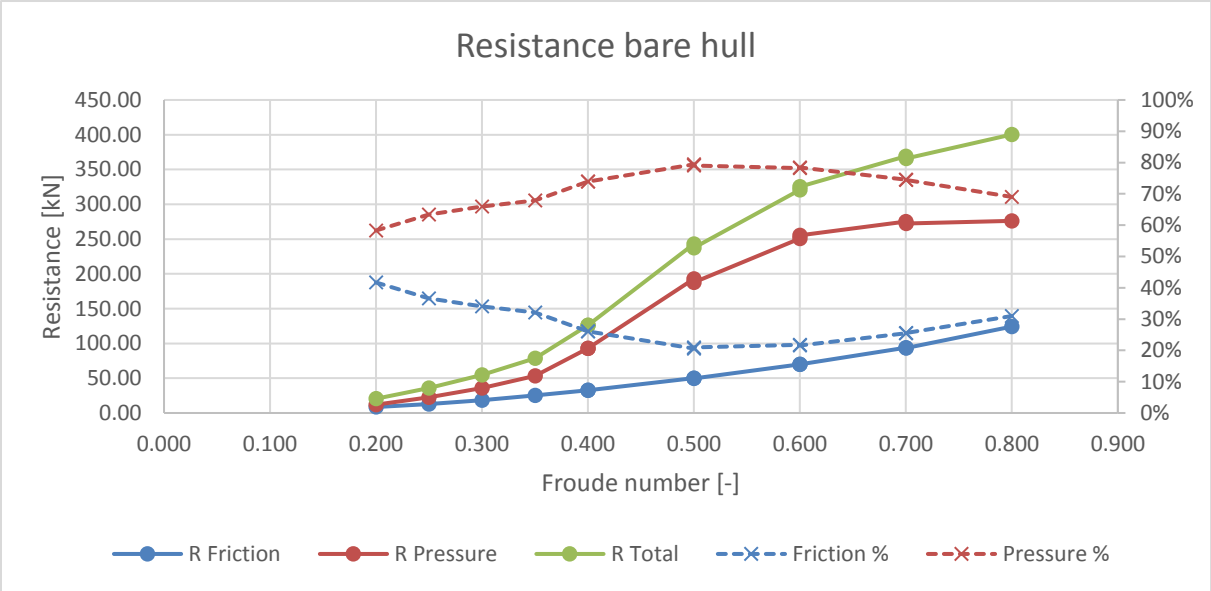

Figure 64: Flat water resistance on AMECRC#13

B. I. COMPARISON OF LIFT ON HULL VANE

First the lift on the Hull Vane is calculated. As the lift is a result of pressure difference, it should be well represented by the Euler flow. One of the differences lies in the influence of the boundary layer on the foil and the wake of the ship. In Figure 65 the lift on the Hull Vane is shown for the simulation of the Euler flow and for the full RANSE simulation. The lift follows the same oscillation for both simulations and the amplitude is similar. The mean is calculated over the last 5 periods and shown in Table 25. The Euler simulation over estimates the lift by around 9%. This is caused by the slower flow of the wake of the ship, but also the neglection of the boundary layer on the foil.

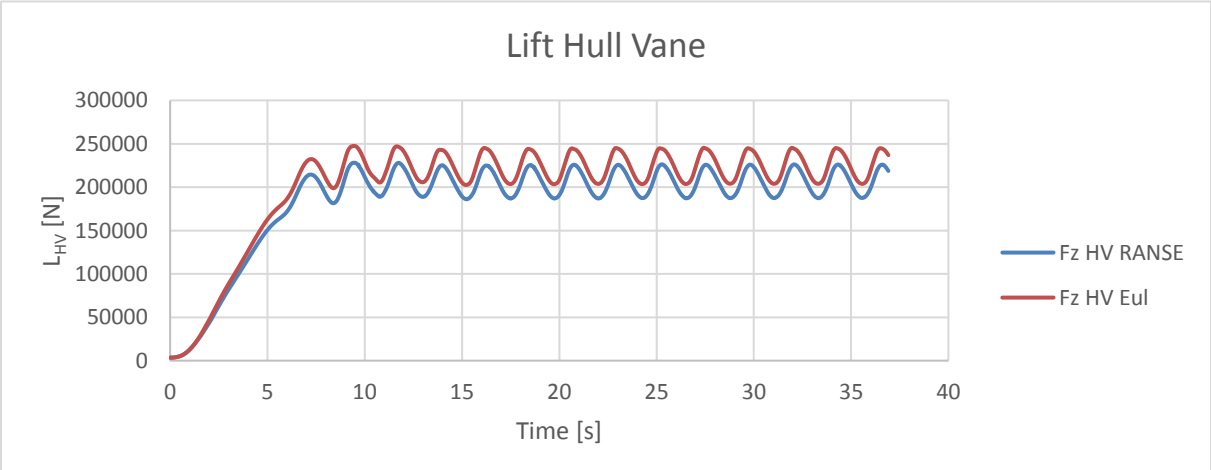

Figure 65: comparison in lift on Hull Vane for Euler and RANSE simulation

Table 25: Comparison of mean lift on Hull Vane for Euler and RANSE simulation

	Mean [N]
RANSE	2.06E+05
Euler	2.24E+05

B. II. COMPARISON OF SHIP MOTIONS

Part of this research is the influence of the Hull Vane on the ship motions. Therefore the Euler flow should be able to give a good representation of the ship motions. The pitch and heave motions are compared to check the performance of the Euler flow solver in waves. In Figure 66 and Figure 67 the pitch and heave motion are shown for both simulations, with and without a Hull Vane. The results show good agreement with and without the Hull Vane. The Euler flow slightly over predicts the movements, this is probably caused by the absence of the viscous damping. The same reasoning can be applied to the heave motion. The mean of the difference in maximum and minimum pitch angle is calculated for the last five wave encounters. The Euler simulation over predicts the amplitude of the oscillation with around 5% with the Hull Vane and around 2% on the bare hull. Because the absolute value of the pitch amplitude for the bare hull is larger, the relative error of the Euler flow is lower.

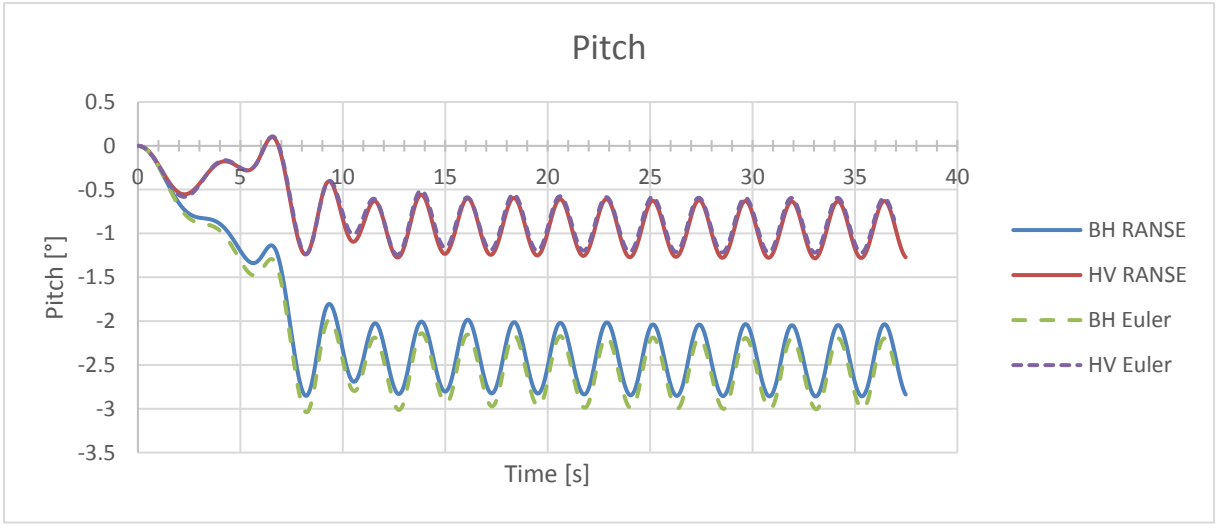

Figure 66: Comparison of pitch angles

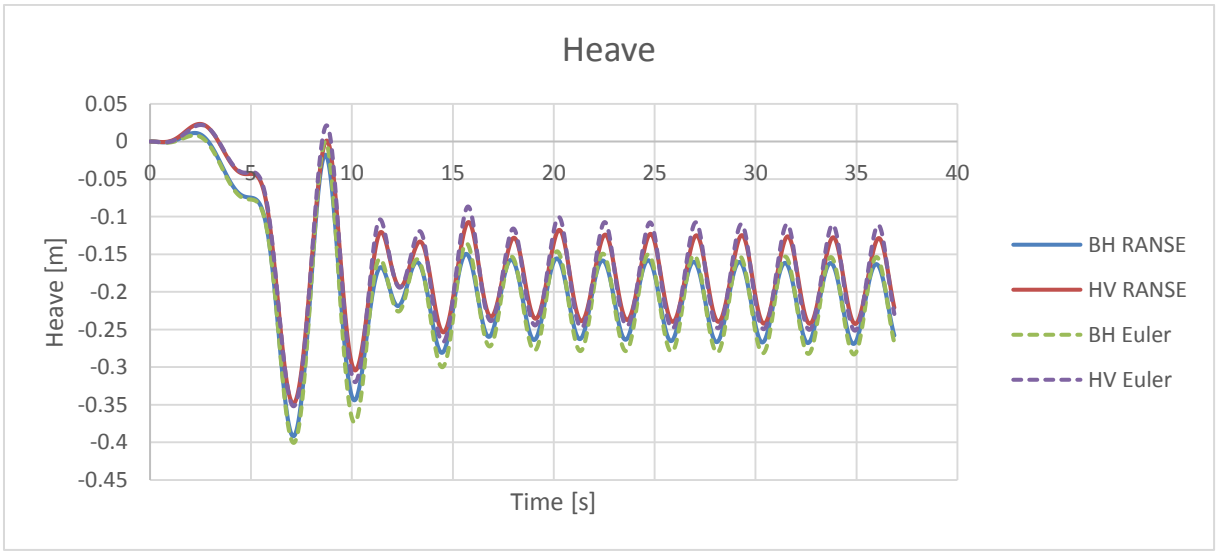

Figure 67: Comparison of heave

B. III. COMPARISON OF RESISTANCE

One of the goals of the Hull Vane is resistance reduction. For successful use of the Euler model, the simulation should provide accurate results on the resistance, at least on the relative difference between simulations with and without a Hull Vane. Therefore the resistance of the Euler simulation and the RANSE simulation are compared. First the absolute resistance between the two simulations is compared in Figure 68. As the Euler simulation only calculates the pressure resistance, the absolute resistance is under predicted by a large offset. The oscillating wave resistance is well represented, and the resistance reduction due to the Hull Vane can also be seen.

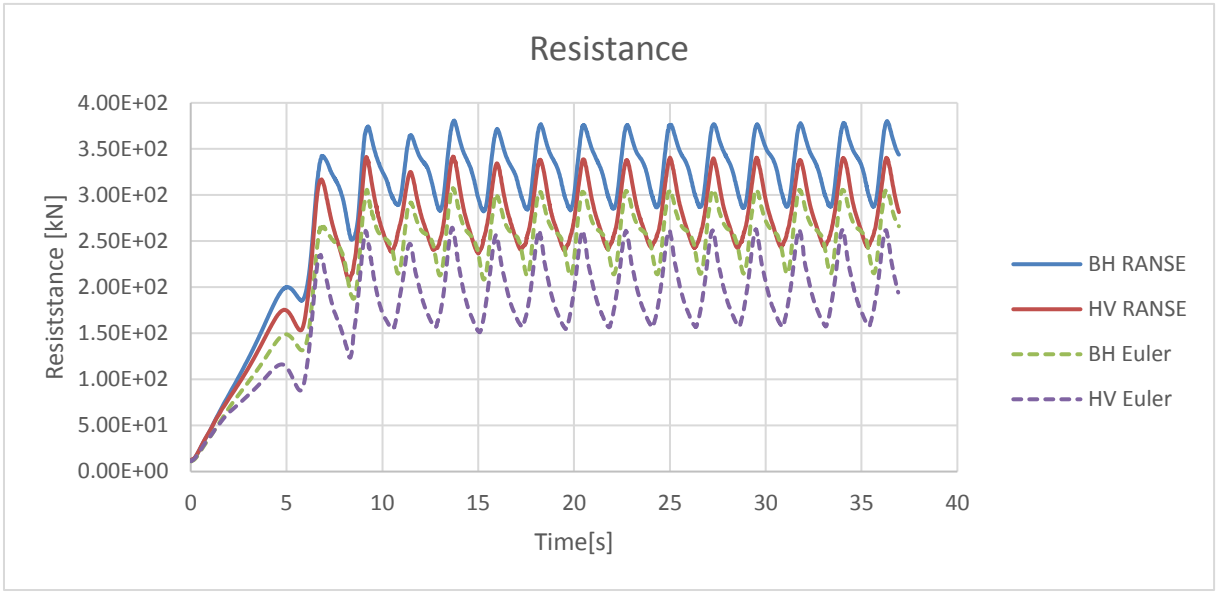

Figure 68: Comparison on resistance

The offset without the viscous resistance causes a misleading resistance reduction with the Hull Vane. The mean of the resistance is taken again over 5 periods. The RANSE simulation then shows a resistance reduction of 15%, while the Euler solver shows 24%. This is not a fair comparison, because the Hull Vane only reduces the pressure resistance, which causes the Euler solver to over predict the reduction. The Hull Vane increases the viscous resistance of the ship, which is not simulated by the Euler flow. If the optimization is done based on Euler simulations, only pressure resistance can be compared between runs. Therefore the pressure resistance of the RANSE simulation and Euler simulation are compared in Figure 69. As expected the pressure resistance is represented fairly accurate with the Euler simulation. The RANSE simulation shows a decrease of pressure resistance of 20%. The difference between the RANSE and Euler runs is caused by the bump that is seen right after the resistance peak of the bare hull Euler simulations. As this only happens for the bare hull it might be caused by the movement of the ship or the different pitch. This has influence the resistance.

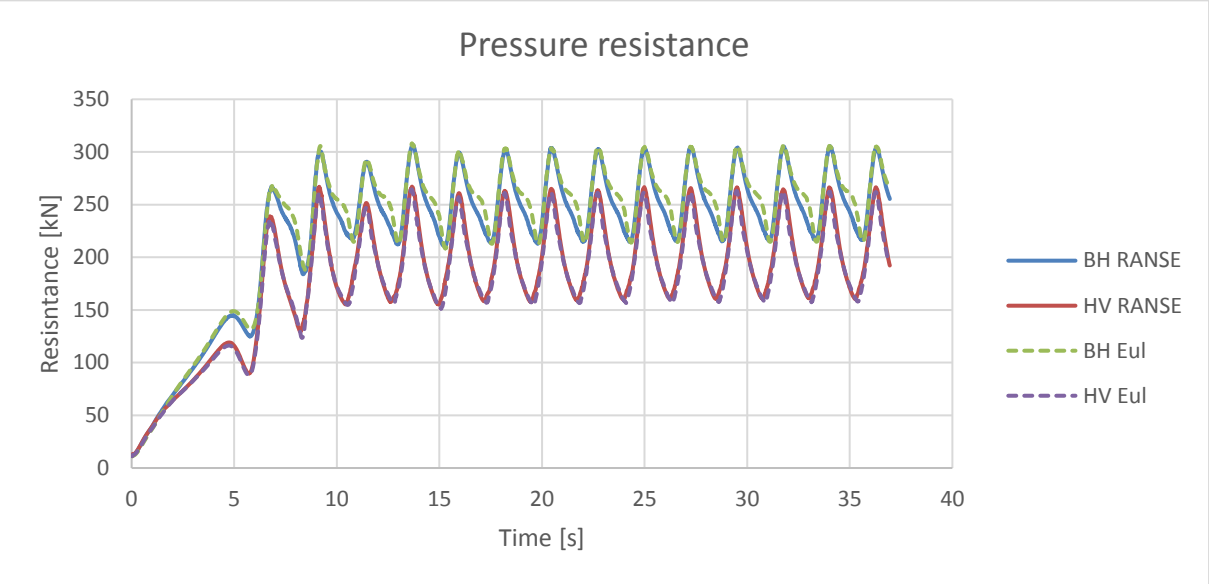

Figure 69: Comparison on pressure resistance

B. IV. Conclusion

The Euler simulations proved to simulate the ship motions fairly accurate, but in the resistance prediction there is still quite a difference. Therefore all results of the Euler simulations would need to be verified with a RANSE simulation. For the Euler simulation the extra refinement in the viscous layer around the hull was removed, this saved a significant amount of cells in the mesh. The computation was done on the same amount of cores, and was for both still within a reasonable amount of cells per cores. This made sure that any difference in computation time was caused by the amount of cells and the simulation, not by difference in cores or a bottleneck in communication between cores. With this setup the Euler simulation took around 70% of the time of the RANSE simulation. The difference in computing was deemed to be not enough to justify the difference in the result. Especially when validation on the Euler simulations increases the total amount of runs.

C. PRE STUDY

The possible effect of the Hull Vane is investigated by simulating the lift and measuring the lift and thrust for a sweep of Hull Vane angles. The result of this can be used as input for the control algorithms.

C. I. MINIMAL WAVE RESISTANCE

As the Hull Vane creates a vertical force at the aft of the ship, it reduces the trim of the ship at high speeds. In flat water the decrease in trim reduces the resistance, as seen in earlier research of Van Oossanen for the AMECRC#13 (Uithof, Hagemeister, Bouckaert, van Oossanen, & Moerke, 2016). The shift of LCG with the flat water runs indicated that a shift of LCG forward reduced the resistance, combined with the thrust force produced with the lift of the Hull Vane, a maximum lift would provide the lowest resistance.

As the goal is to reduce the resistance of the ship in waves, a short study is done to investigate the effect of a varying simulated Hull Vane lift onto the resistance of the ship in waves. Instead of an actual Hull Vane simulations are done with a vertical force at the position of the Hull Vane. The goal of this short study is to check the effect of the vertical force on the resistance and ship motions, without the thrust of the Hull Vane. The ship is accelerated in head waves with an encounter frequency of $\omega = 1.75\,{}^{rad}/_{s}$. After most of the start-up effects have dissipated, the simulation is split in five different simulations each with a different vertical force at the location of the Hull Vane. The vertical force and results are shown in Table 26. For the same conditions with a standard Hull Vane the vertical force varied between 160kN and 260kN on the full ship. The results show a decrease in resistance and an increase in pitching amplitude for an increase in vertical force. Although the mean resistance is lower, the variation in resistance becomes larger. The largest vertical force is also around 20% of the displacement of the ship, this plays a significant role in reducing the resistance.

Table 26: Resistance and pitch amplitude for varying simulated Hull Vane vertical force

	-200 [kN]	0	200 [kN]	400 [kN]	800 [kN]
R_{avg} [kN]	180.6	156.3	138.6	129.4	126.8
R_{avg} relative to 0	116%	100%	89%	83%	81%
$\bar{\theta}$ [deg]	-1.4	-0.7	0	0.6	2
$\hat{\theta}$ [deg]	2.3	2.4	2.5	2.5	2.8

The reduction in resistance now causes extra ship motions. When moving the angle of the Hull Vane with the waves this might be different. The results show that a maximum lift on the Hull Vane, will reduce the total resistance, but for a decrease in added wave resistance a more thoughtful approach is suggested.

C. II. MAXIMUM HULL VANE ANGLE OF ATTACK

The literature research showed what the dynamic Hull Vane should deliver to achieve our goals. In this paragraph we take a look of what the dynamic Hull Vane can deliver. In the literature review the lift and drag coefficients of the 2D and 3D foil profile were presented. Now a short study is done into the performance of the dynamic Hull Vane behind a ship. A simulation is started in which the ship is accelerated, after acceleration the angle of the Hull Vane is varied from -5° to 20°. This provides a lift and drag curve for the actual Hull Vane. In Figure 70 the horizontal and vertical forces on the Hull Vane are shown for a sweep of different angles to the horizontal. As seen the foil begins to stall around a 16° angle to the horizontal. As the flow is not horizontal here, the angle of attack is larger.

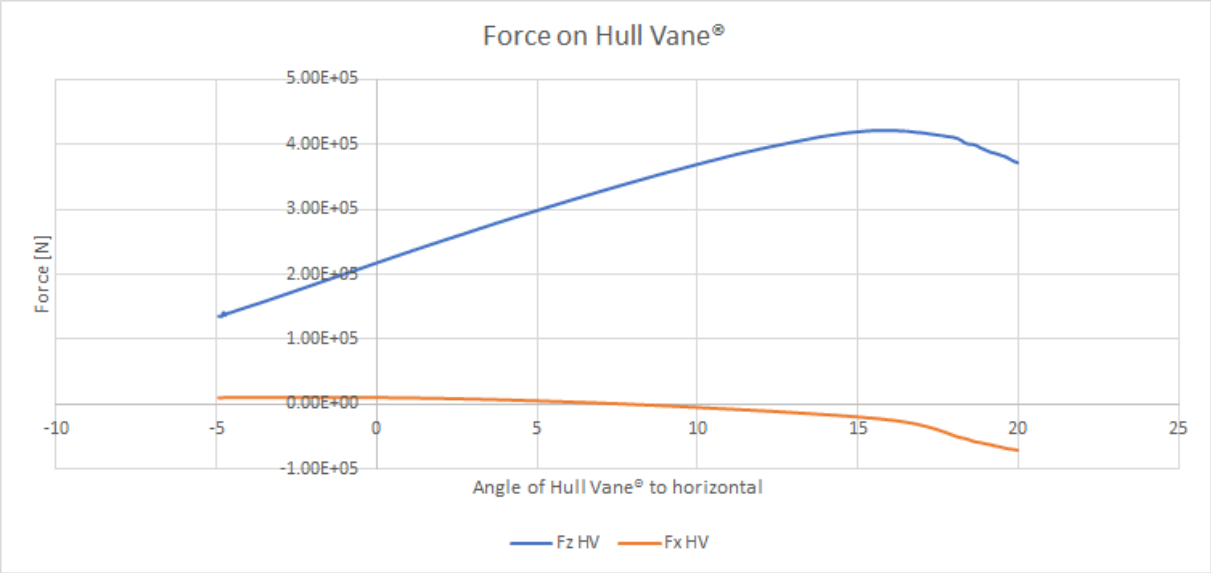

Figure 70: Variation of Hull Vane angle, with fixed ship at Fn 0.40

This experiment also showed that the drag on the Hull Vane becomes a significant part of the total resistance. The ship and Hull Vane combined had the lowest resistance when the Hull Vane had an angle to the horizontal of 0° to 3°, with a resistance reduction of around 14%. A wider optimum with still a positive force on the Hull Vane was found between -5° and 7°, with a resistance reduction of 9%. The resistance significantly increased when the Hull Vane started stalling and had an angle to the horizontal of 15° or more.

For the resistance reduction algorithm Hull Vane it would be best to keep the dynamic Hull Vane between 0° and 3° and definitely inside the limits of -5° and 7°. For the ship motion algorithm it would be best to keep the dynamic Hull Vane under the 15°, but preferably inside the -5° to 7° range.

D. SIMULATION QUANTITIES

D. I. FROUDE = 0.30, ENCOUNTER FREQUENCY = 1.75

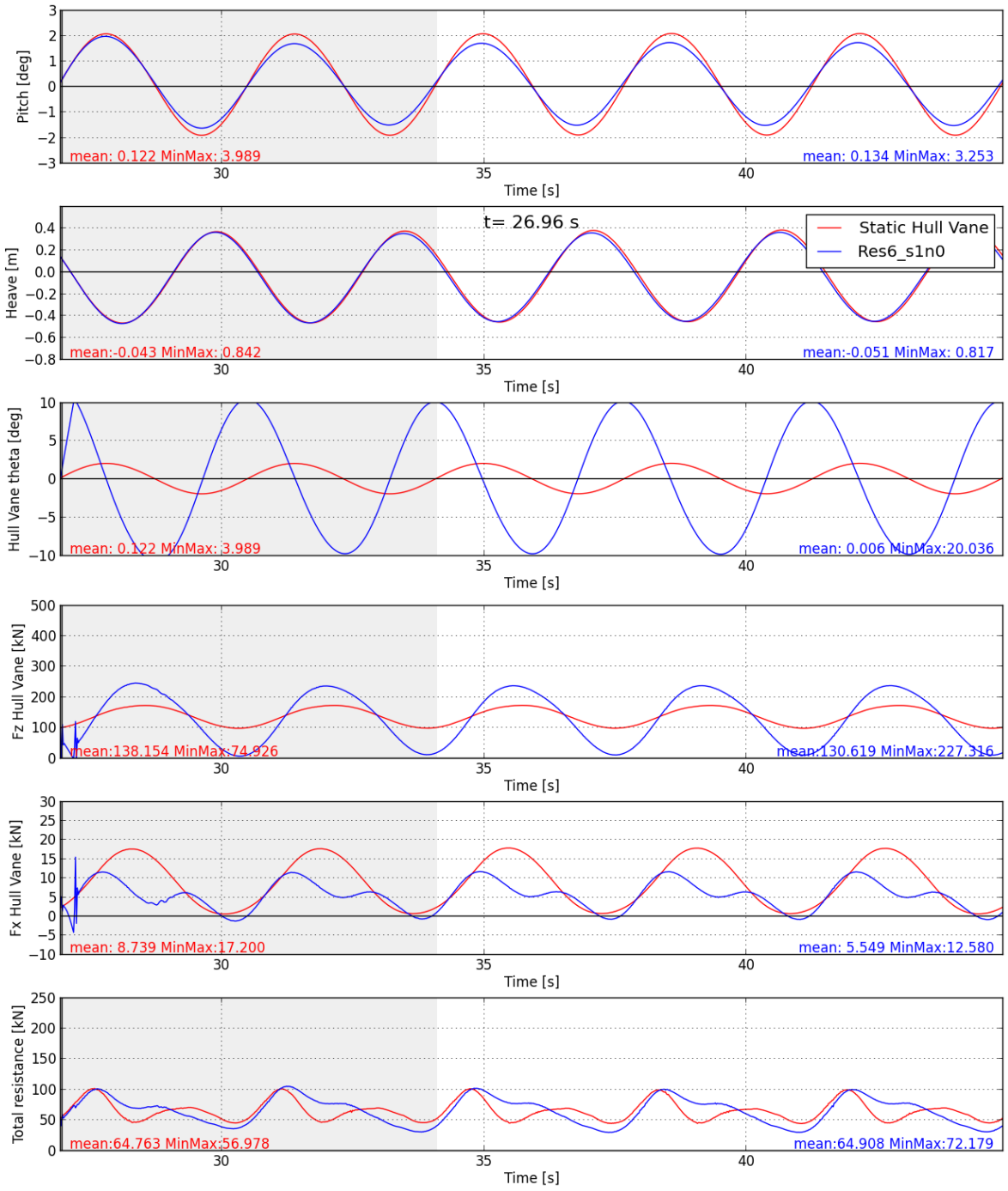

Figure 71: Overview of simulation quantities for Fn=0.30 $\omega_{enc} = 1.75\,{}^{rad}/_{s}$

D. I. FROUDE = 0.40, ENCOUNTER FREQUENCY = 1.25

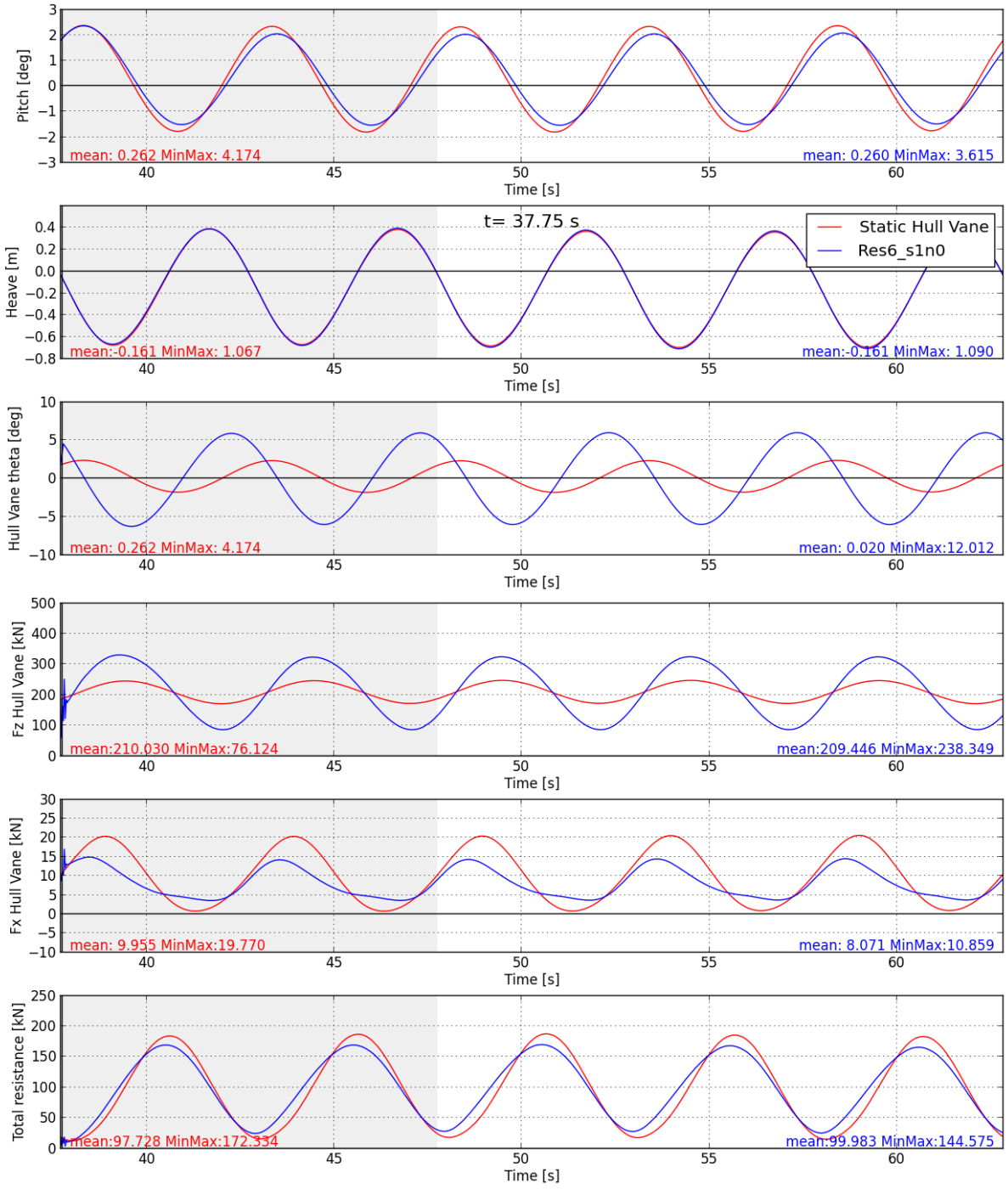

Figure 72: Overview of simulation quantities for Fn=0.40 $\omega_{enc} = 1.25\,{}^{rad}/_{s}$

D. I. FROUDE = 0.40, ENCOUNTER FREQUENCY = 1.75

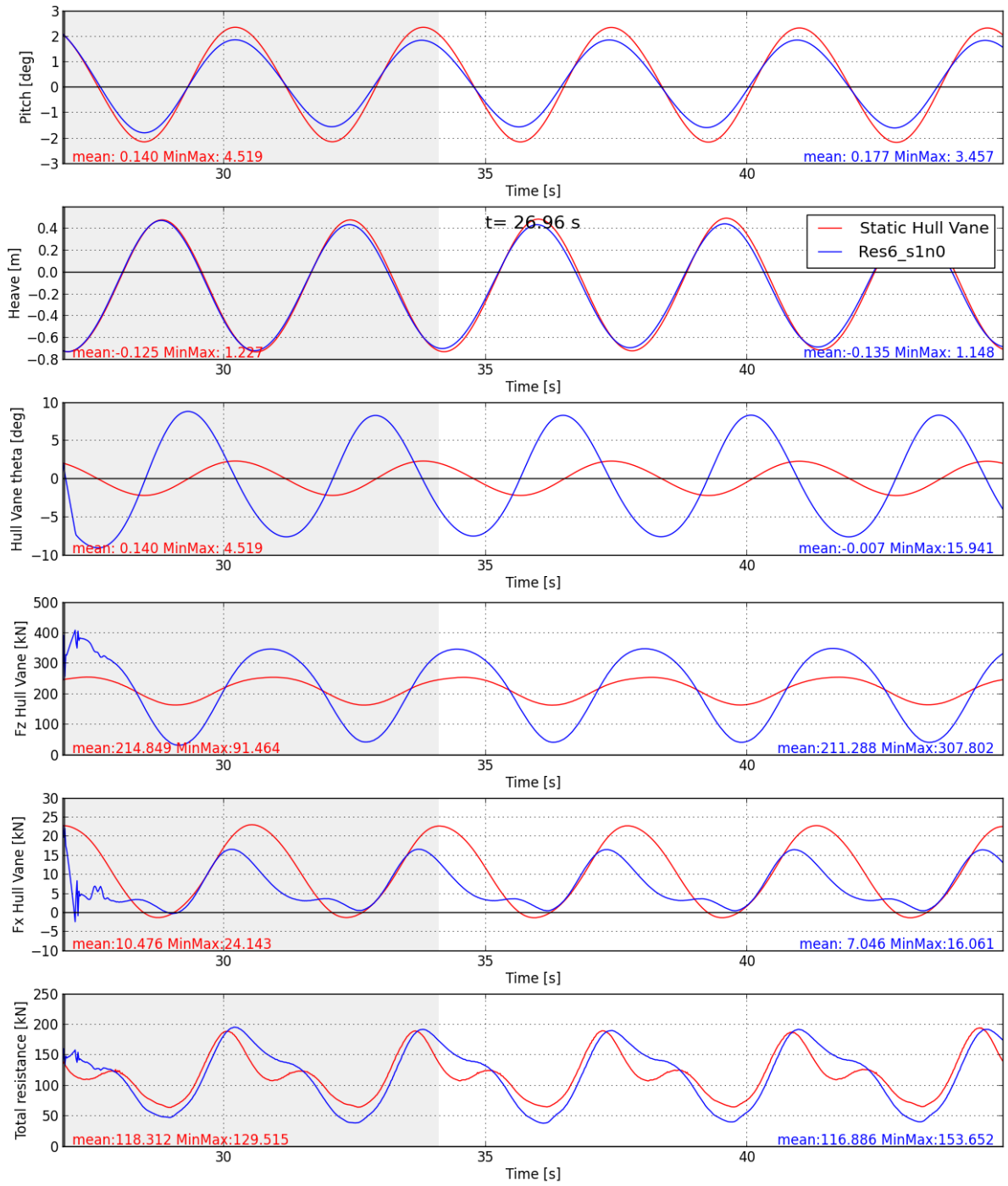

Figure 73: Overview of simulation quantities for Fn=0.40 $\omega_{enc} = 1.75\,^{rad}/_{s}$

D. I. FROUDE = 0.40, ENCOUNTER FREQUENCY = 2.25

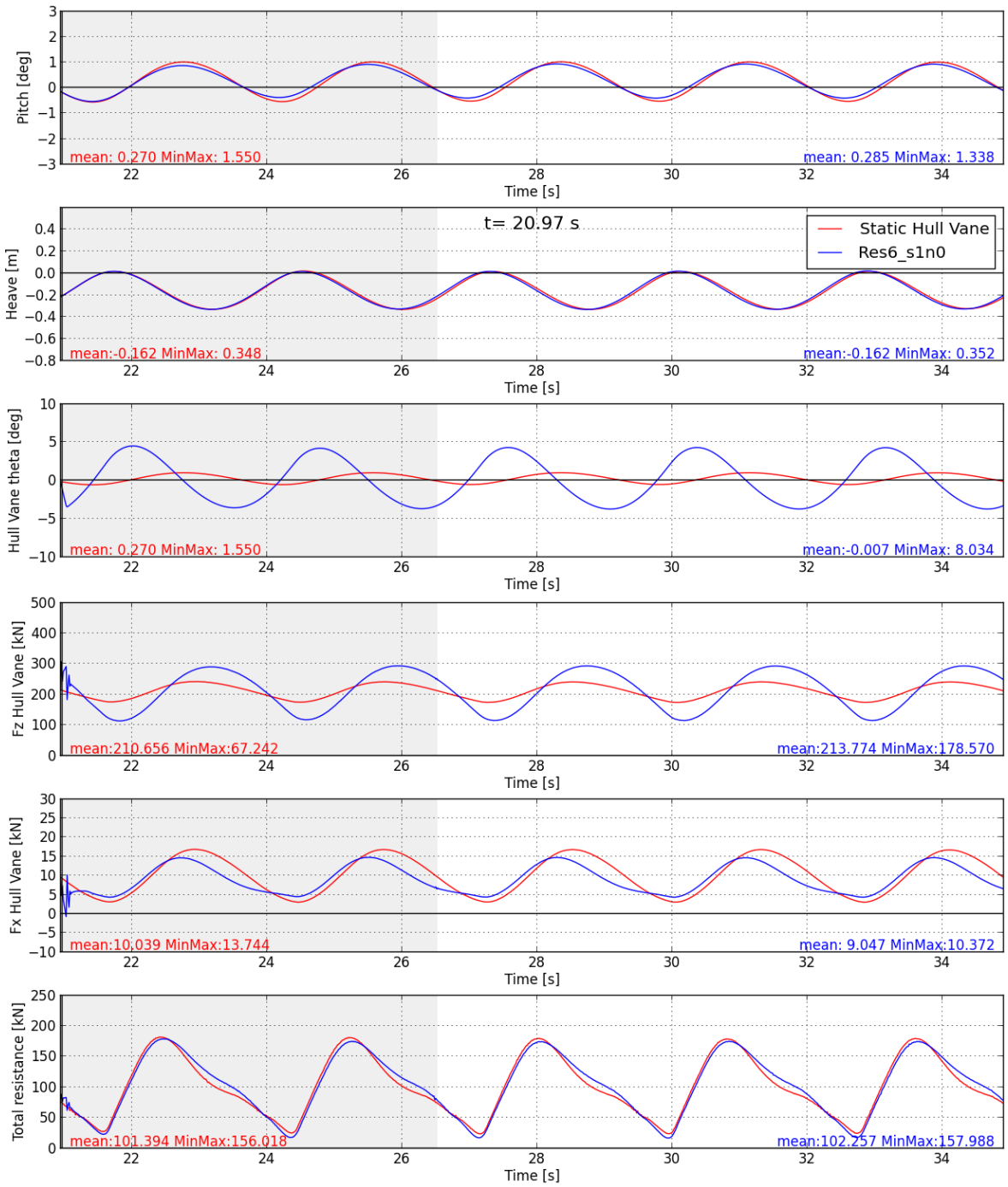

Figure 74: Overview of simulation quantities for Fn=0.40 $\omega_{enc} = 2.25\,^{rad}/_{s}$

D. I. FROUDE = 0.50, ENCOUNTER FREQUENCY = 1.75

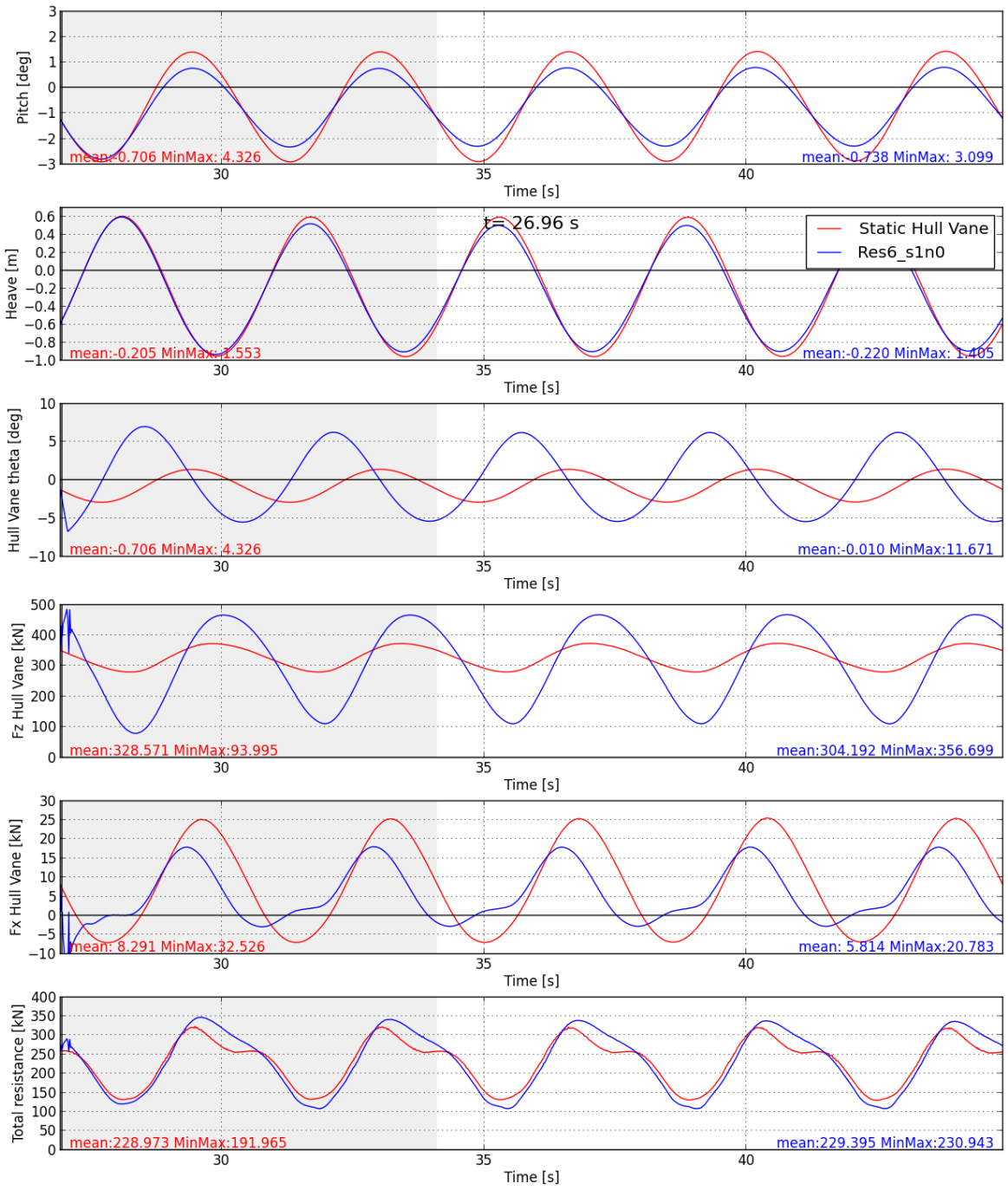

Figure 75: Overview of simulation quantities for Fn=0.50 $\omega_{enc} = 1.75\,{}^{rad}/_{s}$

D. II. FROUDE = 0.30, ENCOUNTER FREQUENCY = 1.75, WAVE HEIGTH = 0.5 M

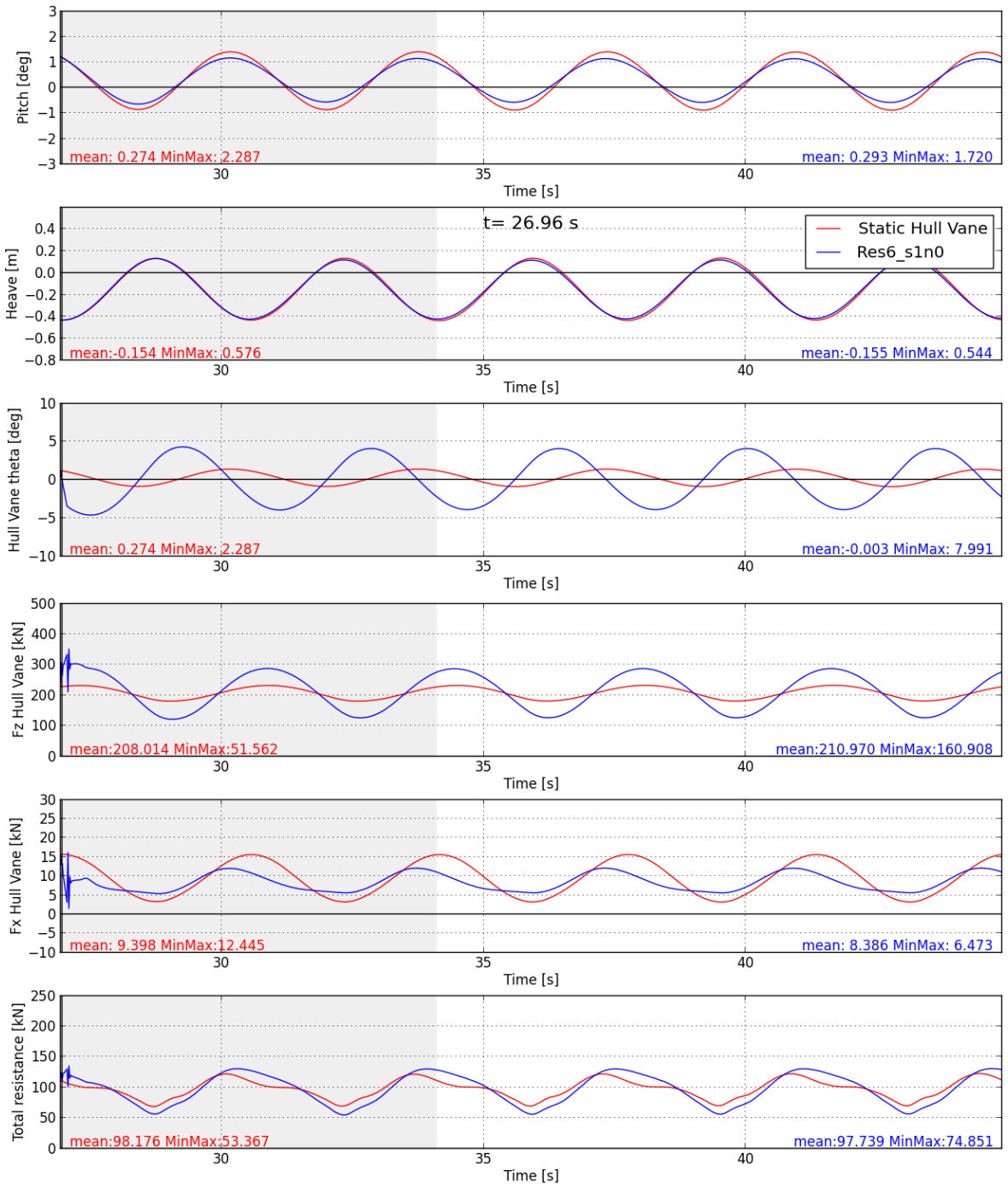

Figure 76: Overview of simulation quantities for Fn=0.40 $\omega_{enc} = 1.75\,{}^{rad}/_{s}$, wave height = 0.5 m

D. III. FROUDE = 0.30, ENCOUNTER FREQUENCY = 1.75, WAVE HEIGTH = 2 M

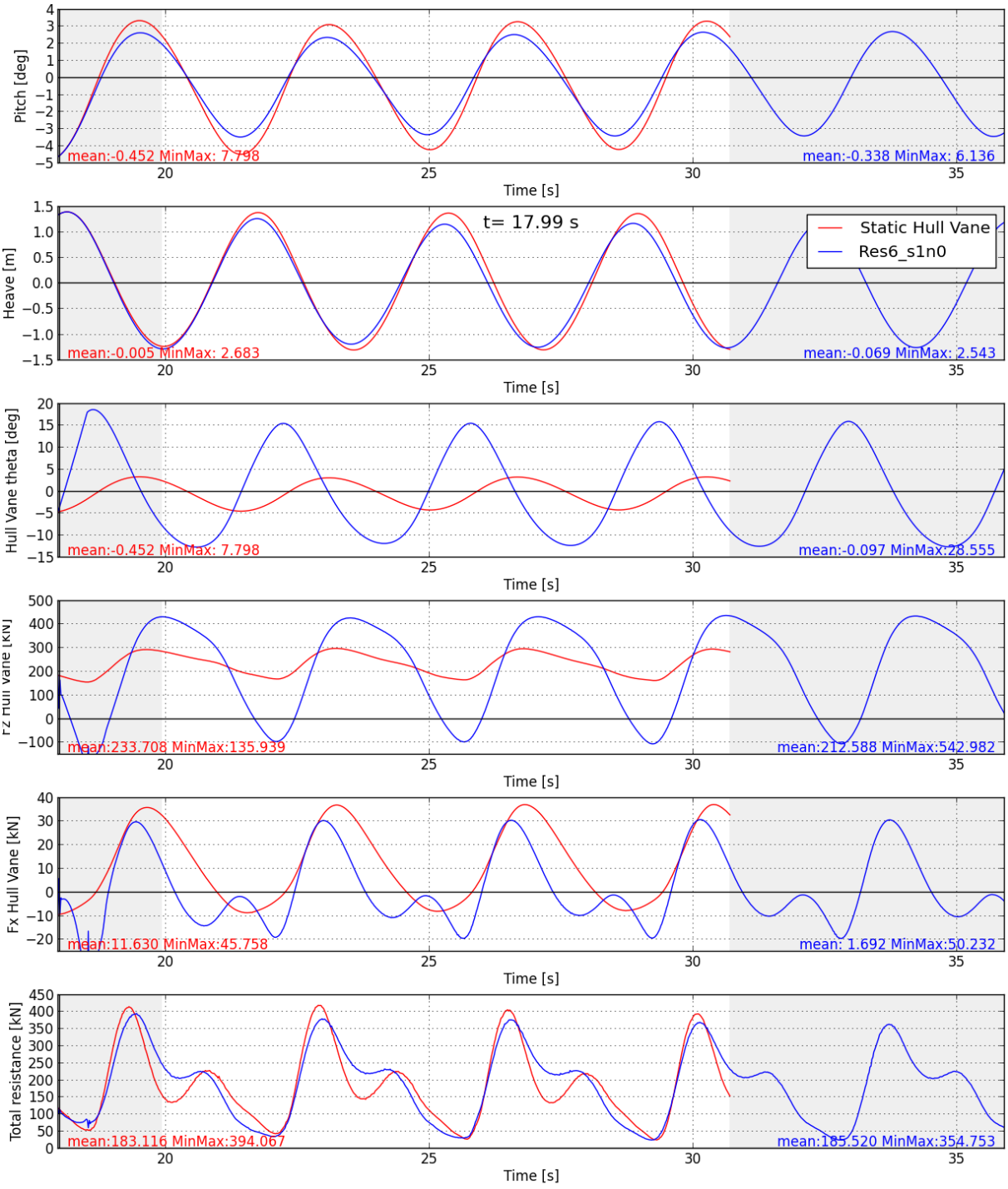

Figure 77: Overview of simulation quantities for Fn=0.40 $\omega_{enc} = 1.75\,{}^{rad}/_{s}$, wave height = 2 m

visit & mail us:

Nude 46

6702 DM, Wageningen

The Netherlands

contact us:

T +31 (0) 317 425818

info@hullvane.com

follow us:

www.hullvane.com